INFORMATION TO USERS

8517197

Geusic, Michael Edward

CLUSTER STUDIES WITHIN A SUPERSONIC MOLECULAR BEAM

Rice University   Ph.D.   1985

University
Microfilms
International 300 N. Zeeb Road, Ann Arbor, MI 48106

RICE UNIVERSITY

CLUSTER STUDIES WITHIN A SUPERSONIC MOLECULAR BEAM

by

MICHAEL E. GEUSIC
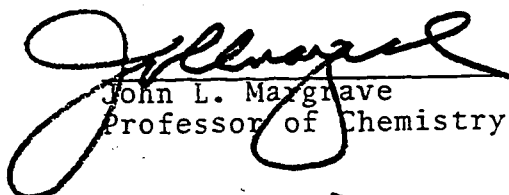
A THESIS SUBMITTED
IN PARTIAL FULFILLMENT CF THE
REQUIREMENTS FOR THE DEGREE

DOCTOR OF PHILOSOPHY
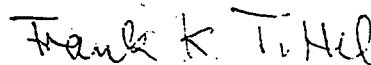
APPROVED, THESIS COMMITTEE:

Richard E. Smalley
Professor of Chemistry, Director

John L. Margrave
Professor of Chemistry

Frank K. Tittel
Professor of Electrical Engineering

Houston, Texas

April, 1985

ABSTRACT

CLUSTER STUDIES WITHIN A SUPERSONIC MOLECULAR BEAM

by

Michael E. Geusic

A novel technique for the production of metal and
semiconductor clusters based on laser vaporization
within the throat of a pulsed supersonic molecular beam
nozzle has been developed within our lab. An outline
of the overall experimental equipment and detection
schemes used for both producing and probing the clusters
within the beam will be delineated. A number of studies
using this technique have been carried out in an effort
to investigate some of the fundamental physical properties
such as bonding and reactivities of these species.

The first set of spectroscopic investigations is
concerned with the nature of the metal-metal bond in
transition metal diatomics. Studies of certain homo-
nuclear transition metal diatomics were conducted using
high resolution resonant two-photon ionization spectroscopy
in an effort to obtain gas phase data on both the ground

state bond lengths and vibrational frequencies of these
species. These investigations, as exemplified by chromium
dimer, attempted to determine the contribution of the
d-orbitals to bonding. Also, data from similar studies
on V_2, Mo_2, and Ni_2 is represented in tabular form.

Subsequently, our spectroscopic investigation of
the astrophysically important triatomic molecule, silicon
dicarbide, is detailed with the ultimate goal of this
study being to determine the ground state and excited
state bond lengths and geometries of this species. For
the past thirty years, the geometry of this molecule was
thought to be asymmetric and linear (Si-C-C), however,
from the resulting data it is clear that silicon dicarbide
is, in actuality, an asymmetric top of C_{2v} symmetry.

The recent development of a reaction tube that when
coupled to the aforementioned cluster source has facili-
tated study of gas phase reaction chemistry on metal
clusters (2-30 atoms). Details of this reaction tube
and pertinent factors regarding gas conditions contained
within the tube during the reaction period will be ex-
plained. Initial studies of the variation of reactivity
as a function of cluster size have been performed using
a select group of reactant molecules (CO, N_2, H_2) and
metals. This work has led to interesting results
suggesting that a significant variation in reactivity
does exist which depends on the metal, cluster size, and
reactant.

ACKNOWLEDGEMENTS

TABLE OF CONTENTS

LIST OF TABLES

LIST OF FIGURES

Figure

I. INTRODUCTION

Research into the production and investigation of clusters has grown substantially during the past few years and led, consequently, to the development of a number of new techniques. One such innovative technique based on laser vaporization within the throat of a supersonic nozzle is outlined in the following presentation. This laser vaporization scheme for producing clusters has provided an alternative to the earlier developed hot-oven based schemes allowing for an easy extension of cluster studies to even the highest boiling point materials. The capability to easily and reliably produce clusters of elements such as tungsten, chromium, and silicon has been demonstrated making this the most powerful and suitable technique for such studies.

Interest in the study of clusters initially developed due to the lack of experimental data relevant to the most fundamental physical properties (electronic structure, ionization potential, etc.) for the simplest of these species. Similar information pertaining to the larger clusters (trimer, etc.) has been even more difficult to obtain. Subsequently, interest developed because of the possibility that transition metal cluster studies could

lead to greater understanding in a number of scientifically and economically important areas such as, catalysis and surface chemistry.

Historically speaking, the study of small metal clusters began in the condensed phase using the method of matrix isolation. Initial researchers included Ozin[1], Moskovits[2], Linday[3], and Bondybey[4]. The technique involves co-condensation of metal vapors and an inert gas (Ar, Kr, etc.) onto a cold finger at a temperature of approximately four degrees kelvin which allows for clusters to be stabilized, cooled, and then investigated spectrally. These studies had obtained an enormous amount of information but certain limitations encouraged the pursuit of alternative methods.

The extension of cluster (alkali metals) studies into the gas phase as first reported by Schumacher and co-workers[5] involved the use of a hot-oven source coupled to a supersonic molecular beam. With this source in combination with mass selective photoionization detection, they obtained information about electronic structure and ionization thresholds for small sodium and potassium clusters. Though this work was a landmark in cluster studies, further advances were sought which would enable even higher boiling point metals (transition metals) to be studied.

In the effort to extend cluster studies to the transition metals, two subsequent designs were reported. The first method which was accomplished by Gold and co-workers[6] involved development of a hot-oven based source capable of producing a Cw free jet expansion of pure copper vapor. The source as reported in their paper had not been sufficiently analysed in order to determine the cluster distribution in their beam, though spectroscopic studies revealed a considerable concentration of Cu_2 being produced. Riley et al.[7] next reported a source that combined a very high temperature vaporization oven with a cryogenically cooled quench cell. This scheme was successfully operated at temperatures up to 2000 K , and produced Cw cluster beams of such relatively refractory metals as Al, Cr, Ni, Cu, and Ag. Unfortunately however, all of these hot-oven based techniques incur the same problem with the design and construction of the equipment due to the fact that these preliminary steps must be carried out with extreme care. Another difficulty is that at these very high temperatures of 2000-6000 K contamination from surfaces and potential nozzle clogging problems may arise.

A further step in the study of clusters was made when the well-studied laser vaporization of metals[8-10] (used in 1969 by Leach[11,12] for the production of Al_2 and C_2) was coupled to both supersonic expansion and quench

flow configurations. The laser vaporization technique developed in our lab[13-15] and also, concurrently by Bondybey,[16,17] has shown that metals can be coaxed into the gas phase, clustered, and then cooled to near zero degrees kelvin. The single most valuable advantage of this technique is that only a very local heating occurs, which in contrast to the oven based schemes, considerably reduces the design and material requirements. The local heating also permits extensive cooling which preserves all of the benefits of a normal supersonic expansion. These sources have been effective in producing clusters of even the highest boiling point metals (see Figure 1) with relative ease and reliability.

Figure 1.   Mass spectrum of iron, nickel,
            tungsten, and molybdenum clusters.

NUMBER OF ATOMS IN CLUSTER
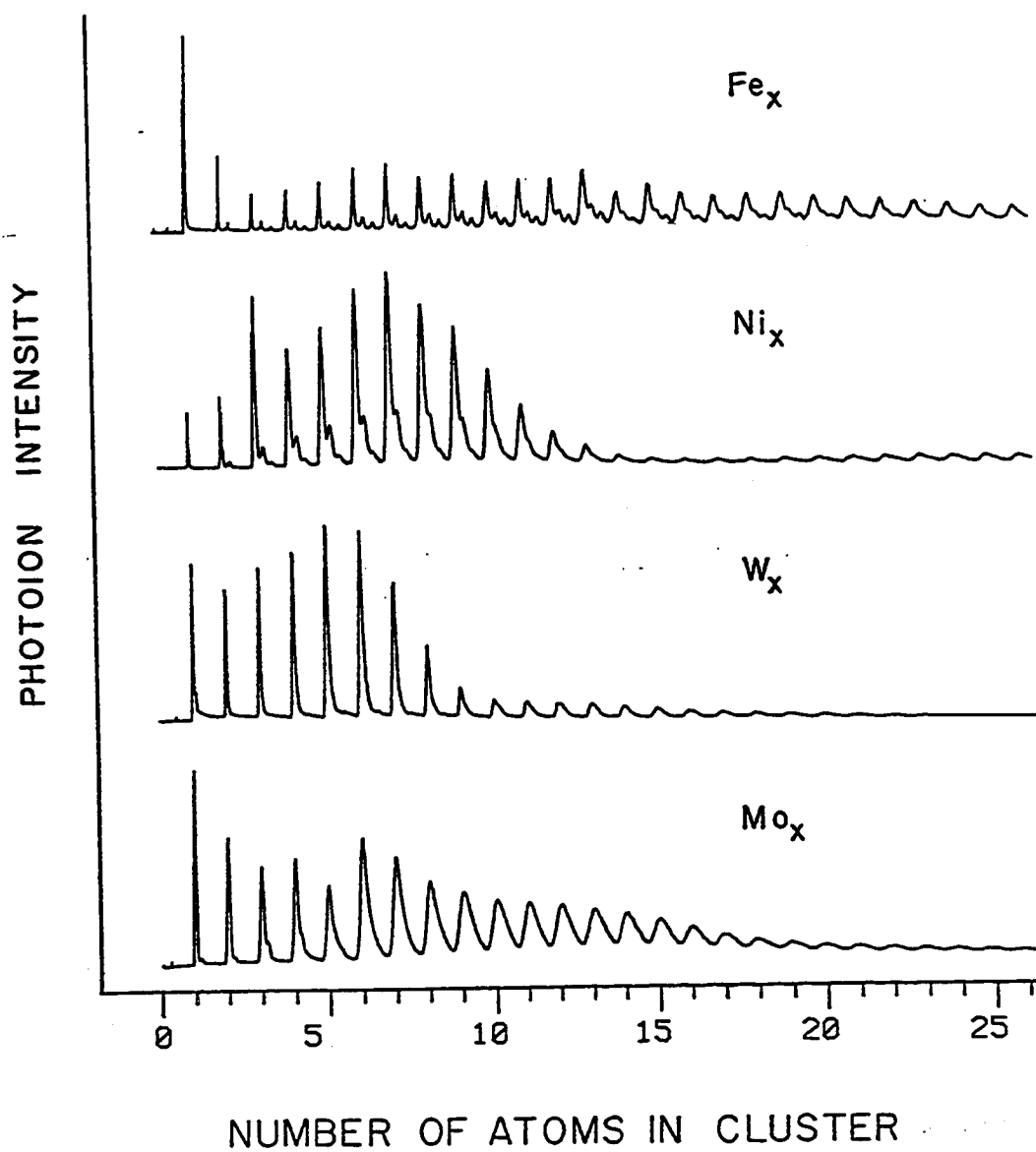
II. EXPERIMENTAL

A. Introduction

Through the use of laser vaporization, clusters of a number of elements in the periodic table have been produced within the throat of a supersonic pulsed nozzle. An overview of events for a typical experiment is sketched below. Supplemental details for certain components[18] follow in the later sections.

A typical experimental sequence begins with a pulsed double solenoid nozzle which is used to produce 200-400 μs pulses of helium (FWHM). This helium pulse flows down a .2 cm diameter tube during which time it passes over a rotating sample target and at the maximum intensity of this pulse over the sample, a Q-switched Nd:YAG laser (second harmonic), focused to a .1 cm diameter spot upon the target rod, is fired. The laser pulse vaporizes the sample producing a plasma which is entrained within the helium carrier gas. An exit channel, .2 cm in diameter and of variable length, enables sufficient three-body collisions to produce clusters prior to expansion. The helium plus cluster beam then proceeds downstream where it is skimmed twice for collimation purposes and

the beam then enters into a collisionless high vacuum ionization region of a time of flight mass spectrometer (TOFMS).

Once in this region a number of lasers may be used to investigate cluster distributions. Vibronic absorption spectra may also be taken using resonant two-photon ionization. Mass selective detection is accomplished with a time of flight mass spectrometer used to monitor the resulting signal. This signal is then multiplied and digitized using a fast 20 MHz transient digitizer. Once digitized, the signal is read through the Camac dataway to a lab minicomputer (MIK RT-11/2) for processing. This final step allows for averaging and normalization of the incoming signal in order to correct for intensity fluctuation within the source.

B. Vacuum System

A side view of the overall vacuum system as seen in Figure 2 consists of three chambers which are labeled "main, A, and B". The main chamber is a large stainless steel cylindrical can with a volume of approximately 600 liters and encircled by four flanges equally disposed about its diameter. The two side flanges are equipped with laser input windows, electrical feed-throughs, and gas-line inlets. A tri-directional translation stage

Figure 2. Side view of overall vacuum system consisting of three chambers: main, A, and B.

B

A

Main

6" DIFF. PUMPS

20" DIFF. PUMP

1.2 METERS
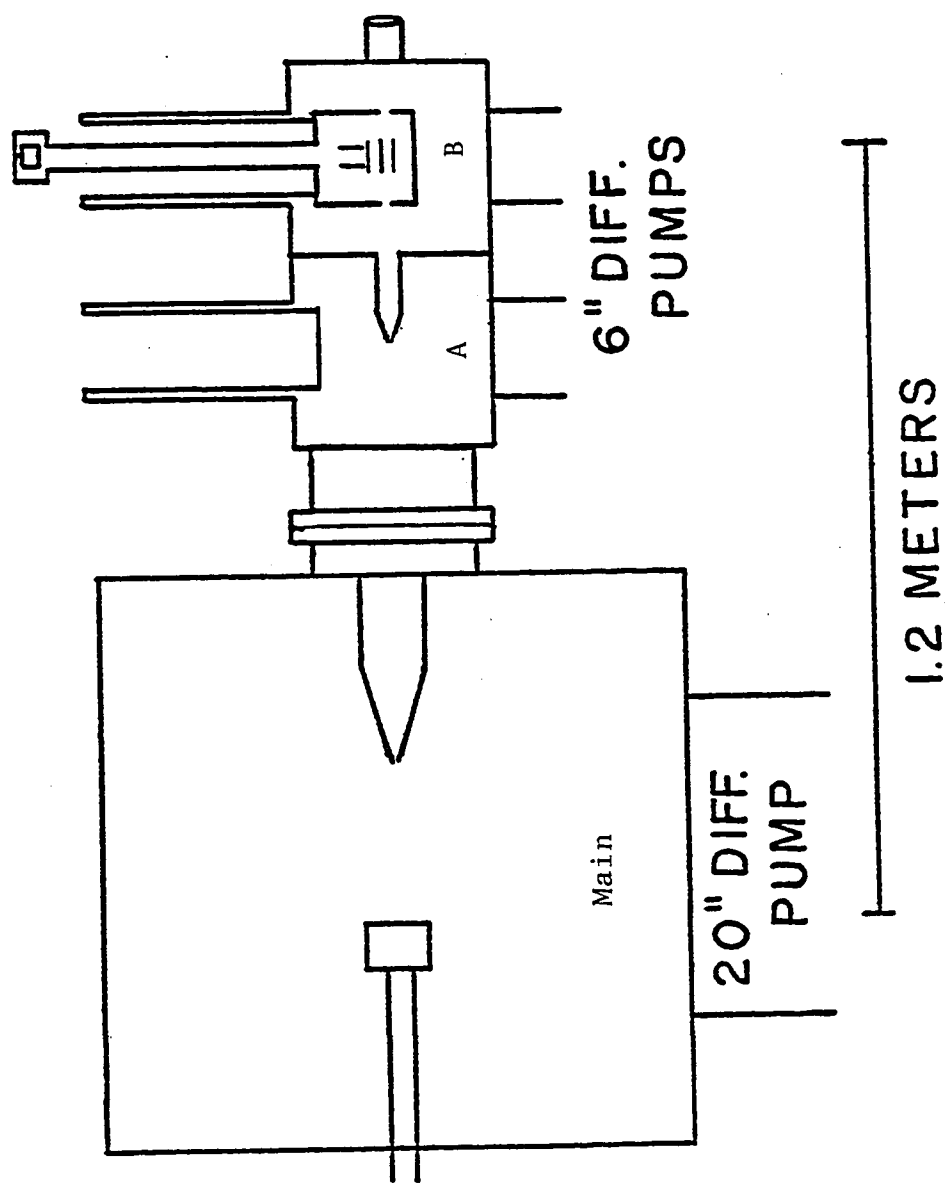
is mounted upon the back flange supporting the nozzle
and vaporization source and permitting alignment of
the molecular beam. The top of the main chamber is
removable which makes sample changes or nozzle adjust-
ments a simple procedure. Inside the chamber, a skimmer
(Beam Dynamics .3 cm diameter, 30° conical angle) is
mounted off the front wall and positioned approximately
35 cm downstream of the nozzle. A HS20 Varian diffusion
pump (20 inch diameter, type 165) which is capable of
pumping 21,000 liter/s of helium in the range of 1×10^{-4}
to 1×10^{-9} torr is backed by a Ruvac WA-series roots pump
and provides adequate pumping. Under normal operating
conditions, a base pressure of 1×10^{-4} and 1×10^{-6} torr is
maintained with the molecular beam on and off, respectively.
Separation of the main chamber from "A" and "B" is accom-
plished through the use of a four inch namatic gate valve.

The "A" chamber is also a stainless steel cube but
much smaller with a volume of approximately 30 liters.
Side flanges are equipped with laser input windows and
ionization gauges, while the top is fit with a liquid
nitrogen cryotrap used for additional pumping of con-
densable gases. The "A" chamber is pumped by a VHS-6
Varian diffusion pump (6 inch diameter, type 184) with
the capability of pumping 3,000 liters/s of helium in
the range of 1×10^{-3} to 1×10^{-9} torr), and backed by a

Welch Duo Seal vacuum pump (model #1397). The base
pressure of this chamber is 1×10^{-6} and 1×10^{-8} torr
with the beam on and off, respectively. Another col-
limating skimmer (1.5 cm diameter, 30° conical angle)
is mounted inside and situated approximately 65 cm
downstream of the nozzle.

The final chamber is also constructed of a stainless
steel cube (volume approximately 30 liters) with two
side flanges equipped with laser input windows, elec-
trical feed-throughs, and ionization gauge. The end
wall has been fit with a 1 inch diameter laser input
window, and the top with a liquid nitrogen cryotrap in
which the drift tube of a time of flight is placed. This
"B" chamber houses the acceleration and draw-out regions
of the time of flight mass spectrometer. These units are
enclosed within a copper shroud in contact with the liquid
nitrogen dewar. The pumping system is identical to "A"
with a slight variation in the base pressure being 1×10^{-7}
to 1×10^{-8} torr with the beam on and off, respectively.

c. Mass Spectrometer

The time of flight mass spectrometer used in these
cluster studies (see Figure 3) is of the Wiley-McLaren[19,20]
design and consists of several basic components: a double
stage acceleration region (labeled A-C), deflection plates,
a drift tube, and an ion multiplier. A copper shroud

encases the acceleration region connecting directly to
the liquid nitrogen dewar in an effort to keep this
area free from contamination (ex: backing streaming oil).

Ions are created in region A-B by way of photoioni-
zation using either an excimer or Nd:YAG laser system.
These ions are then accelerated through region B-C to
constant kinetic energy. And from here the ions pass
through a field-free drift tube until they strike an ion
multiplier (Johnson MM-1) for detection. A deflection
area is contained within the drift tube so that a compen-
sation of the initial beam velocities can be made helping
to direct the ions onto the multiplier.

Acceleration of all singly charged ions to constant
kinetic energy leads to the fact that their flight time
will be proportional to the square root of the mass.
This means that the ions separate into individual packets
within the drift tube according to mass. Consequently,
the lighter ion packets will strike the detector first
and heavier packets will come later. This feature
allows for a complete mass spectrum to be monitored in
a single laser shot which enables the isotopes of a
particular species to be detected simultaneously, but
independent of each other.

In normal operation, the voltages listed below
are applied to the corresponding components of the

Figure 3. Time of Flight Mass Spectrometer:
A. Repeller plate
B. Draw-out grid
C. Flight tube grid
D. Deflection plates
E. Flight tube
F. Ceramic support rods
G. Copper cryoshield
H. Stainless steel liquid nitrogen dewar
I. Ion multiplier

The spacing between the grids and plates is:
A-B = 2.54 cm   B-C = 1.27 cm   C-I = 112 cm

I

O   2 cm

H

G

F

E

D

C

B

A
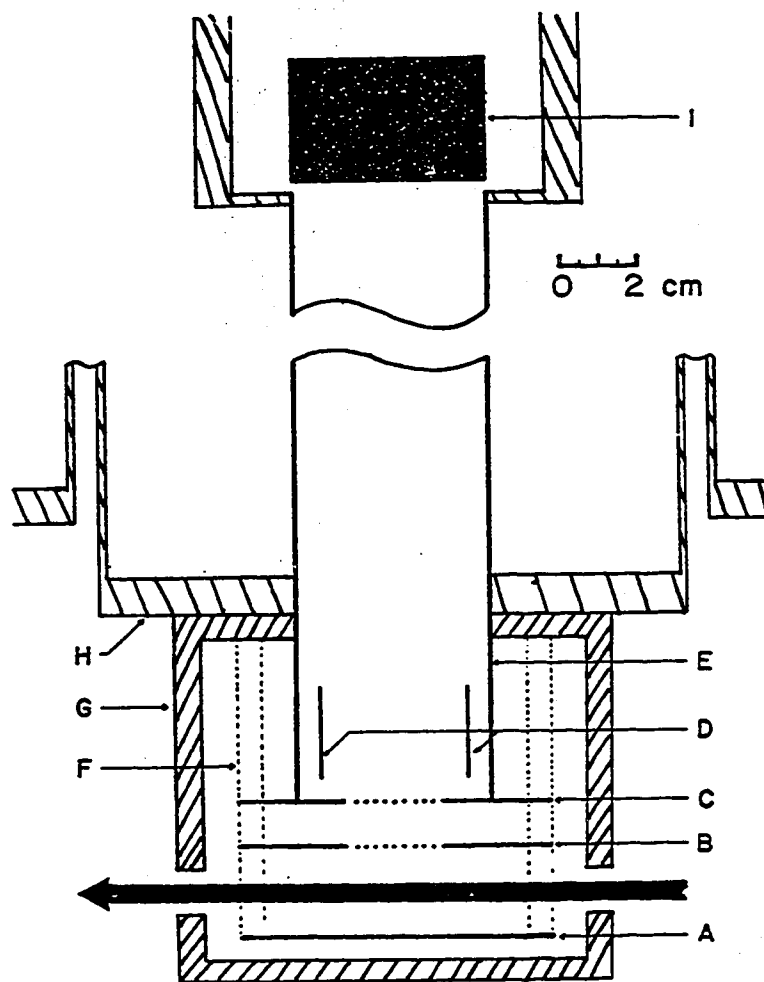
mass spectrometer:

repeller plate	+ 3,100 volts
draw-out grid	+ 2,600 volts
flight tube grid	0 volts
flight tube	0 volts
deflection plates	+ 0-500 volts

These voltages were determined using the equations outlined by Wiley-McLaren[20] for maximum resolution.

All components of the mass spectrometer were constructed of either stainless steel or ceramic with two notable exceptions being the teflon insulation on the electrical lead wires and the copper shroud. The grids are 70 line per inch, 90 per cent transmission, stainless steel mesh (Buckbee Mears).

D. Nozzle

The pulsed nozzle used in these experiments is conceptually similar to the double solenoid design of Grant[21,22] (see Figure 4 for side view). The valve is driven by two electromagnetic solenoid coils allowing for the nozzle to easily produce pulses of 200-400 µs duration. The magnetic actuator (labeled C) consists of a disk (.3 mm thick, 12.8 mm diameter) and a plunger (2.5 mm diameter, .5 mm long) constructed from a single piece of ferromagnetic material for strength. The disk is placed between the pole faces of the coils which are separated by a 1.3 mm thick aluminum ring. The plunger

Figure 4. Nozzle and Cluster Source:
        A. Close coils
        B. Open coils
        C. Magnetic actuator
        D. Sealing o-ring
        E. Spring
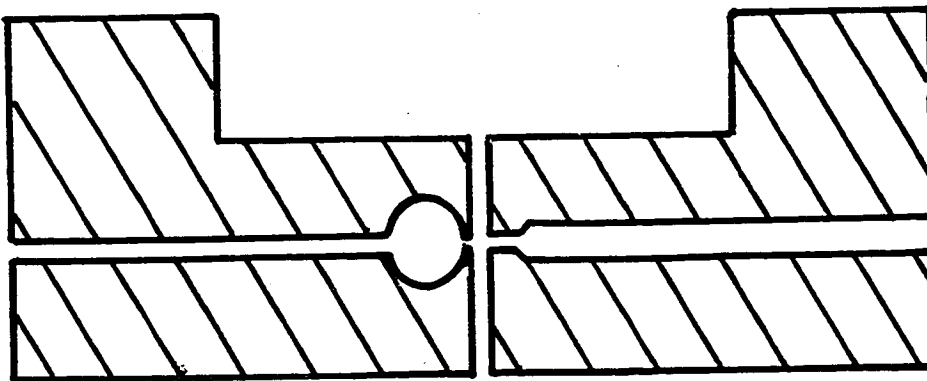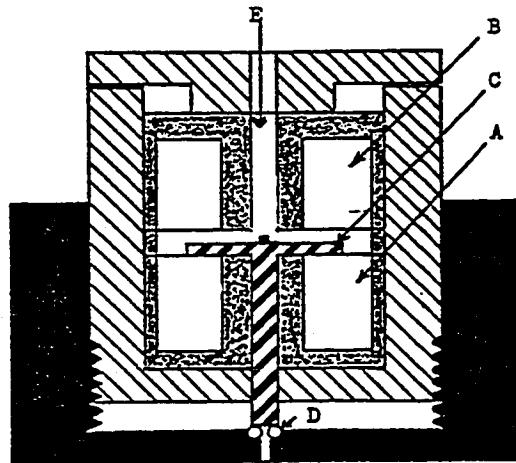
extends through a bronze bearing fit within the center
of the front (close) coil. The face of the plunger is
what actually seals against an o-ring (Parker 0.002-2)
on the face plate of the nozzle housing.

The nozzle control unit (see Figure 5) has been
designed to allow for variable current pulses to be
applied to both the front and back coils. The pulses
are adjustable in length with the close coil being
turned on as soon as the open coil is turned off. In
normal operation the back coil is pulsed which causes
the actuator to be pulled back off the sealing o-ring.
The travel of the actuator (between 0.25-1 mm) is de-
termined by an adjustable spacer or the tension of a
small spring extending through the back coil as seen in
the figure. A second pulse is then generated causing
the close coil to turn on, pulling and holding the actu-
ator back down onto the o-ring. The nozzle parameters
(voltage, pulse length, spring tension, etc.) are adjusted
such that a helium pulse of betwen 200-400 μs (FWHM)
duration (see Figure 6) is produced, with a flow rate of
approximately 1.5 torr liter at a backing pressure of 8
atmospheres.

Cooling of the nozzle housing is required since
heating results from the eddy currents that are produced
within the coils and actuator. Both the coils and actu-
ator are constructed of mild steel chosen for its high

Figure 5.   Schematic of Nozzle Control Unit
            A. Solenoid driver logic board
            B. Solenoid driver power switching
               section (continued on next page)

Solenoid Driver
Logic Board

input 270 Ω

50 Ω

2N2222A

5 KΩ

+5

5417

+5

+5

12 KΩ

10 µf

74123

74123

+5

+5

+5

10 K

18 K

+.1 µf

+5

R=3 KΩ
C=.47 µf

+5

LH0002C

+5

LH0002C

-5

-5

CLOSE

OPEN

COIL = .6 Ω

Solenoid Driver Power
Switching Section

input

+5

30 Ω

1 Ω

TIP642

2N6306
(xB)

IN4007

(+ 0-100v)

+5

1 Ω

TIP642
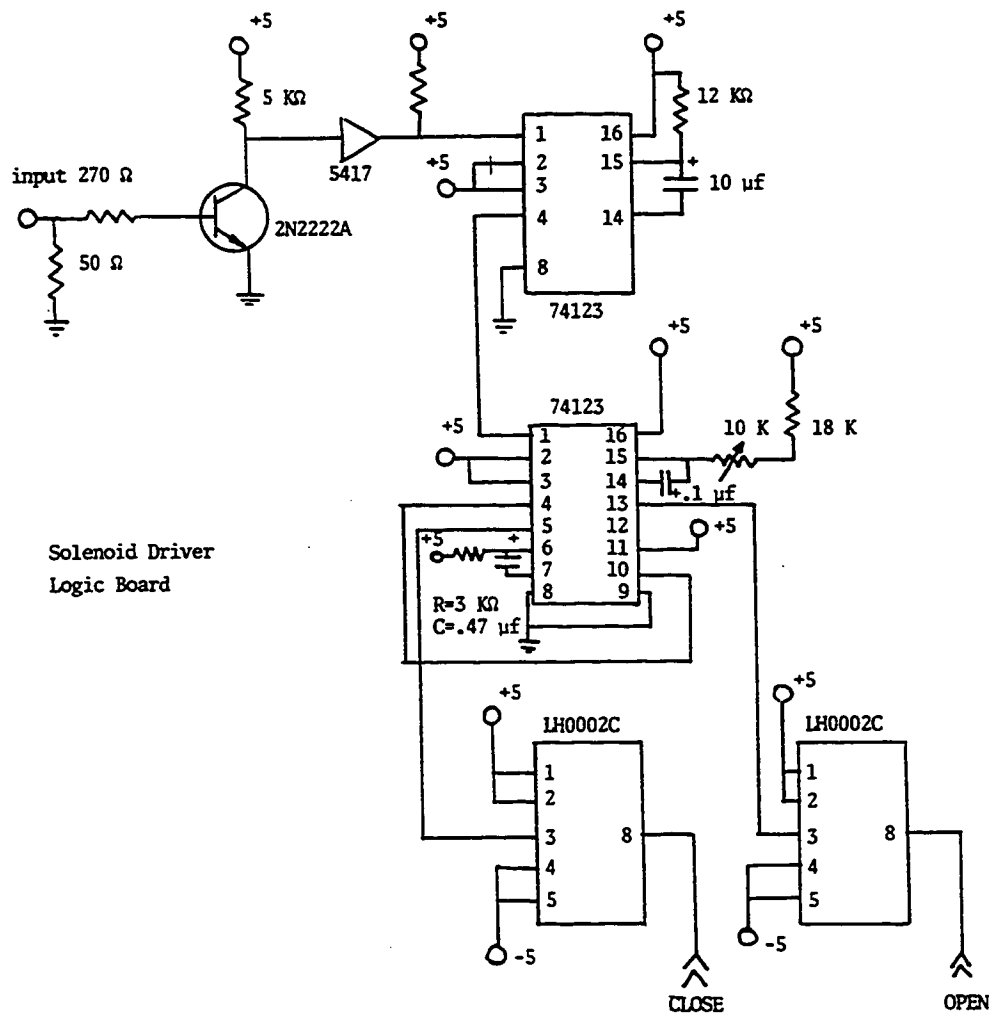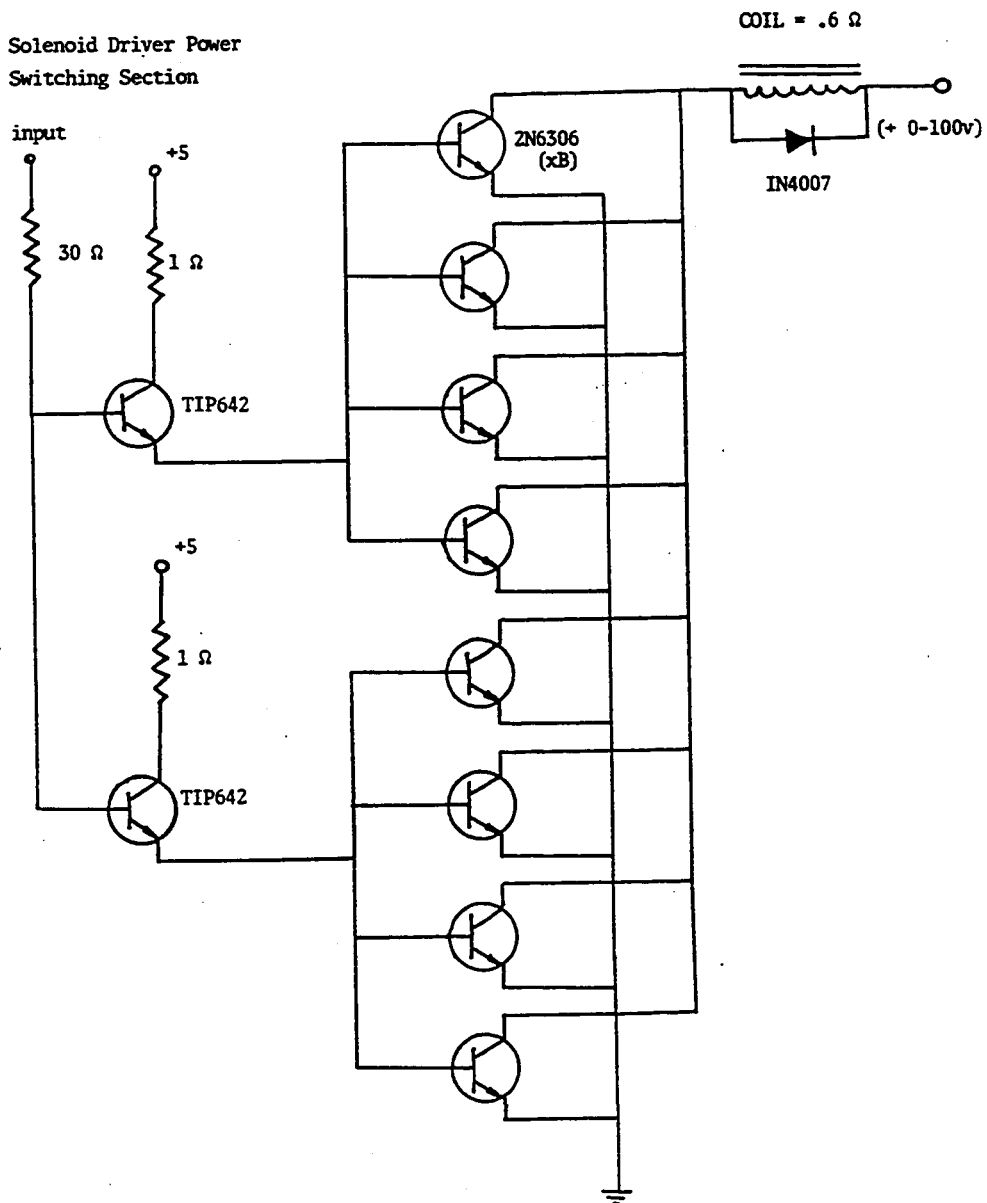
Figure 6. Time of arrival profile for helium. ArF
is used for photoionization, although the
helium signal is seen to go linearly with
laser power. Therefore, the signal must
be produced by electron impact caused by
scattered light hitting the mass spectrum
plates.

HELIUM BEAM PULSE

He$^+$ PHOTOION INTENSITY

MICROSECONDS
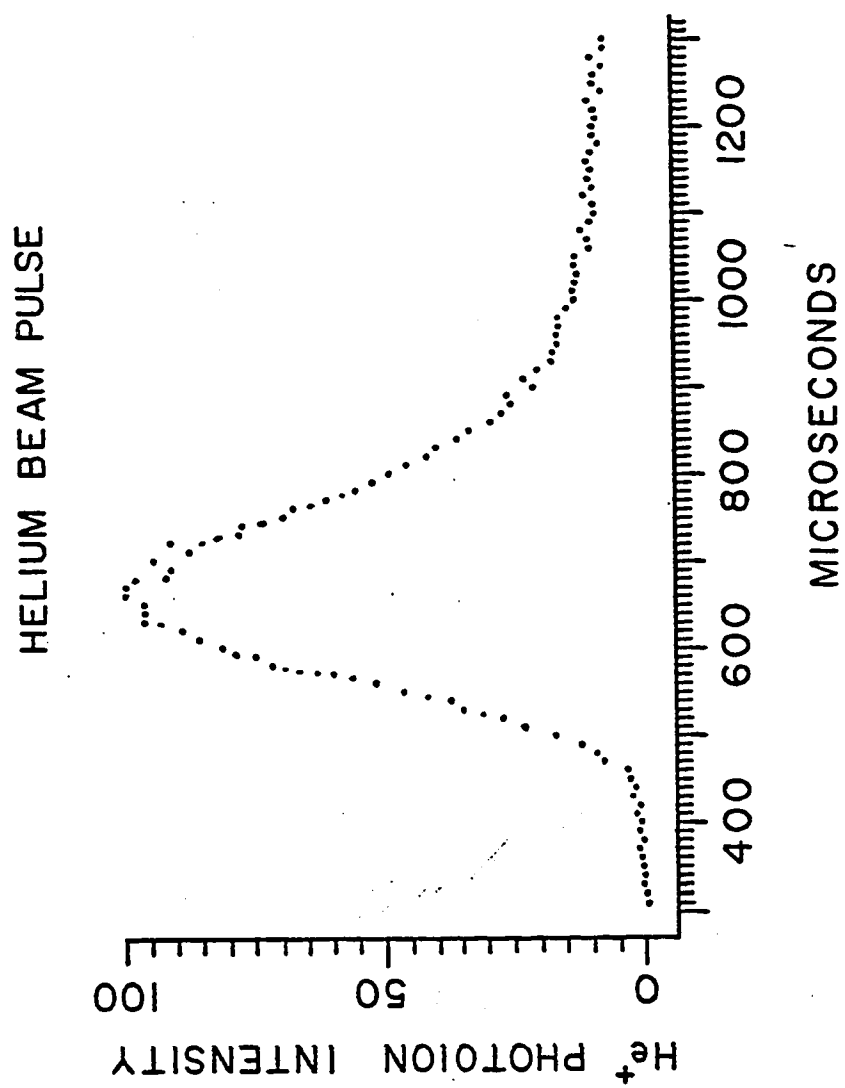
magnetic saturation property but whose low resistivity fosters the large production of eddy currents. The temperature problem is somewhat alleviated when we slot the coil housing, thereby causing a reduction in the eddy currents.

E. Laser Vaporization Source

The source is mounted on the front of the pulsed nozzle as shown in Figure 4. In this top view, two channels which lie orthogonal to each other within the same plane have been drilled. One is a .2 cm diameter channel along the molecular beam and the other is a .1 cm channel which is used for the laser input. A third channel of .25 inch diameter, which is mutually perpendicular to the other two, is drilled through the .1 cm channel directly after the point of bisection with the .2 cm channel. The sample rod is inserted within this third channel forming a portion of the .2 cm channel wall.

Through the .1 cm channel, the second harmonic of a Nd:YAG laser is focused with a 1.0 m lense such that it is incident upon the target sample. The target rod is continuously rotated at a rate of .5 rpm on a micrometer screw with a 15 turn per cm pitch. If this rotation is not performed, then the reproducibility and stability of the metal cluster signal is rather poor. These results are caused by the drilling of deep holes in the target

which makes subsequent vaporization extremely difficult.
This rotation rate produces a uniform vaporization area
when irradiated at 10 Hz, with 10-70 mj's pulses of the
second harmonic of a Q-switched Nd:YAG.

The cluster distribution which is achieved is governed
by a number of parameters. The most important (with the
exception of the third body: helium) is the length of the
.3 cm channel from the point of vaporization to free expan-
sion. This distance is critical in determining the maxi-
mum size cluster which is to be formed. Figure 7 illus-
trates a comparison between a .3 cm and 3.0 cm extension.
These results are explained simply as permitting additional
time for recombination to occur. There also has been ob-
served a small effect on the cluster distribution which
depends on the intensity of the vaporization laser and
the time at which it is fired within the helium pulse.

F. Detection and Processing Scheme

Once the ions have been created by way of photoioniza-
tion, they are accelerated to constant kinetic energy and
separated in time within the drift tube of the time of flight
mass spectrometer. These ion packets then strike a Johnson
multiplier (Model #MM-1) with a gain of up to 10^9 at 5000
volts. The analog signal is multiplied by an additional
factor of 100 by two comlinear CLC-11 video amplifiers
placed in series. From here the signal is digitized by

Camac-based fast Lecroy transient digitizer (Model #
2256AS), capable of sampling the analog waveform at a
maximum rate of 50 nanosecond intervals. The digitizer
then preforms an 8-bit analog to ditigal conversation
storing the results in a 1024 word (16-bit) random
accessible memory (RAM). The RAM is readout through
the dataway into a lab minicomputer (MIK RT-11/2) located
within the Camac crate. At this point, the mass spectrum
is processed so that it may be readout onto a terminal or
written onto a floppy disk. From considering the digi-
tizer's memory size it can be calculated that the maximum
mass range in a single shot is 850 amu.

There are two other Camac-based modules besides the
digitizer and computer. The first is a Bi-Ra (Model #
3101) 32 channel, 16-bit multiplexed analog to digital
converter. This module enables the analog signals, such
as etalon fringes or laser power measurements, to be
monitored for each shot of the experiment, and allows
this type of information to be processed along with the
mass spectrum. The second module is a kinetic system
(Model #3112), 8 channel, 12-bit digital to analog con-
verter. The second system allows the user to take any
of the digitized signals discussed above and reconvert
them to analog in order that they may be simultaneously
plotted on a stripe chart recorder. In this particular

Figure 7. Comparison of cluster distribution
           for a .3 cm and 3.0 cm extension tube
           on the cluster source.

COPPER CLUSTERS

A) 3mm Extension Channel

B) 30mm Extension Channel
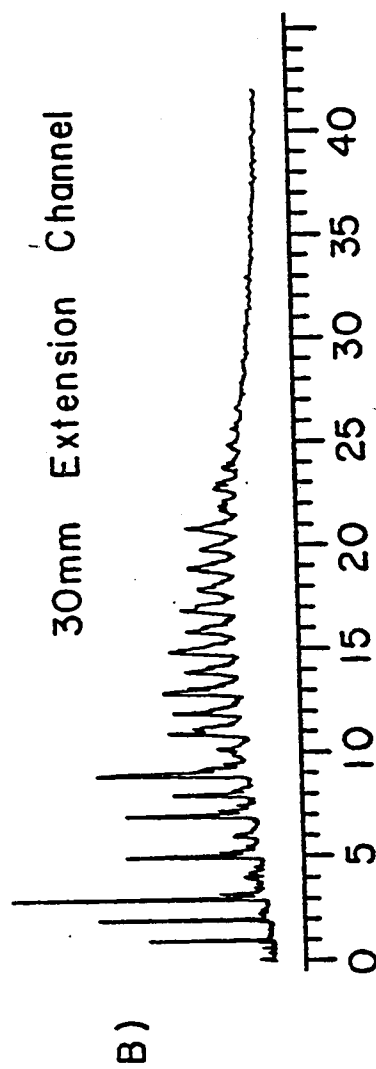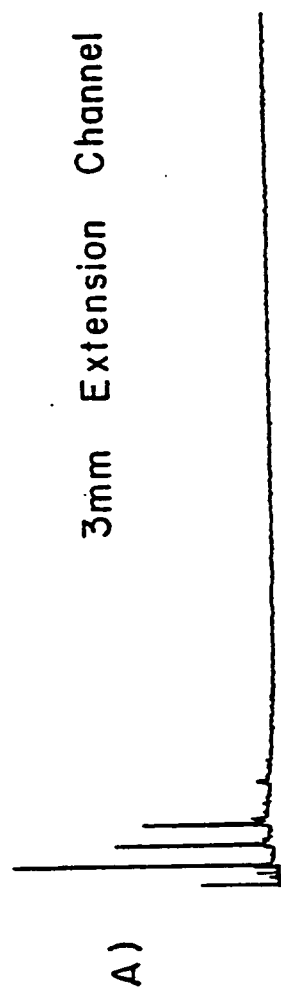
NUMBER OF ATOMS IN CLUSTER

case, the digital signals are read from the computer
through the dataway to the converter in order that
averaging of the signal can be done before plotting.
Due to the computer's capability to handle and process
incoming data, the detection scheme is run at a maxi-
mum of 10 Hz. Figure 8 presents a block diagram showing
the overall detection and processing scheme.

G. Photoionization

The production of ions by way of photoionization[23-26]
has been shown to be an extremely gentle technique. The
technique's major advantage is that under certain experi-
mental conditions (low photon fluence) little or no
fragmentation occurs. In clusters study this turns out
to be an important consideration because if fragmentation
on a large scale has taken place, then interpretation of
the data becomes extremely complex, if not impossible.

In this lab photoionization is accomplished using
two basic schemes. These two types are presented in
Figure 9 and can be seen to involve either a one or
two-photon process. The first type scheme involves a
direct one-photon ionization of all species within the
molecular beam. This process is mainly used for investi-
gations of cluster distributions and relative intensities
although, in order to intensity information to be useful
one must assume similar absorption cross sections for all

the species present. Normally with this scheme the F_2
excimer laser (7.98 eV) line is used. The only major
factor which must be considered with this type of ioni-
zation is the laser intensity. The photon flux must
be kept low enough so that no multiphoton processess
will occur.

The second scheme, a resonant two-photon ionization,
is used in this lab mainly for the probing of bound
excited electronic states of the species under study.
This type of ionization can be accomplished through
either a two-photon, one or two color scheme. In the
two color process, two photons of different energies
are involved. The first photon (excitation) is generated
from a scanning Nd:YAG pumped dye laser. The second
photon (ionization), chosen to be incapable of ionization,
is supplied from a fixed frequency laser (either an exci-
mer or Nd:YAG). The overall process is a resonant absorp-
tion of the excitation photon to a bound level of an
excited state from where the ionization photon promotes
the electron into the ionization continuium. In the two-
photon, one color scheme, both photons are of the same
energy and are supplied by the same laser. In this later
case, it is understood that only bound states of equal to
or greater than one-half the ionization energy, will result
in ion production.

Figure 8. Block diagram of detection and
processing scheme.

M-1
Johnston
Multiplier

Dual Pre-amp →

MIK 11/02

Trans.
Dig.

ADC

DAC

Camac
Crate →

Terminal

Stripe Chart Recorder
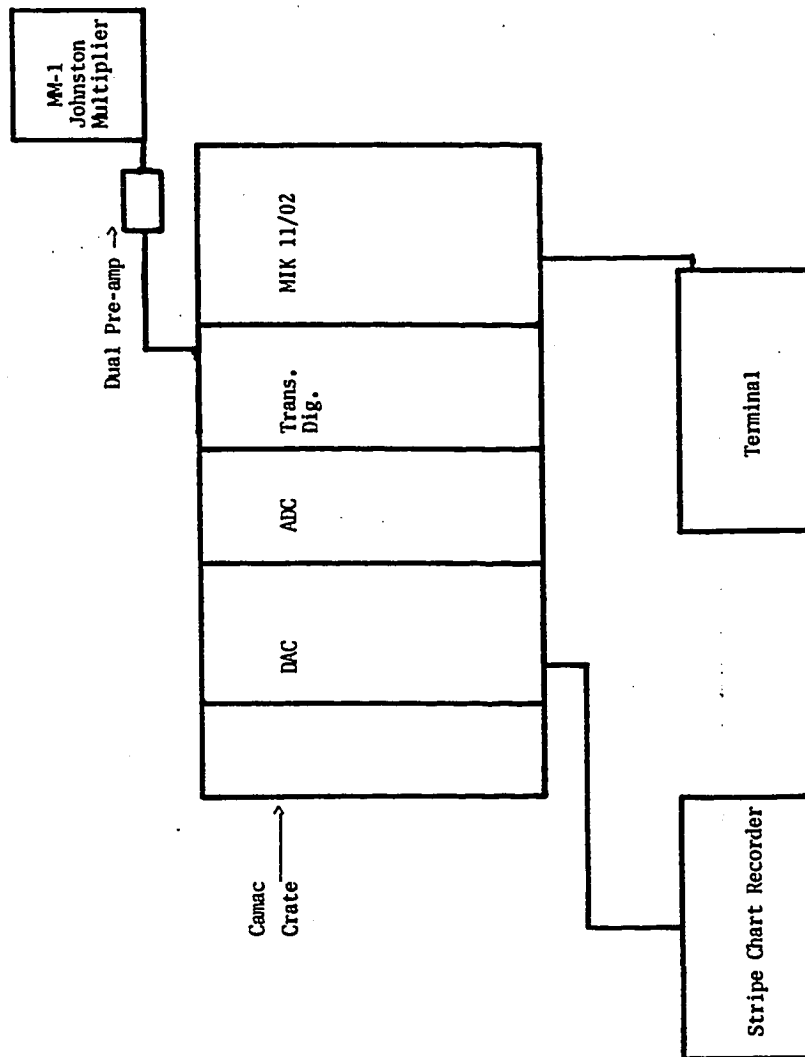
Figure 9. Photoionization schemes:
           A. Direct one photon ionization
           B. Two photon, one color ionization
           C. Two photon, two color ionization

Ionization Laser

Ionization Laser

Excitation Laser

Bound Excited State

A

B

C
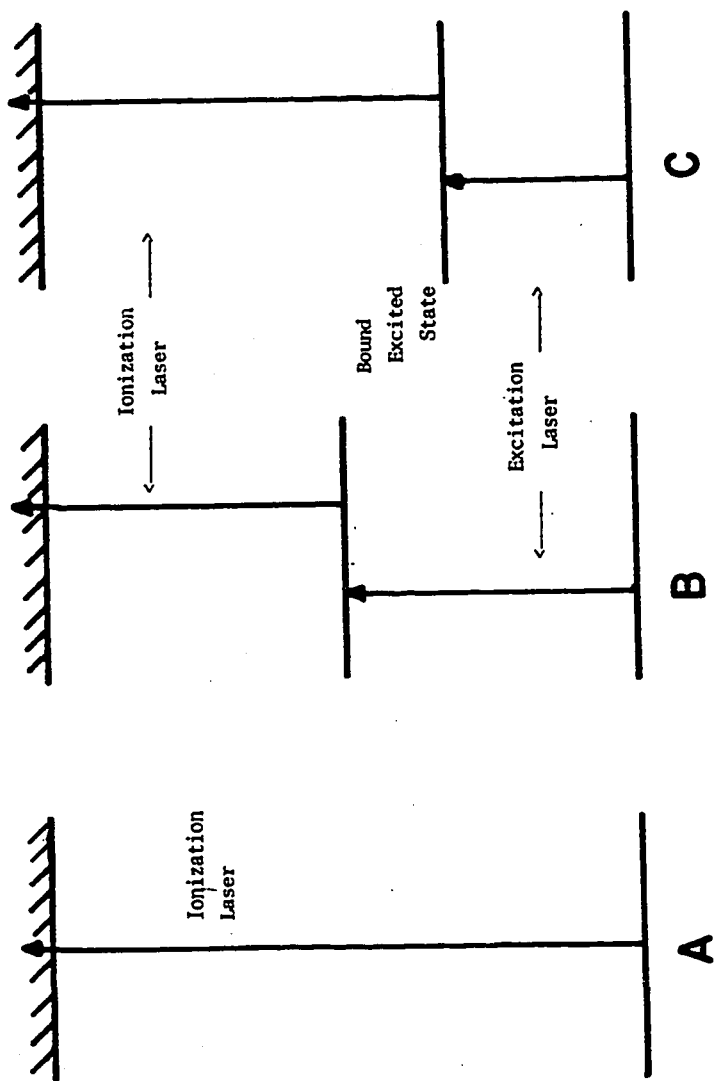
H. Timing Sequences

For the production and probing of these clusters,
a sequential timing scheme is needed in order to control
the precise firing of the independent components of the
experiment. The timing sequence is initiated by a mas-
ter oscillator which drives a series of Nimbin-based
delay generators at a repetition rate of 10 Hz. Two
schemes have been used for the experiments in this
thesis and are shown in Figure 10 (labeled A and B).
Timing scheme A is used to acquire simple mass spectrum;
while scheme B is used for spectroscopic investigations
via resonant two-photon ionization.

The master oscillator consists of a 3.5 MHz crystal
oscillator divided down to 10 Hz. Also, within this unit
is contained an Evans Associate delay generator which
allows for an initial delay to be set with respect to
time zero of the experiment. This then triggers a series
of other delay generators, which in turn allows one to
set delays between the various required events. These
are all accurate to within ±1 ns. The master oscillator
and delay generators (Evans Associate) are Nim-based
and have been equipped with thumbwheel switches so the
delays can be set accurately, in real time, without the
need for an oscilloscope.

Figure 10. Experimental timing sequence for
acquiring:

A. Mass spectra
B. Resonant two-photon ionization
spectroscopy

B

30 ms   680 us   830 us   600 us   270 us   370 us   270 us

Excimer
Charge
On
Demand

Vaporization
Laser
Relay

Spectroscopy
Laser
Relay

Nozzle
Fire

Vaporization
Laser
Lamp   Q-Switch

Spectroscopy
Laser
Lamp

Excimer

Transient
Digitizer

Spectroscopy
Laser
Q-Switch

A

30 ms   1510 us   600 us   270 us   640 us

Excimer
Charge
On
Demand

Vaporization
Laser
Relay

Nozzle
Fire

Vaporization
Laser
Lamp   Q-Switch

Excimer

Transient
Digitizer

III. SPECTROSCOPIC INVESTIGATIONS OF TRANSITION METAL DIATOMICS (CHROMIUM DIMER)

A. Introduction

The gas phase spectroscopic investigations of transiton metal diatomics have lagged behind as compared to similar studies of other elements within the periodic table. This is primarily due to the extremely high boiling points (approximately 2000-6000 K) of these metals, making their spectroscopic studies extemely difficult, if not impossible, with the techniques used for the alkali and coinage metals. Although about one half of all transition metal diamtomics have been studied in the condensed phase by matrix isolation,[27] some of the answers to important scientific questions have been elusive mainly because of the inability of this technique to permit investigation of high resolution rotational spectra. One of the most important and also controversial questions surrounding the transition metal diatomics has been the nature of the metal-metal bond, or more specifically, the role of d-orbitals in the bonding of these molecules.

In an effort to obtain experimental data pertaining to this question, the cluster source previously described

was used to produce and cool (Vib $\leq$ 125 K, Rot $\leq$ 10 K)
beams of these transition metal clusters. The diatomics
could then be spectroscopically probed using high reso-
lution resonant two-photon ionization.

At the start of these studies, it was apparent
that chromium dimer had become a central issue in the
controversy over the nature of multiple metal-metal
bonding. The ground state of the chromium atom is a
half-filled $3d^5$ $4s'$ configuration in a high spin ^7S
state. One might argue that this would lead to chromium
dimer having a very tightly bound ground state with
a bond order of perhaps as high as six. This would be
accomplished through a single $4s\sigma$ bond and five d-d
bonds involving $3d\sigma,\pi$, and δ orbitals. If this argument
were accepted, all the valence electrons would be paired
making the ground state electronic symmetry that of
$^1\Sigma$, and most likely $^1\Sigma_g^+$. With six bonds one would expect
an exceedingly short bond length, high vibrational
frequency, and dissociation energy.

Up until the time of our experiments, the experimental
gas phase data pertaining to chromium dimer consisted of
two studies. The first, done by Kant,[37] used mass spec-
troscopic measurements of the Cr/Cr_2 equilibrium ratio
in a Knudsen effusion cell to determine the binding energy
(D_e = 1.56 $\pm$ .03 eV) of Cr_2. The other experiment relevant

to the binding in chromium dimer was reported by Efremov et al.[38] in 1974. In a flash photolysis study of chromium hexacarbonyl vapor, a transient absorption was observed in the 4600 Å region. Rotational analysis of this spectrum indicated a bond length of r_0 = 1.68 Å, but the analysis could not rule out the possibility of this spectrum being due to CrO_2 or CrC_2.

Since then, the idea of a sextuplet bond has been the subject of extensive theoretical calculations.[30-36] Some of these calculations supported the idea; others suggested an effective bond order of considerably less than six. The most recent calculation (at the time of this reinvestigation), done by Goodgame and Goddard[36] using a self-consistent 6000 confiration wave function corresponding to spin-optimized generalized valence bond plus inter-pair correlations and van der Waals interactions, suggests that chromium dimer is not best described as a sextuplet bond, but rather as an anti-ferromagnetic dimer. This calculation yielded a ground state bond length of r_e = 3.0 Å and a binding energy of D_e = .03 eV. In this same paper, they also recalculated the binding energy obtained by Kant arguing that the value may have been too high because of the failure to consider substantial population of the low-lying high spin electronic states, and also that effusive flow was not maintained during the experiment.

Because of the lack of firmly established experimental data and unrestrained theoretical calculations, we felt that reinvestigation[39] of the 4600 Å band of Efremov et al.[38] was necessary in order to establish whether the carrier was chromium dimer. We also hoped to obtain more extensive data in our reinvestigations. This work will be presented in full. Similar investigations of other transition metal diatomics will be discussed briefly and presented in tabular form.

B. Experimental

Chromium clusters were produced within a supersonic molecular beam using the laser vaporization technique previously described. In this experiment, a pulsed solenoid nozzle is used to produce a 200-400 us pulse of helium (FWHM). As the helium flows over a chrome-plated steel target (.06 cm diameter, plating depth of .013 cm), a Q-switched Nd:YAG laser of the second harmonic and focused to a 0.15 cm diameter spot, is fired at a chosen time within the helium pulse. The laser pulse vaporizes the target material and produces a plasma which is entrained in the helium carrier gas. An exit channel (.2 cm diameter, .32 cm length) enables sufficient three-body collisions to produce clusters prior to expansion. The supersonic free jet (He + chromium clusters) then expands proceeding downstream during which time it is skimmed

twice at positions 32 and 65 cm away from the nozzle before entering the ionization region of a time of flight mass spectrometer (TOF MS). The resonant two-photon ionization with mass-selective detection is obtained using a Nd:YAG-pumped dye laser as the excitation with a KrF excimer laser (4.98 eV) providing the ionization photon. For high resolution scans, the dye laser line width is narrowed to approximately 0.05 cm^{-1} by the insertion of an inter-cavity etalon and then pressure-tuned using either SF_6 or N_2. Both lasers are overlapped temporally and spatially in the ionization region. The ionization laser is chosen such that it is incapable of one-photon ionizing the cluster of interest but can directly ionize an excited state produced by absorption of a photon from the excitation (dye) laser. This provides a resonant enhancement when the dye laser is tuned to an absorbing transition. Mass-selective detection is accomplished using a time of flight mass spectrometer to monitor the resulting photoion signal. The signal is then multiplied and digitized. The intensity of each photoion can then be averaged and recorded by a lab minicomputer (MIK RT-11/2). In this way, the spectrum of chromium dimer can be determined simultaneously (but independently) for the various isotopic species.

C. Selection Rules

In these experiments the information pertaining to the bonding in transition metal (chromium dimer) diatomics was obtained through spectroscopically probing rovibronic transitions. The probability that a transition between two different electronic states will be induced by the oscillating electric field of light is proportional to the square of the transition moment integral,[40]

$$M = <\Psi' |\hat{\partial}| \Psi''> = \int \Psi_N'^* \Psi_N'' [\int \Psi_{el}'^* \hat{d}_{el} \Psi_{el}'' \hat{d}\tau_{el}] \hat{d}\tau_n$$

where, the single prime indicates the upper of the electronic states. From this integral the overall selection rules for a one-photon electric dipole transition for diatomic molecules (with an emphasis on a $^1\Sigma$-$^1\Sigma$ transition) are seen to be:[41]

1) The spin multiplicity cannot change.

$$\Delta S = 0$$

Singlet <——> Singlet

Triplet <——> Triplet

Singlet <—|—> Triplet

2) The electronic orbital angular momentum can change at most by one quantum.

$$\Delta \Lambda = 0, \pm 1$$

3) For homonuclear diatomics, even electronic

   states combine only with odd electronic states.

$$\text{gerade} \longleftrightarrow \text{ungerade}$$

$$\text{gerade} \longleftrightarrow\!\!\!|\!\!\!\longrightarrow \text{gerade}$$

$$\text{ungerade} \longleftrightarrow\!\!\!|\!\!\!\longrightarrow \text{ungerade}$$

4) Σ^+ states cannot combine with Σ^- states.

$$\Sigma^+ \longleftrightarrow \Sigma^+$$

$$\Sigma^- \longleftrightarrow \Sigma^-$$

$$\Sigma^+ \longleftrightarrow\!\!\!|\!\!\!\longrightarrow \Sigma^-$$

5) The vibrational quantum number may change by

$$\Delta V = 0, \pm 1, \pm 2, \pm 3 \ldots \text{etc.}$$

6) The rotational quantum number may change by

   at most one.

$$\Delta J = 0, \pm 1$$

$$\Delta J = \pm 1 \text{ for } \Sigma\text{-}\Sigma \text{ transition}$$

Along with these selection rules, there are factors
which modulate the intensity of individual vibrational
and rotational lines within an electronic transition.
For the vibrational bands, it is seen that the square
of the integral,

$$\int \Psi'_{vib} \; \Psi''_{vib} \; \hat{d\tau}_n$$

is proportional to the intensity of the band. Therefore,
the magnitude of the overlap between the two vibrational
wave functions is the determining factor of the strength
of a particular vibrational band within the electronic

transition. The square of this integral is called the Franck-Condon factor. For rotational lines within a particular vibrational band, there is also a modulation in intensity. These intensities can be shown to be proportional to the Honl London factors[41] whose formulae are given below for a $\Delta\Lambda=0$ transition:

$$S_J^R = \frac{(J'+\Lambda')(J'-\Lambda')}{J'}$$

$$S_J^Q = \frac{(2J'+1)\Lambda'^2}{J'(J'+1)}$$

$$S_J^P = \frac{(J'+1+\Lambda')(J'+1-\Lambda')}{J'+1} \quad .$$

When dealing with homonuclear diatomic molecules with $\Lambda=0$, one must also consider the effects of nuclear spin[40] because of the fact that either the even or odd rotational levels will have a greater statistical weight. The ratio of the intensity between the even and odd levels can be shown to be $(\frac{I+1}{I})$. In the case of a homoclear diatomic with zero nuclear spin, it can be seen that either the odd or even rotational levels will be non-existent.

D. Results

The supersonic beam version of the chromium dimer absorption band in the 4600 Å region as reported by Efremov et al.[38] is shown under low resolution to consist

of a single vibronic transition (see Figure 11). In this figure, the resonant two-photon ionization signal corresponds to a certain isotopic species (52-52) of chromium dimer versus the frequency of the scanning dye laser. In trying to understand the appearance of the low resolution scan as consisting of a single band assigned as the (0-0) transtition due to the small isotope shift, two possible explanations are conceivable. The first is that the transition was between two nearly identical states that is at least near the minimum of their potential energy wells. If this were the case, one might expect to observe a $\Delta v = 0$ progression. The second explanation is that the higher vibrational levels of the excited state are predissociative. Measurement of the lifetime shows the $v=0$ level of the excited state to be 30 ns which is supportive of the predissociative argument. Further evidence however is needed before either or both possibilities may be ruled out.

Higher resolution scans of the (0-0) band are shown in Figures 12 and 13 corresponding to the 52-52 and 50-52 isotopic species, respectively. From the well-resolved rotational structure, it is quite apparent that a Q branch is not present. This type of rotational structure, consisting of a P and R branch, is what would be expected for a Σ-Σ rovibronic transition. Since the 52-52

Figure 11. Resonant two-photon ionization scan
of chromium dimer (52-52) in the
4600 Å region.
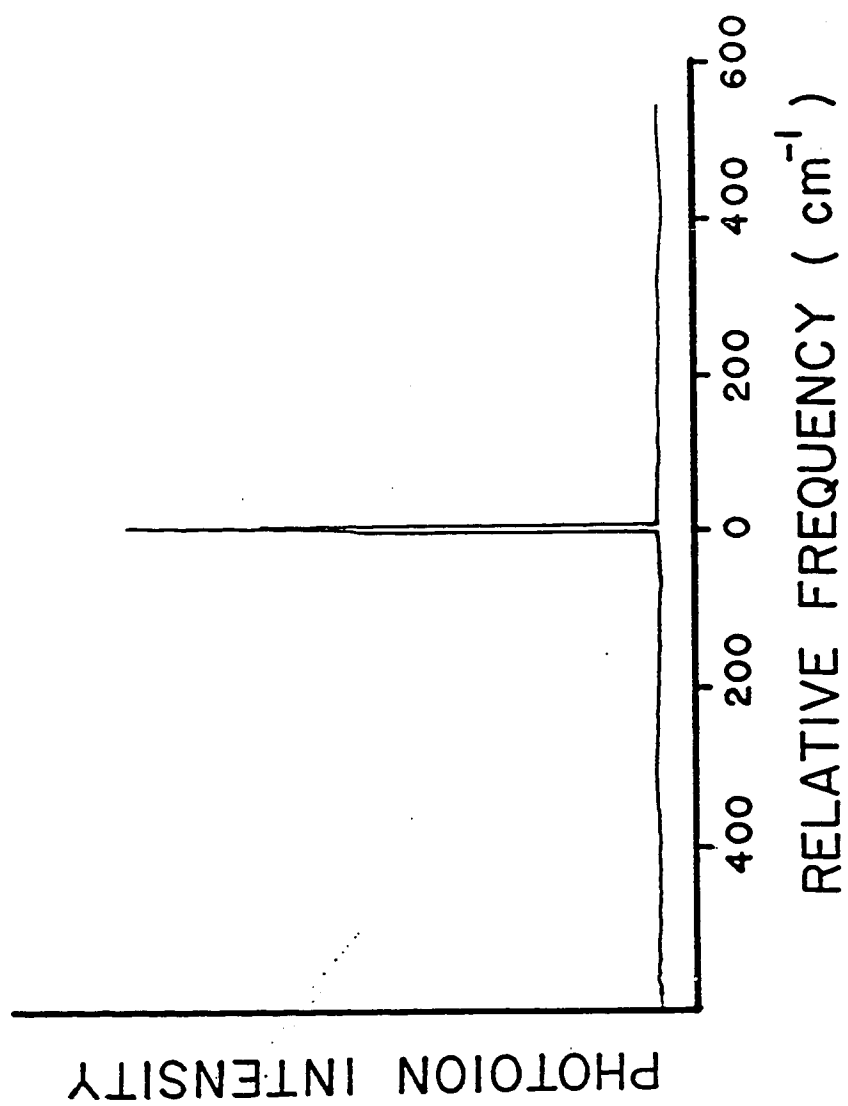
isotopic species has zero nuclear spin, one also expects
that alternating rotational lines would be absent in
the spectrum, due to nuclear spin statistics. This is
easily confirmed by examining the band gap (spacing be-
tween the inner most lines of the P and R branches) in
Figure 12. When all lines are present the ratio of the
spacing of the band gap to any two consecutive lines in
either the P or R branch will be two. If only alterna-
ting lines are present this ratio will be three-halves.
Also since the 50-52 isotopic species has no symmetry
restrictions on the existence of its rotational levels,
a quick comparison of Figure 13 to Figure 12 would fur-
ther confirm the absence of alternating lines in the
52-52 rotational structure. High resolution spectra of
the 52-54 isotopic species has also been obtained showing
a similar rotational structure as that for the 50-52
isotopic species as would be expected.

Using the selection rules for a $\Sigma \leftarrow \Sigma$ transition and
the Honl London factors presented in the last section,
symmetries of the states involved can be narrowed to
either

$$\Sigma_u^+ \leftarrow \Sigma_g^+ \quad \text{or} \quad \Sigma_g^- \leftarrow \Sigma_u^- \ .$$

The first of these is more likely and therefore, the
transition is assigned as $^1\Sigma_u^+ \leftarrow {}^1\Sigma_g^+$.

Figure 12. Rotationally resolved 0-0 band
of the A $^1\Sigma_u^+$ ← X $^1\Sigma_g^+$ electron
transition of $^{52}Cr_2$ in a super-
sonic molecular beam. The spectrum
was recorded by monitoring the in-
tensity of mass (m/e)=104 photoions
produced by resonant two-photon ion-
ization using a pulsed, pressure-
tuned dye laser to scan over the
spectrum and a simultaneous KrF
exciplex laser to ionize the A $^1\Sigma_u^+$
molecules produced when the dye laser
was on resonance. Photoion signal was
observed only when the two lasers were
overlapped in time, indicating the A
state lifetime was less than 10 nano-
seconds.
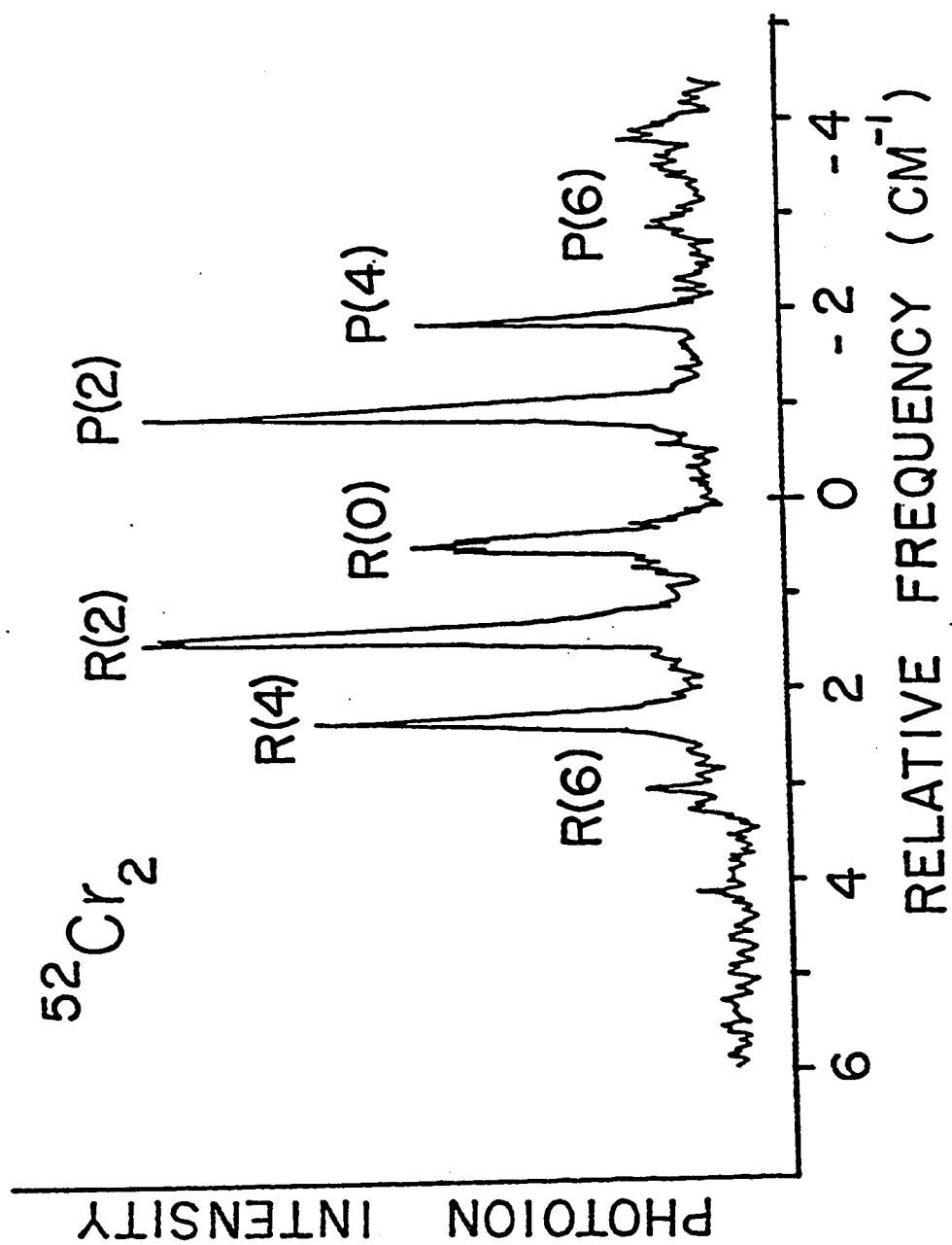
Figure 13. Rotationally resolved 0-0 band of
the A $^1\Sigma_u^+ \leftarrow$ X $^1\Sigma_g^+$ electronic transi-
tion of the isotopically mixed molecule
$^{50}Cr^{52}Cr$ in a supersonic molecular beam.

Figure showing photoion intensity versus relative frequency for $^{50}Cr^{52}Cr$, with R(J) branch labeled 6 5 4 3 2 1 0 and P(J) branch labeled 1 2 3 4 5. X-axis: RELATIVE FREQUENCY (CM^{-1}), values 6 4 2 0 -2 -4. Y-axis: PHOTOION INTENSITY.
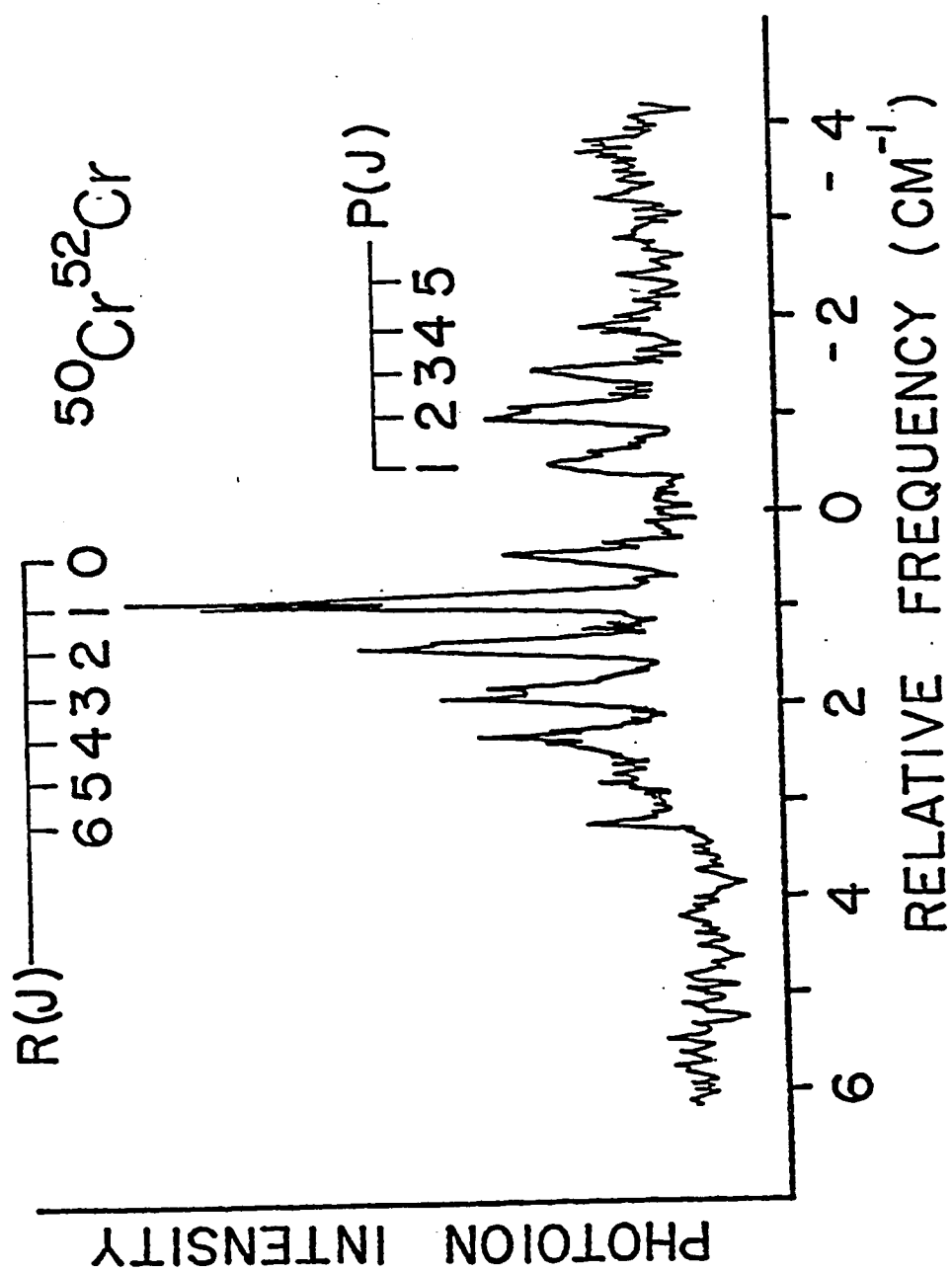
Sc	Ti	V	Cr	Mn	Fe	Co	Ni	Cu	Zn
(1.65)	(1.30)	1.83	2.06	(0.43)	(1.04)	(1.73)	2.06	2.03	(0.19)
Y	Zr	Nb	Mo	Tc	Ru	Rh	Pd	Ag	Cd
(1.62)		(5.21)	(4.19)			(2.92)	(1.09)	1.66	(0.08)
La	Hf	Ta	W	Re	Os	Ir	Pt	Au	Hg
(2.52)							(3.71)	2.30	(0.08)

Figure 14.   Ground state binding energies (eV) for transition metal homonuclear diatomics.

See Refs. 28, 29, 39, 42-47

The assignments and measured positions of all
observed rotational lines are listed (see Table I) for
each of the three isotopic species mentioned above.
These line positions were then fit simultaneously to
the formula[41]

$$\nu\pm = F'(J''+1) - F''(J'')$$

where the + and - refer to the $R(\Delta J=+1)$ and $P(\Delta J=-1)$
branches of the rovibronic transition, respectively,

where $\quad F'(J) = \nu_{00} + \tfrac{1}{2}\rho we' + \rho^2 \beta_0' \ J(J+1)$

$\qquad\qquad F''(J) = \tfrac{1}{2}\rho we'' + \rho^2 \ \beta_0'' \ J(J+1)$

and $\qquad \rho = (\frac{\mu}{\mu_i})^{\tfrac{1}{2}}$

$\qquad\qquad \mu$ = the reduced mass of the 52-52 isotopic species

$\qquad\qquad \mu_i$ = the reduced mass of the other isotopic species

$\qquad\qquad$ of chromium dimer being measured.

Results of the fit are listed in Table I. The parameters
are presented in Table II and compared to the results of
Efremov et al.[38]

As shown in Table I, the fit of the measured data
to the suggested model is excellent. It should be pointed
out that due to the extensive rotational cooling (approxi-
mately 4 K which has been determined by computer simula-
tion of a rovibronic band) in the supersonic molecular
beam, only the low rotational levels are populated. This
leads to a spectrum consisting of a limited number of
lines in both the P and R branches. The accuracy of the

Table I. Measured·Rotational Line Positions for the
A $^1\Sigma_u^+ \leftarrow$ X $^1\Sigma_g^+$ 0-0 Band of Chromium Dimer.

Transition	Observed Position(cm^{-1})	Calculated Position(cm^{-1})	Residual(cm^{-1})
	$^{50}Cr^{52}Cr$		
P(4)	-2.06	-2.09	-.03
P(3)	-1.63	-1.61	.02
P(2)	-1.15	-1.14	.01
P(1)	-0.68	-0.67	.01
R(0)	0.25	0.27	-.02
R(1)	0.73	0.73	.00
R(2)	1.19	1.20	-.01
R(3)	1.69	1.66	.03
R(4)	2.12	2.12	.00
R(6)	3.01	3.03	-.02
	$^{52}Cr^{52}Cr$		
P(6)	-2.81	-2.79	.02
P(4)	-1.84	-1.85	-.01
P(2)	-0.91	-0.93	-.02
R(0)	0.45	0.45	.00
R(4)	2.27	2.27	.00
	$^{52}Cr^{54}Cr$		
P(4)	-1.64	-1.64	.00
P(3)	-1.24	-1.18	.06
P(2)	-0.75	-0.73	.02
R(1)	1.09	1.73	.02
R(2)	1.52	1.52	.00
R(3)	1.95	1.97	-.02
R(4)	2.40	2.41	-.01

[a]All observed line positions were measured relative to the band origin of the $^{52}Cr_2$ molecule. This 0-0 band origin was found to lie at 21,751.5 ± 1.0^{-1}(76.2 ± 1 cm^{-1} from the 21,827.7 cm^{-1} line of atomic Cr corresponding to the transition y $^5P_1(3d^44s^14p^1)\leftarrow$a $^5S(3d^54s^1$) which was also observed in this molecular beam experiment).

[b]See text and Table II for parameters used for this cal-culation.

Table II. Molecular Constants for the A $^1\Sigma_u^+ \leftarrow$ X $^1\Sigma_g^+$
Transition of Chromium Dimer ($^{52}Cr_2$).

	This Work[a]	Efremov et al.[b]
ν_{00}	$21{,}751 \pm 1$ cm^{-1}	$21{,}751{,}52$ cm^{-1}
$\omega_e{}' - \omega_e{}''$	-39.1 ± 4.4 cm^{-1}	----
$B_0{}'$	$0.2290 \pm .0023$ cm^{-1}	$0.2276 \pm .0004$ cm^{-1}
$B_0{}''$	$0.2298 \pm .0028$ cm^{-1}	$0.2287 \pm .0002$ cm^{-1}
$r_0{}'$	$1.684 \pm .009$ Å	$1.6888 \pm .0015$ Å
$r_e{}''$	$1.671 \pm .010$ Å[c]	----

[a]Indicated error is estimated 95% confidence limits.

[b]Reference 38.

[c]Calculated from $B_e{}'' = B_0{}'' + \frac{1}{2}\alpha_e{}''$ where $\alpha_e{}''$ was estimated from Moskovits' et al. measurement of $\omega_e{}'' = 427.5$ cm^{-1} and $\omega_e x_e{}''$ = 15.8 cm^{-1}(reference 74b), and the Pekeris Relation (reference 41).

data is limited but is still sufficient to determine
that the ground state and excited state bond lengths
for v=0 lie within the range of 1.67 to 1.69 Å.

Similar gas phase studies have been published by
both Bondybey[42] and Riley.[43] Bondybey has reported
data concerning the ground state vibrational frequency
which he estimated to be approximately 460 cm^{-1}. In
both of these studies, information regarding the pre-
dissociation of the v=0 level is presented and shown
to have a strong rotational dependence.

Independent studies on nickel dimer,[44] vanadium
dimer,[45] and molybdenum dimer[46,47] have also been carried
out in our laboratory. The measurement of bond lengths
and some vibrational frequencies for these species were
obtained and are presented in tabular form in Table III.
According to this data the contribution of the d-orbital
to bonding in transition metal diatomics can be inter-
preted as a function of position within the periodic table.

E. Conclusion

In examining the data presented one can see that our
results are in excellent agreement with those of Efremov
et al. This firmly establishes the carrier of the 4600 Å
vibronic band to be chromium dimer. From the bond length
measurement and estimated ground state vibrational fre-
quency, one may reasonably conclude that the d-orbitals

Table III. Ground state constants for a few
transition metal homonuclear dia-
tomics.

	Ground State Constants		
	w_e''	r_e''	D_o''
V_2	535 cm^{-1}	1.77 Å	1.85 eV
Cr_2	460 cm^{-1}	1.68 Å	2.0 eV
Ni_2		2.20 Å	2.068 eV
Mo_2		1.94 Å	4.2 eV

See Refs. 39, 42-47

play a significant role in the bonding. The extremely short bond length of 1.68 Å and high vibrational frequency ($\simeq$460 cm^{-1}) suggest a quintuplet or sextuplet bond.

Recent calculations using a modified generalized valence bond method[48] and local spin density formalisms[49] have both yielded results predicting a tightly bound dimer with an equilibrium bond length of 1.68 Å. This is in agreement with the experimental data, although these calculations lead to differences in the actual shape of the ground state potential energy curve and binding energies. The modified generalized valence bond method predicts a double minimum with the inner minimum at 1.68 Å which is due to a quintuplet bond involving only the d-orbitals. The outer minimum at 3.06 Å is suggested to arise from bonding of 4s-4sσ_g orbital with the d-shells coupled (antiferromagnetically) into a net singlet state. Using the new values for r_e, w_e and an electronic degeneracy of 1, the experimental binding energy has been recalculated to be 2.0 $\pm$ .03 eV. The calculation using the local spin density formalisms is in agreement with the equilibrium bond length, although this calculation yields no double minimum in the ground state potential energy curve. Also, the binding energy was calculated to be .05 to 1 eV higher than the modified generalized valence bond method.

Our results in conjunction with those of Bondybey[42] and Riley[43] suggest that the presence of the single vibronic band is due to a combination of both Franck-Condon factors and predissociation. The data shows both the ground and excited states to have nearly identical equilibrium bond lengths, while predissociation was also observed in the v=0 and v=1 levels of the excited state (see Appendix 1 for further spectroscopic studies of Cr_2).

Similar studies concerning a few other transition metal diatomics have also been carried out within this lab. Listed in Table III are the bond lengths and vibrational frequencies obtained. From this data, one can suggest that the bonding in vanadium and molybdenum dimer must involve contributions from the d-orbitals. Theoretical calculations[50] concerning Mo_2 have predicted the bonding contribtuions to be identical to Cr_2.

In contrast, the results from Ni_2 suggest little or no contribution from the d-orbitals. When compared to Cu_2, whose bonding is accepted as being due to only the $4s$-$4s\sigma_g$ orbital, one can conclude from its similar bond length that only a single $4s$-$4s\sigma_g$ bond is present in Ni_2. This agrees with the predictions of theoretical calculations.[51,52]

Spectroscopic studies of the remaining first row transition metal diatomics and triatomics (with the exception of Cu_3[53]) have been carried out in the same

spectral region with no observation of any excited state features. A possible explanation for these results is that the open d-shell leads to a large density of states which gives rise to a fast subnanosecond nonradiative decay into states inaccessible to detection by resonant two-photon ionization. A plausible solution to this problem is to probe excited states whose potential energy minimum lies below the dissociation energy of the ground state. Results obtained on Ni_2 support the explanation that a high density of states exists leading to a fast nonradiative decay. It also shows that these low-lying states can be probed by way of R2PI.

Figure 14 presents bonding information for the transition metal diatomics. This information shows that in some cases the use of tunable infrared sources will be needed in order to obtain spectral information necessary to examine these low-lying excited states. Such tunable infrared sources are now available, and so the study of the first row diatomics may continue.

In extending similar studies to the second and third row transition metals the same fast nonradiative decay is likely to exist, however, an additional complication may arise. Due to the heavier masses and an expected increase in bond length, an additional requirement of higher resolution lasers than available in our lab would

be needed to resolve the rotational structure of these species. At this time a possible solution which involves the use of a pulse amplified Cw ring laser is being set up and tested in our lab.

IV. SPECTROSCOPIC INVESTIGATIONS
OF SILICON DICARBIDE

A. Introduction

Silicon dicarbide was first observed[54] in 1928 in

the spectra of certain cool carbon stars although not

identified at this time. Some thirty years later in 1956,

the carrier of the 4980 Å band system was tentatively

identified as SiC_2 by Kleman.[55] Using a silicon charged

graphite tube of a King furnace heated to over 2500 K,

he was able to obtain spectra proving that the carrier of

this band system was due to a compound consisting of only

silicon and carbon. Based on a partial vibrational anal-

ysis, Kleman postulated the molecule to be linear SiCC and

suggested it to be the analog of 4050 Å cometary spectrum

of C_3.[56]

Subsequently, a matrix isolation study by Weltner and

McLeod[57] was carried out. They trapped vapors from a hot

oven in cryogenic neon and argon matrices, obtaining both

optical and infrared spectra that supported previous con-

clusions. But their vibrational assignment was somewhat

different than that of Kleman. Next, Verma and Nagaraj[58]

reported an improved gas phase study obtaining an absorp-

tion spectra using a flash discharge technique. From their

vibrational analysis they also were in agreement that silicon dicarbide was linear SiCC. Most recently, Bondybey[59] re-examined the 4980 Å band system using laser vaporization to produce SiC_2. This band was reinvestigated both in the gas phase and matrices being probed by laser-induced fluorescence along with absorption in the matrix. From the observed spectra, Bondybey agreed with the previous structure (due to a lack of any evidence to the contrary), although a reassignment of the vibrational spectra was proposed. He also pointed out that the linearity of SiC_2 was not a priori obvious.

A theoretical study by Green[61] was done in an effort to establish whether the linear SiCC configuration was correct. Using a self-consistent field (SCF) calculation he concluded that the ground state should be linear SiCC with a closed shell $^1\Sigma^+$ electronic structure, agreeing with previous experimental results. In this publication he also pointed out that in recent radioastronomical[60] observation of the molecular envelope of the evolved carbon star IRC + 10216, unidentified lines in the millimeter-wave region needed to be investigated. He observed that these lines were not harmonically related as would be the case for rotational transitions in linear molecules. But, he suggested that they have a pattern reminiscent of b-type transitions as in a bent symmetric structure such as might be postulated for CSiC.

In light of what has been presented above, Michalopoulos and I felt the reinvestigation of SiC_2[62] under high resolution (so that the rotational structure could be analyzed) was necessary in order to determine the true structure of silicon dicarbide. This study has been carried out and will be presented within. Also mentioned will be the negative results of a similar spectroscopic investigation of SiC whose search was actually the initial intent of these studies.

B. Experimental

The technique used for the production of SiC_2 is the same as described earlier. The target sample used was a polycrystalline silicon carbide rod (99.9% pure, Atomergic Chemetals Corp., Plainview, N. Y.). In this case, the vaporization laser was the second harmonic of a Nd:YAG focused to a .1 cm spot, and operating at 60-70 mj's per pulse. The predominant species in the beam were seen to be Si_x (x=1-6), SiC_2, Si_2C, Si_3C, Si_2C_2, and Si_2C_3 using the F_2 excimer laser line (7.98 eV). Silicon carbide was present but only in very small quantities (less than 1% of SiC_2).

Resonant two-photon ionization (R2PI) was used with mass selective detection to record the visible absorption spectra of SiC_2 in the 4980 Å region. The origin band (0-0) was rotationally resolved by inserting a pressure-tuned

intracavity etalon, narrowing the dye laser line width
to .05 cm^{-1} FWHM.

In this study, it was also necessary as will become
apparent shortly, to reheat the rotational temperature
of the molecular beam so that higher lying rotational
transitions could be observed. In a supersonic jet
it is a simple matter to adjust the rotational tempera-
ture by decreasing backing pressure of the nozzle. Al-
though, when using this laser vaporization technique, it
is important that the helium density above the target is
as high as possible in order to efficiently produce
clusters. Therefore, the decrease in backing pressure
normally used would be unsatisfactory. A solution to this
problem was found to be the use of a short tube mounted
on the end of a pulsed nozzle source. The tube used was
5 cm long with 1 cm internal diameter and mounted co-axial
along the beam axis. The carrier gas expanding into this
tube reflects off the walls and causes turbulence in the
flow. The effect of the turbulence is to reheat the gas
before expanding out of the 1 cm diameter orifice. Under
these conditions, the final rotational temperature is
found to be somewhat higher (15 K) than expansion from
the normal nozzle orifice. The rise in temperature de-
pends on the length and diameter of the reheat tube.

C. Selection Rules

In this study of silicon dicarbide, information pertaining to the bond lengths and geometry was obtained through probing one-photon rovibronic absorption spectra using two-photon ionization. If the molecule was linear and asymmetric, as thought for the past thirty years, then the selection rules given in Chapter III, Section C would apply. This transition $^1\pi \leftarrow {}^1\Sigma$ would be expected to show a rotational structure consisting of a P, Q, and R branch for the origin (0-0) rovibronic transition.

Although, if the molecule were bent, it would be an asymmetric top. A transition between two different electronic states will be allowed by the oscillating electric field of light, if and only if, the matrix element[63,64]

$$M_{e'v'e''v''} = \int \Psi'^*_{esvr}\, \hat{d}\Psi''_{esvr}\, \hat{d}\tau_{esvr} = \int \Psi'^*_{vr}\Psi''_{vr}\, d\tau_v \int \Psi'^*_{es}\, \hat{d}\tau_e \Psi''_{es}\, d\tau_e$$

is different from zero. Here the single prime indicates the upper of the electronic states. In the preceding discussion, it has been assumed that the geometry of the molecule is the same in both the electronic states involved. Therefore, for an allowed transition the product $\Psi'_e{}^* M_e \Psi''_e$ must be symmetric (A_1) with respect to the symmetry elements of the point group. As an example, for the point group of C_{2v}, it can be shown that the product

of $\Psi_e' {}^* M_e \Psi_e''$ will be symmetric depending on the electronic symmetries and the orientation of the dipole moment.

C_{2v}	A_1	A_2	B_1	B_2	
	M_z	f.	M_x	M_y	A_1
		M_z	M_y	M_x	A_2
			M_z	f.	B_1
				M_z	B_2

The species of the electronic states involved are given on the top and right hand side of the table. A transition between any two states can be seen to be allowed or forbidden (f.) depending on the orientation of the dipole moment (M_x, M_y, M_z). This same type of table may be constructed for any other point group. If the electronic states have different symmetries, then only the common symmetry element of these point groups must be considered.

From the transition moment integral, the selection rules for a rovibronic transition of an asymmetric top can be seen to be (for non-multiplet state):[63,64]

1). The spin multiplicity cannot change.

$$\Delta S = 0$$

Singlet $<\longrightarrow>$ Singlet

Triplet $<\longrightarrow>$ Triplet

Singlet $<\!-\!\!|\!-\!\!>$ Triplet

2). An electronic transition is orbitally
   allowed, if and only if,

   $\int \Psi_e'^* \hat{d} \Psi_e'' d\tau_e$ is non zero.

   (An electron transition is orbitally allowed
   if the triplet direct product

   $\Gamma(\Psi_e'^*) \times \Gamma(\hat{d}_e) \times \Gamma(\Psi_e'')$

   contains the totally symmetric irreducible
   representation of the point group of the
   molecule.)

3). Vibronic transition is allowed, if and only if,
   the integral

   $\int \Psi_e'^* \Psi_v'^* \hat{d}_e \Psi_e \Psi_v d\tau_{en}$ is non zero.

4). The rotational quantum number may be at most, one
   $\Delta J=0, \pm 1$ (with the restriction $J=0 \longleftrightarrow J=0$)

5). Combination of the level of a given J value of
   one electronic state with those of a given J value
   of another electronic state are subject of re-
   strictions depending upon the symmetry properties
   of the asymmetric top rotational eigenfunctions.

   If the transition moment is in the direction
   of the a-axis, only the transitions

   $+ + \longleftrightarrow - +$ and $+ - \longleftrightarrow - -$

   can occur.

   If the transition moment is in the direction
   of the b-axis, only the transitions

   $+ + \longleftrightarrow - -$ and $+ - \longleftrightarrow - +$

can occur.

If the transition moment is in the direction
of the c-axis, only the transitions

$$+ \; + \; <\!\!-\!\!-\!\!> \; + \; - \;\; \text{and} \;\; - \; + \; <\!\!-\!\!-\!\!> \; - \; -$$

can occur.

If the transition moment does not lie along
one of the principal axes, then the selection
rules are determined by which components along
the axes are non zero. Although, even in the
most general case, transitions between levels
of the same symmetry are forbidden.

$$+ \; + \; <\!\!-\!\!-\!\!|\!\!-\!\!-\!\!> \; + \; +$$

$$- \; - \; <\!\!-\!\!-\!\!|\!\!-\!\!-\!\!> \; - \; -$$

$$+ \; - \; <\!\!-\!\!-\!\!|\!\!-\!\!-\!\!> \; + \; -$$

$$- \; + \; <\!\!-\!\!-\!\!|\!\!-\!\!-\!\!> \; - \; +$$

The symbols ++, -+, etc. are determined by the
behavior of the rotational eigenfunctions with
respect to 180° rotation about the c and a prin-
cipal axes, repsectively.

6). The overall (rovibronic) species must not change

$$A \; <\!\!-\!\!-\!\!-\!\!> A, \;\; B \; <\!\!-\!\!-\!\!-\!\!> \; B.$$

For the overall species based on the full sym-
metry group, the product of the overall species
of the upper and lower states must be the pro-
duct $T_z R_z$ of a translation and a rotation. This

is shown below for a few point groups.

Point Group	Species of $T_z R_z$	Allowed Rovibronic Transition
C_2	A	$A-A, B-B$
C_{2h}	A_u	A_u-A_g, B_u-B_g
C_{2v}	A_2	A_1-A_2, B_1-B_2
D_2	A	$A-A, B_1-B_1, B_2-B_2, B_3-B_3$
D_{2h}	A_u	$A_u-A_g, B_{1u}-B_{1g}, B_{2u}-B_{2g}, B_{3u}-B_{3g}$

Along with these selection rules, there are factors which modulate the intenstiy of the individual vibrational and rotational lines within an electronic transition. For the vibrational bands, the intensity is proportional to the Franck-Condon factor. The rotational lines within a particular vibrational band also have a modulation in their intensities which are given by Cross.[65]

Consideration of nuclear spin[63,64] can also have an effect on the intensity of the rotational levels depending on symmetry of the molecule. In the case of silicon dicarbide, the point group is C_{2v} and interchange of identical carbons with zero nuclear spin around the a-axis will lead to an intensity alteration between the A and B rovibronic species. The ratio of the intensities between the A and B rovibronic levels can be shown to be $(\frac{I + 1}{I})$. Therefore, in this case the B rovibronic levels will be nonexistent.

D. Results

In order to determine the geometry of SiC_2, a high resolution scan of the (0-0) origin band of the SiC_2 $\tilde{A} \leftarrow \tilde{X}$ spectrum, found at the 4980 Å region, was obtained under normal expansion conditions. Figure 15 shows the observed rotation structure of this band. This spectrum corresponds to a plot of photoion intensity of $^{28}SiC_2$ versus the frequency of a pressure-tuned dye laser. A similar spectrum was observed simultaneously for both $^{29}SiC_2$ and $^{30}SiC_2$ minority isotopic species. The low natural abundance of these species resulted in such a weak spectra that accurate rotational line measurement could not be made. These spectra have therefore not been presented here. Although, the observed isotopic shifts of these species support the assignment of this band as being the origin (0-0) transition.

In examining the spectra shown in Figure 15, it is seen to be exactly what would be expected for a $^1\Pi \leftarrow {}^1\Sigma$ transition in a linear molecule. There is a strong Q branch, and the R branch is more intense than the P branch. In trying to fit the spectrum to the model:[64]

$F(J',J'') = B'J'(J'+1) \pm .5qJ'(J'+1)-B''J''(J''+1)$

the rotational constants and quantum numbers follow the standard notation. The (+) sign in front of the lambda doubling term is used for the Q branch, while the (-)

sign is used for both the P and R branches. One finds
the calculated constants such as the lambda doubling
parameter and bond lengths to be somewhat odd. The
actual fit is reasonable, but the lambda doubling
parameter is .043 cm^{-1} which is 100 times greater than
in C_3 (which is known to be linear), and both the Si-C
and C-C bond lengths are extremely short (1.0-1.2 $\overset{\circ}{A}$).
The shortness of these bond lengths could be explained
if one assumes that the geometry of SiC_2 is linear and
symmetric (C-Si-C). The interchange of equivalent car-
bon with zero nuclear spin would eliminate alternate
rotational levels in the $^1\Sigma$ ground state. This would
lead to reasonable bond lengths but whose actual fit
to the model is rather poor. From these facts the
linearity of silicon dicarbide was dismissed leaving
the explanation that its geometry is that of an asym-
metric top.

The cold spectrum (5 K rotational) in Figure 15
was then submitted to a fit for the model of an asym-
metric top. As shown, it turns out that this band is
really the r-form ($\Delta K = ^+1$) subband from K"=0 in a per-
pendicular transition of an asymmetric top which is
near the prolate top limit. The fit to this model was
good and the larger lambda doubling parameter becomes
a normal K-doubling due to the asymmetry splitting of
K'=1 levels of the excited state.

Figure 15.   The high resolution R2PI spectrum
             of the origin region of the 4980 Å
             system in SiC_2.   The rotational tem-
             perature is estimated to be on the
             order of 5 K.   The notation used is
             that of the prolate symmetric top.
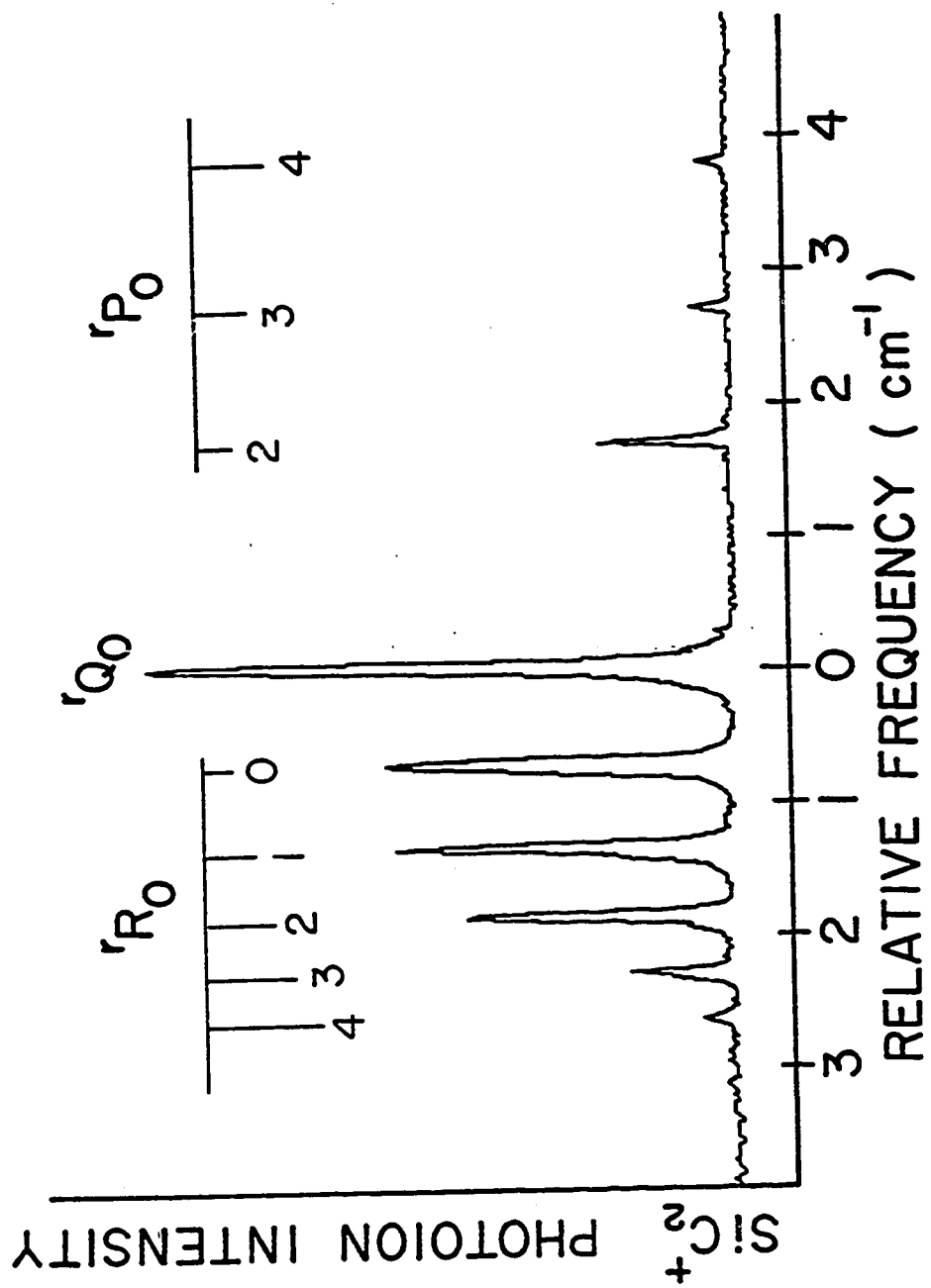
If the rotational constant A of this asymmetric
top if fairly large, then the levels belonging to
higher K'' values would not be expected to be populated
at the very low rotational temperatures. So, in order
to test the model further and to obtain more rovibronic
lines for analysis, the jet reheat tube discussed earlier
was put in place. Figure 16 shows the spectra of the
origin (0-0) band under these conditions. The rotational
temperature in this figure is estimated to be 15 K. This
more extended scan now shows the expected p and r form
bands due to the increased population of the higher K''
levels in the rotationally heated SiC_2.

In fitting this higher rotational temperature spectrum
it was found that these new subbands do not arise from
the next higher K'' level. These features can be explained
by the fact that they originate from $K''=2$. The correct
assignments are shown in Figure 16 and diagrammed on a
schematic energy level chart in Figure 17. Examination
of a number of spectra similar to that presented were
analyzed, but revealed no evidence of subbands originating
from $K''=1$ or $K''=3$. The reason for missing odd K'' levels
can only be understood if the two carbon atoms in this
molecule are equivalent and are interchanged by rotation
about the a-axis. In a near prolate asymmetric top,
interchange of identical nuclei with zero nuclear spin
by rotation about the a-axis would produce an alternation

Figure 16.   The high resolution R2PI spectrum
             of the origin region of the 4980 Å
             system in SiC_2. The rotational tem-
             perature of the molecule has been
             raised by perturbing the flow of the
             molecular beam as described in the
             text, leading to the observation of
             transitions originating from higher
             K levels. As in Figure 15, the nota-
             tion used is that of the prolate
             symmetric top.
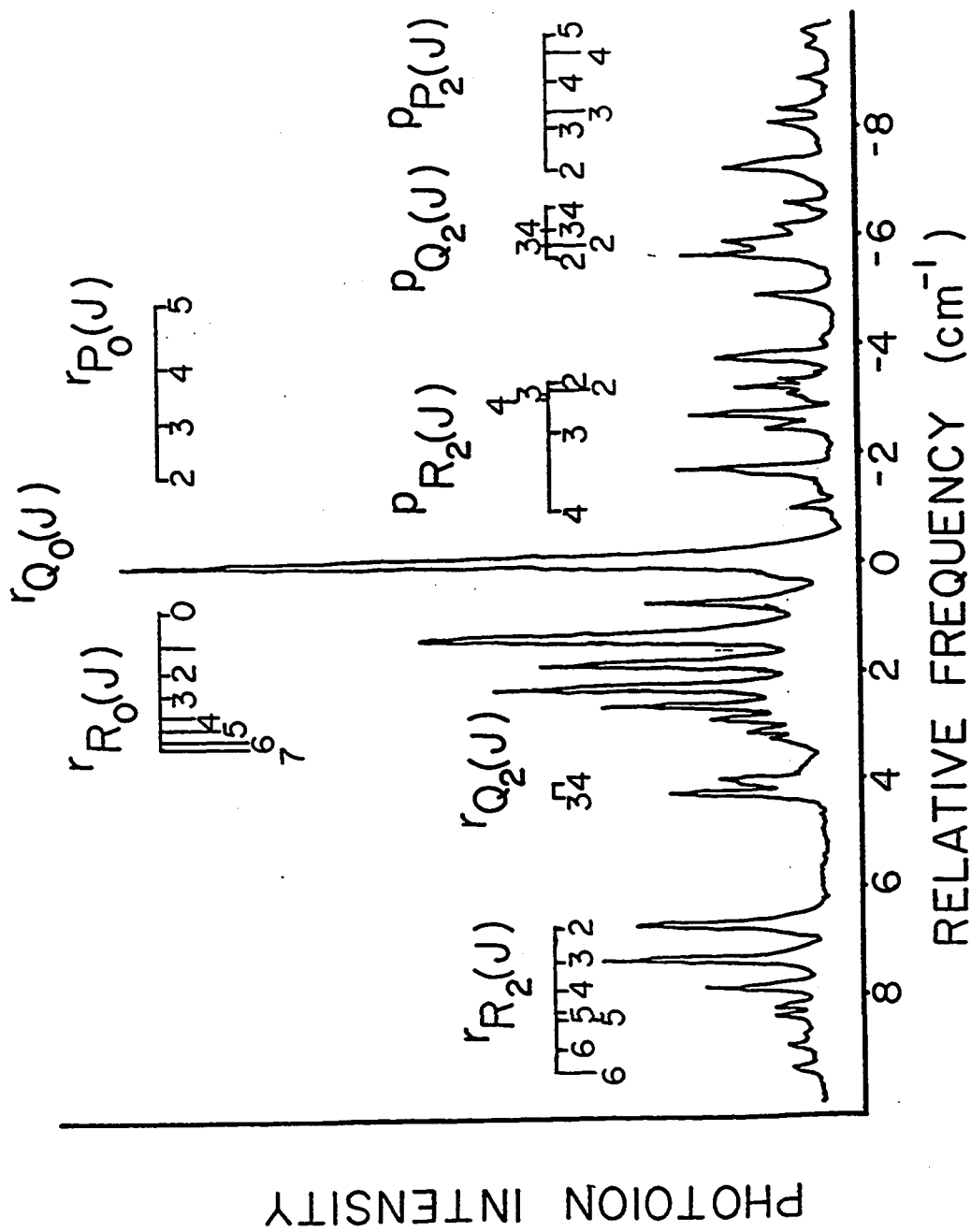
Figure 17.   A schematic energy level diagram of
the lower rotational levels of the
bent symmetric SiC_2 molecule in the
limit of the prolate symmetric top.
Asymmetry splittings are included for
levels with nonzero K.   Levels drawn
with a broken line are absent in SiC_2
due to the presence of equivalent car-
bon nuclei with zero spin.   Assuming a
b-polarized electronic transition, some
possible rotational transitions are
indicated.
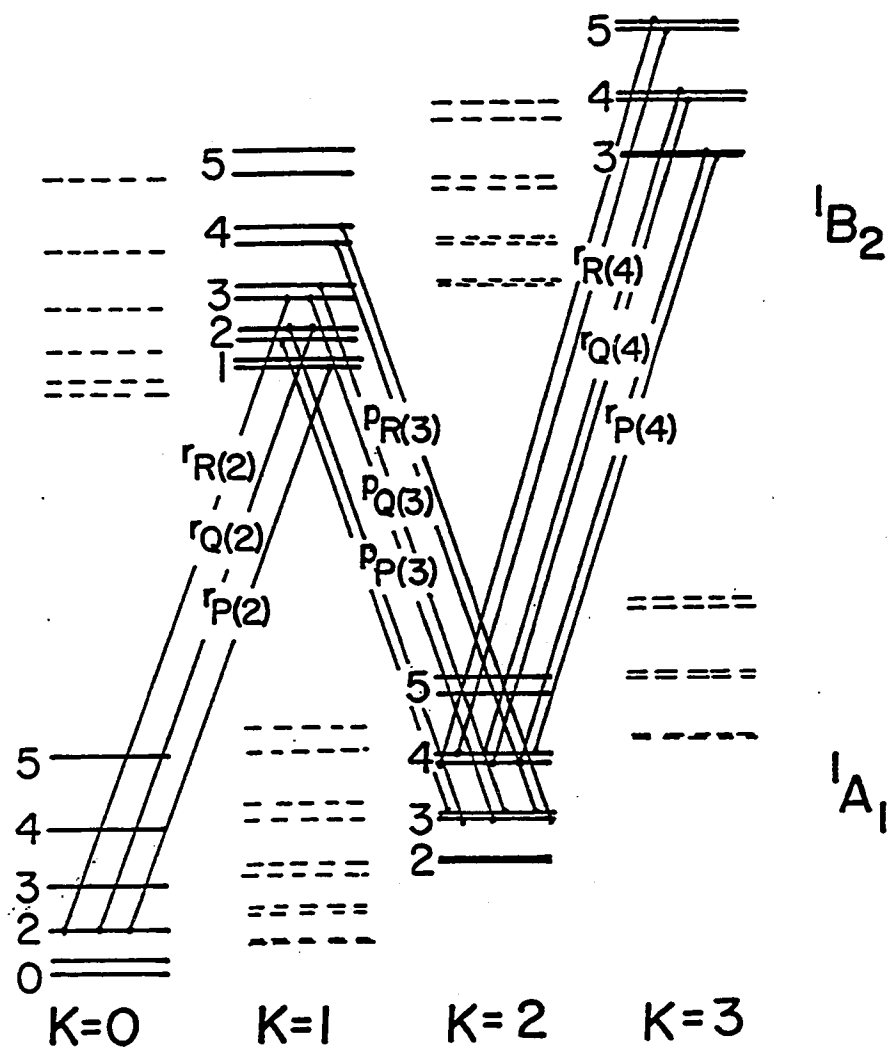
in the K structure. With the data from these fits it
is evident that the ground state is of C_{2v} geometry
as shown in Figure 18. Here, the two principal axes
of the inertial tensors are marked, with the third
being perpendicular to the plane of the paper.

In Table IV are presented the measured line
positions for the 15 K rotational spectrum. Also
tabulated here are the measured relative intensities
of each transition and their assignment. Each line
is labeled both with the conventional J subscript K
prolate, K oblate asymmetric top labels and the ap-
propriate prolate symmetric top labels (since the mole-
cule is a very near prolate symmetric top as seen by
the Rays asymmetry parameter[41] K=$^-$.87).

All lines from Table IV were submitted to a non-
linear least squares program.[66] This program calculated
the asymmetric top eigenvalues and eigenfunctions in
the ground and excited states by direct matrix diagonal-
ization of the rigid rotor Hamiltonian in the prolate
symmetric top limit. The fit resulted in the measure-
ment of rotational constants in the ground and excited
states along with the band origin.

With the rotational constants and fact that the
two carbons are equivalent (with rotation around the
a-axis), the bond lengths and angles were calculated

Figure 18. The SiC_2 molecule drawn to scale with
the princiapl inertial axes indicated
(the inertial c-axis is perpendicular
to the plane of the figure). The bond
lengths and bond angle have been deter-
mined from an analysis of the high re-
solution R2PI spectrum of the 4980 Å
origin region.
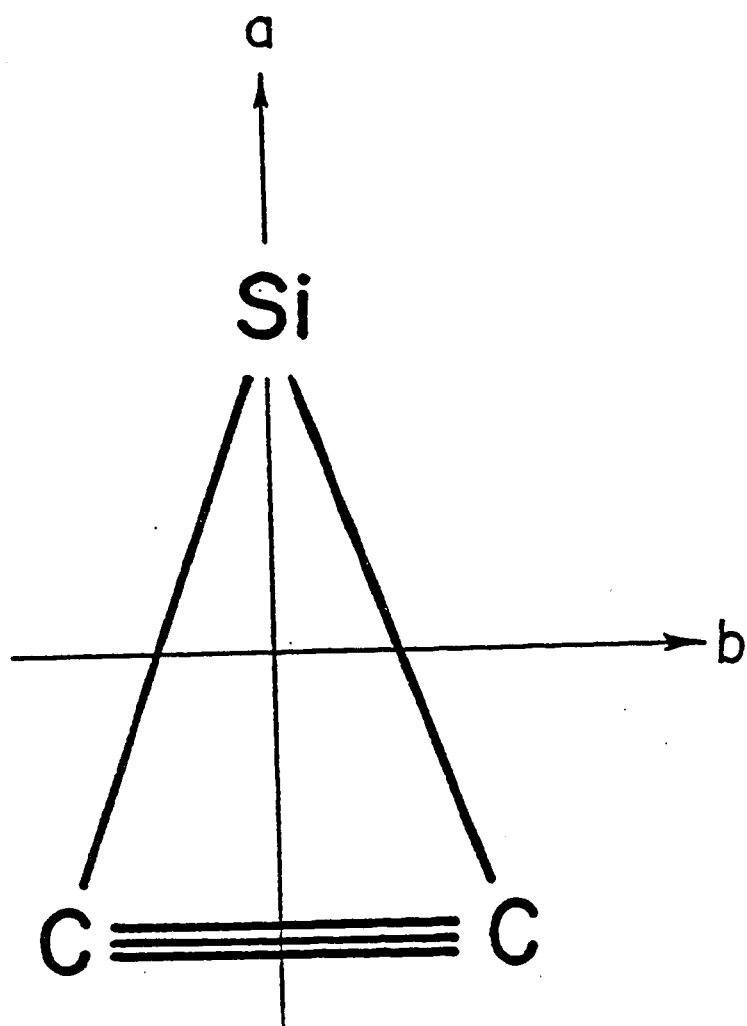
Table IV. Relative line positions and intensities
of the features shown in Figures 15 and 16.
The numbers in parentheses are the residuals
of the fit dicussed in the text. For con-
venience the assignments are given in the
limit of both the prolate symmetric and the
asymmetric top. For the asymmetric top the
notation J_{KaKc} is used, where Ka and Kc are
the projections of J along the top axis in
the limit of the prolate and oblate symmetric
top, respectively. The intensity scale is
linear and has been set so that 10 corresponds
to the most intense transition observed.

Energy (cm^{-1})	Assignment		Intensity
8.352(-0.029)	$^rR_2(5)$	$6_{33} \leftarrow 5_{24}$	0.6
8.196(-0.016)	$^rR_2(5)$	$6_{34} \leftarrow 5_{23}$	0.6
7.821(0.025)	$^rR_2(4)$	$5_{33} \leftarrow 4_{22}$	1.6
7.290(-0.004)	$^rR_2(3)$	$4_{32} \leftarrow 3_{21}$	3.1
6.680(-0.037)	$^rR_2(2)$	$3_{31} \leftarrow 2_{20}$	2.8
4.290(0.021)	$^rQ_2(3)$	$3_{30} \leftarrow 3_{21}$	2.4
4.055(0.042)	$^rQ_2(4)$	$4_{31} \leftarrow 4_{22}$	1.6
3.125(0.004)	$^rR_0(6)$	$7_{17} \leftarrow 6_{06}$	1.0
2.891(-0.003)	$^rR_0(5)$	$6_{16} \leftarrow 5_{05}$	1.6
2.625(0.011)	$^rR_0(4)$	$5_{15} \leftarrow 4_{04}$	2.8
2.290(0.024)	$^rR_0(3)$	$4_{14} \leftarrow 3_{03}$	4.5
1.836(-0.002)	$^rR_0(2)$	$3_{13} \leftarrow 2_{02}$	4.1
1.352(0.032)	$^rR_0(1)$	$2_{12} \leftarrow 1_{01}$	5.5
0.704(-0.003)	$^rR_0(0)$	$1_{11} \leftarrow 0_{00}$	2.8
-0.040(-0.022)	$^rQ_0(1)$	$1_{10} \leftarrow 1_{01}$	10.0
-1.053(0.002)	$^pR_2(5)$	$6_{15} \leftarrow 5_{24}$	0.7
-1.728(-0.010)	$^rP_0(2)$	$1_{11} \leftarrow 2_{02}$	2.2
-2.459(0.025)	$^pR_2(3)$	$4_{13} \leftarrow 3_{22}$	1.0
-2.731(-0.025)	$^rP_0(3)$	$2_{12} \leftarrow 3_{03}$	2.1
-3.237(-0.006)	$^pR_2(2)$	$3_{12} \leftarrow 2_{21}$	1.4
-3.368(-0.015)	$^pR_2(3)$	$4_{12} \leftarrow 3_{21}$	0.7

Energy (cm^{-1})	Assignment		Intensity
-3.781(-0.014)	$^rP_0(4)$	$3_{13} \leftarrow 4_{04}$	1.7
-4.875(0.013)	$^rP_0(5)$	$4_{14} \leftarrow 5_{05}$	1.2
-5.632(-0.009)	$^PQ_2(2)$	$2_{11} \leftarrow 2_{20}$	2.2
-5.882(-0.010)	$^PQ_2(2), ^PQ_2(3)$	$2_{12} \leftarrow 2_{21}, 3_{13} \leftarrow 3_{22}$	1.4
-6.179(-0.010)	$^PQ_2(3)$	$3_{13} \leftarrow 3_{22}$	0.7
-6.570)-0.004)	$^PQ_2(4)$	$4_{14} \leftarrow 4_{23}$	0.7
-7.250(0.050)	$^PP_2(2)$	$1_{11} \leftarrow 2_{20}$	1.7
-8.054(-0.006)	$^PP_2(3)$	$2_{11} \leftarrow 3_{22}$	0.8
-8.345(-0.018)	$^PP_2(3)$	$2_{12} \leftarrow 3_{21}$	0.7
-8.890(0.007)	$^PP_2(4)$	$3_{12} \leftarrow 4_{23}$	0.5
-9.476(-0.003)	$^PP_2(4)$	$3_{13} \leftarrow 4_{22}$	0.3

and are presented in Table V. The 1.25 Å C-C bond
length in the ground state is close to that for a
C-C triple bond while the 1.30 Å in the excited state
is approximately that of a C-C double bond. This would
suggest that the transition is a $\pi^* \leftarrow \pi$ on the carbon-
carbon triple bond.

From the fit the r-form subband, originating from
K"=0 and terminating in K'=1 of the excited state, is
seen to go to the upper of the two K' doublet levels
for the Q branch transition, and the lower for the R
and P branch transitions. This determines that the
transition moment lies along the inertial b-axis of
the molecule. If one assumes the ground electronic
state symmetry to be $^1A_1$, then the selection rules
require an excited electronic symmetry of $^1B_2$ in the
point group C_{2v}.

E. Conclusions

Silicon dicarbide has been shown to be an asymmetric
top in the near prolate symmetric top limit which is not
in agreement with previous researches. The ground state
of this molecule is best described as a silicon atom
bound to the side of triplely bonded carbon atoms,
forming a planar triangular molecule of C_{2v} symmetry.
If the ground state is assumed to be $^1A_1$, the selection
rules require the excited electronic state symmetry to

Table V. Rotational constants are shown as
determined from a least square fit
to the data listed in Table I using
the asymmetric top model discussed
in the text. The error shown in
parentheses immediately after each
value corresponds to an estimated
95% confidence limit. Also shown
are the derived quantities: inertial
defect, bond lengths, and angles
which were calculated from the mea-
sured rotational constants (but uncor-
rected for zero-point motion).

	Electronic State	
	$\tilde{X} \ ^1A_1$	$\tilde{A} \ ^1B_2$
Rotational Constants:		
A_0 (cm^{-1})	1.7982(48)	1.6523(26)
B_0 (cm^{-1})	0.4513(46)	0.4194(16)
C_0 (cm^{-1})	0.3586(40)	0.3347(14)
Inertial Defect:		
(amu-A^2)	0.28(15)	-0.03(7)
Bond Lengths and Angles:		
d_{SiC}(A)	1.812(12)	1.881(6)
d_{CC} (A)	1.250(16)	1.304(8)
$\angle CSiC$ (deg)	40.36(34)	40.57(10)

be $^1B_2$ in the C_{2v} point group. The transition moment is seen to be polarized along the inertial b-axis of the molecule and the transition is best understood as a $\pi^* \leftarrow \pi$ excitation on the carbon-carbon triple bond.

During the analysis of this spectrum ab initio calculations of SiC_2 were carried out by Grev and Schaefer[67] in a cooperative effort to understand the spectrum observed. These calculations showed the linear configuration to be the most stable. However, a series of calculations which show the triangular geometry to be increasingly stabilized relative to the linear form at successively higher levels of theory, were also achieved. Although, even at their highest level, the $^1A_1$ triangular form is just barely more stable than the linear form and is still calculated to be a transition state rather than a true minimum. This SCF optimized calculation though is in good agreement with our experimental results.

The suggested explanation of Grene[61] concerning the unidentified lines in the reported radioastronomical observation of the evolved carbon star IRC + 10216, in fact, turns out to be correct. A recent publication by Thaddeus et al[68] shows that the original SiC_2 lines plus the other unidentified lines can be explained by silicon

dicarbide being an asymmetric top. Also, with their
more accurate measurement they have determined our
constants to be approximately 3% high.

One might also consider the possibility that the
linear configuration of SiCC is also present in the
molecular beam, but no evidence for its existence has
been seen. Scans to both higher and lower frequencies
of the origin band were carried out. No other spectral
features (within 5% of the intensity of $^1B_2 \leftarrow {}^1A_1$ origin)
were observed other than the already reported 4980 Å
band system. This of course, does not completely rule
out the linear configuration. It is certain that the
spectrum of SiC$_2$ previously reported is from the triangular
species. In Bondybey's[59] recent assignment, the bending
frequency should be increased by a factor of two since
there is no prohibition against single quantum transition
for a molecule of this geometry.

An ionization potential of SiC$_2$ has also been
bracketed to lie between 8.91 and 10.38 eV. These limits
were determined by the fact that photoion production from
this excited state could not be observed when the ioniza-
tion photon was ArF 6.4 eV, whereas, it was observable
with F$_2$ 7.98 eV.

As mentioned earlier, this study actually had the
initial intent of spectrally investigating SiC. Scans

both in the visible and ultraviolet were carried out

using resonant two-photon absorption, although no

spectral information was obtained. This result could

be explained in two ways. The first is that SiC is

not formed to any substantial amount making the spectral

signal extremely weak, or secondly, the combined ener-

gies of the excitation and ionization photons may not

have been, in fact, energetic enough to produce photo-

ions. In Bondybey's[59] study of SiC_2, he also reported

the absence of spectral features of SiC using laser

induced fluorscence which indicates that the first

explanation is more likely.

V. GAS PHASE CLUSTER REACTION STUDIES

A. Introdution

   The study of reactions, on or with, transition
metals has been the subject of wide interest. Much of
the impetus for these investigations comes from their
behavior as catalysts which is both scientifically
intriguing and economically important. Suprisingly
though, for many years there have been only two main
techniques used to study these reactivities. The first
is ultra high vacuum single crystal experiments[69,70] in
which the single crystal is used as a model for the poly-
crystalline bulk. The second technique approaches the
reactivity from the opposite view point, that is, the
atomic and molecular scale. The use of matrix isolation
for these type studies has been, in fact, the only way
to study these species easily.

   Using this technique controlled amounts of metal
vapors and reactants are co-condensed with an inert gas
(ex:Ar) onto a cold surface allowing for low temperature
(or photochemically induced) reaction products to be
stabilized and then probed spectroscopically. The appli-
cation of this technique has led to a vast literature[27,71-74]
concerning the reaction chemistry of transition metal

atoms along with some diatomic and triatomic species. However, the extension of this technique to larger species is hindered by complications such as indentification of the reactant products and multiple matrix sites. This makes the study of clusters beyond the trimer extremely difficult, if not impossible.

Recently, there has been the development of several techniques[75-77] to study gas phase reactions of transition metal clusters. One of these was developed in our lab and has been used to obtain some initial data concerning the reactivity of metal clusters as a function of size. This technique is based on the previously developed cluster source coupled to a reaction tube. A complete description of the reaction tube[75b] and data[75c] obtained will be presented in full below.

B. Experimental

The clusters used in these studies were produced by the laser vaporization cluster source previously described,[14,15,47] but modified slightly to allow the attachment of the reaction tube. Briefly, a pulsed double solenoid nozzle is used to produce a 200-400 μs pulse of helium that flows down a .2 cm diameter channel passing over the target rod. As this helium pulse flows over the sample, a Q-switched Nd:YAG laser, second harmonic, focused to a .15 cm diameter spot, is fired producing a plasma

which is entrained within the carrier gas. This plasma
is then neutralized, thermalized, and clustered within
the remaining 1.8 cm length of the .2 cm diameter channel.
The helium plus clusters then flow through a diverging
adaptor region into a 1 cm diameter, 10 cm long reaction
tube. All cluster information is accomplished in the
.2 cm diameter channel since expansion into the 1 cm
diameter reaction causes a 25 fold decrease in both
helium and cluster density.

The reaction tube design[75b] is shown from both a side
and end-on view in Figure 19. Four hypodermic needles,
positioned approximately 2 cm downstream of the .2 cm
diameter channel and protruding .3 cm into the reaction
tube are used to inject dilute reactants into the flowing
helium plus metal clusters. These needles are equally
disposed around the diameter of the reaction tube and
are supplied by a common annular reservoir of .5 cm^3 in
volume.

This reservoir is fed by four independently controlled
pulsed reactant nozzles (General Value, Model #9-199-902)
each being supplied by independent gas-lines. These noz-
zles were adjusted to deliver pulses 3 ms wide (FWHM),
with a backing pressure of 2.7 atmospheres. Their firing
was synchronized 1 ms before the main cluster nozzle, so
as to provide a steady flow of the reactant gas during

Figure 19. Schematic of gas phase metal cluster
            reaction tube. Both side and end
            view are shown.

REACTANT INJECTION ASSEMBLY

VAPORIZATION LASER

IO ATM HELIUM

TARGET ROD

FAST FLOW REACTION ZONE

2

3

4
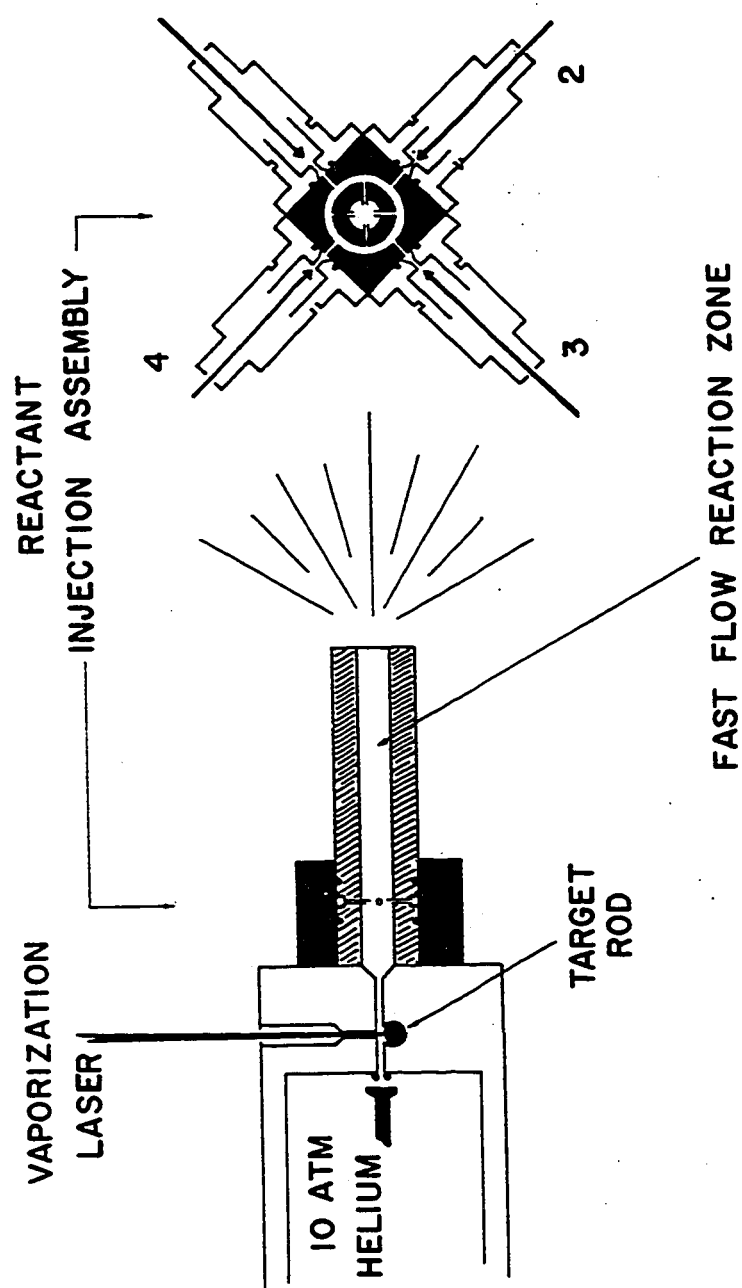
the 400 μs of the main nozzle pulse. The annular reservoir served as a gas ballast feeding each of the four injection needles equally, thus ensuring that the flow of reactant into the reaction tube is independent of which nozzle is fired.

The overall design of this injection scheme is necessary in order to eliminate a number of possible errors. In measuring relative rates of reaction, one must make sure the results are independent of which reactant nozzle is used, eliminating systematic errors that would otherwise be present. The extension of the needles .3 cm into the reaction tube, along with their ends being filed at 45 degrees and positioned such that the flow will be towards the oncoming helium plus clusers, has been designed to ensure turbulent flow causing a complete mixing of reactants.

The reactants were diluted in helium before injection. Reagents were metered through a Hastings Teledyne (Model NA11-100) digital flow meter and mixed with a flow of pure helium. The mixture was then passed through a catalytic purifier (Airco Model #98) which served mainly to remove molecular oxygen from the system. This mixture then entered a ballast tank used to keep the nozzle backing pressure constant.

In these experiments, although the reaction tube was designed to house four reactant nozzles, only two were actually used. The multiple nozzle scheme was designed to permit direct comparison of reactivities of a number of reactant gases. This is accomplished simply by alternating which nozzle is fired. Since all the reactants were diluted in helium, each mixture was compared to a pure helium pulse from the other nozzle. This was done in an effort to negate any error introduced by scattering of the metal clusters from the beam. The extent of reaction is best monitored by depletion of the metal clusters within the beam. Therefore, by using the alternating nozzle arrangement and comparing, shot for shot, the reactant mixture and pure helium injections, one can easily observe any resulting differences in the monitored photoion intensity of the metal clusters.

After some (approximately 175 μs) time within the reaction tube, the resulting beam was then expanded from the 1 cm diameter orifice into the main chamber. The beam is then skimmed twice after which it enters the final B chamber. Once inside the photoionization region of the time of flight mass spectrometer, the photoion signal of the metal clusters and reaction products is monitored by direct one-photon ionization using the F_2 (7.98 eV) excimer

laser line. The fluence of the laser was kept low enough (10^{14} photon/cm^2) to ensure that multipohoton dissociative events would not contribute to the observed mass spectrum.

The resulting analog time of flight photoion signal was then multiplied and digitized using a fast 20 MHz transient digitizer. The entire experiment was run at a repetition rate of 10 Hz.

C. Reaction Tube Characteristics

In order for the results of these experiments to be interpretable certain critical parameters, such as, temperature, pressure, and contact time during the reaction must be reasonably known. With this in mind the next few sections will present estimates of these parameters. Although the complexity of the formation and reaction of the metal clusters using this technique may seem hopeless, it turns out that it is not. Gas dynamics[78-82] for flows in the .1 to 2 atmostphere gas densities are well developed which allows for reasonable estimates of the above parameters to be made.

D. Flow From the Main Nozzle

Of course, before one can hope to understand conditions within the reaction tube, there must be a thorough grasp of the pulsed nozzle cluster source

without the reaction tube in place. From earlier
studies published,[47] the behavior of this source is
well understood. The nozzle has been measured to de-
liver 1.5 torr liters of helium in a pulse of approxi-
mately 400 μs duration. This helium pulse flows
directly down the .2 cm diameter tube where vapori-
zation, cluster formation, and thermalization take
place with only small losses out of the vaporization
laser input hole. The mass flow rate,[80] F, through this
sonic orifice is:

$$F = A \cdot C \cdot P$$

where, A is the cross-sectional area of the orifice

C is the speed of sound at the nozzle temperature

P is the backing pressure

This can be used to calculate an average density at the
.2 cm orifice. From the pulse duration and flow per
pulse the average density is calculated to be 1.6 atm
at 300 K.

The helium carrier gas then expands freely from the
.2 cm diameter orifice to form a supersonic jet whose
flow velocity rapidly increases to a terminal velocity
speed,[80] μ_t:

$$\mu_t = (2T_o C_p/M)^{\frac{1}{2}}$$

where, C_p is the constant pressure heat capacity

T_o is the temperature of the helium before expansion

M is the molecular weight of the gas

From the equation it can be calculated that for
helium at 300 K, the terminal velocity would be
1.77×10^5 cm/s. Although, if one considers the ef-
fects of the vaporization laser firing within the
helium pulse, then there might be additional heating
which needs to be taken into account. By measuring
the time of arrival for the clusters, it is possible
to estimate the effective stagnation temperature, in-
cluding the vaporization process. The clusters'
arrival time is seen to be 10 μs wide (FWHM) centered
about a total delay of 640 μs. For a total distance
of 122 cm travel, the 640 μs flight time implies a
terminal velocity of 1.9×10^5 cm/s. Using this velocity
one can back calculate solving for the effective tem-
perature of the source to be 350 K. This is approxi-
mately 50 K above what is expected without the vapor-
ization laser firing which suggests that thermalization
is quite efficient within the .2 cm diameter tube prior
to expansion.

E. Flow with Reaction Tube

    The presence of the reaction tube on the exit of
the cluster source will no doubt have an effect on the
previously mentioned parameters of the gas entering it.
The major effects are most likely to be a reheating of
the gas due to shock waves and turbulence, along with a

reduction of the flow velocity to subsonic. In order
to understand these effects and their influence on the
experimental results, the next few sections will pre-
sent discussions on temperature, time and density
within the reaction tube.

Temperature

From the discussion of the main nozzle, one might
suspect that the expansion from the .2 cm orifice would
leave the gas in the reaction tube extremely cold. Al-
though in considering the downstream boundary conditions,[78]
it is understood that some kind of shock wave will be
set-up within the first couple of centimeters of the
reaction tube. The most likely effect of these boundary
conditions (ex: sudden inward turn of flow by reaction
tube wall, pressure downstream, etc.) will be to set up
an oblique shock attached to the inside corner at the
end of the diverging adaptor region. In the limiting
case the shock wave system will move up into this diverging
region becoming a normal shock wave.

The effect of this shock wave will be to reheat and
partially compress the gas. This heating however is not
unbound because the flow across the shock wave is so fast
that the overall process is adiabatic. Therefore, the
only source of energy to support the reheating is the
directed translational energy of the flowing gas. For an

adiabatic expansion the enthalpy (per unit mass) of the
original gas prior to expansion, h_o, is related to the
enthalpy of the flowing gas, h, by the energy equation:[78]

$$h_o = h + u^2/2$$

where, u is the flow velocity of the gas. From this equa-
tion it can be seen that, as long as the flow is adiabatic,
the enthalpy of the flowing gas can never be higher than
the original static gas. For a near perfect gas the en-
thalpy is a function of temperature (5/2 KT per atom), so
that for helium the temperature cannot be any higher than
that of the static gas. In fact, since the gas is flowing
it should be somewhat cooler than the source.

Once the gas has entered into the reaction tube the
flow may not remain adiabatic. In fact, the reactant in-
jection needles with their opposing flow were designed to
produce turbulent mixing and boundary interactions which
would introduce heat exchange between the gas and the walls
of the reaction tube. Although, since the walls are at
300 K, the only effect would be to help heat the gas to
this temperature.

With this information above and consideration of the
vaporization process (heating) taken into account, a
reasonable estimate of the reaction temperature would be
300-400 °K, with the best estimate being 320 K.

Residence Time

     The best way to estimate the actual residence time
is to measure the cluster arrival time in the photoioniza-
tion region and compare it to the arrival time without
the reaction tube on. The arrival time of the latter
case (no reaction tube), was measured to be 640 us. To
consider the reaction tube, a few cases were investigated
in order to understand the effect of each of the elements
(walls of the tube, injection needles, injected gas) sep-
arately. First of all, when the tube was put in place
without the injection needles, an additional 60 µs was
observed. With the needles inserted but without any gas
having been injected, an additional 80 µs was observed
as compared to without the reaction tube. Finally, if
gas was also injected a total delay of 120 µs was observed,
giving an overall arrival time of 760 us.

     The major portion of these added arrival times is
most likely due to the time spent in the reaction tube.
By considering the estimated temperature of 320 K (pre-
sented above) in the reaction tube, the terminal velocity
of the beam would be nearly the same as the main nozzle
itself, except for a small delay (5 µs)[83] due to a
slower acceleration to terminal velocity from the 1 cm
diameter orifice of the tube. From the average velocity
of 1.9×10^5 cm/s it is known that a travel of 10 cm would

under normal expansion conditions take 53 us. Therefore,
with the added delay of 120 μs, the total residence time
is 120 + 53 + 173 μs.

The observed delay of 120 μs can be explained in
terms of two effects. The first is a slowing of the
gas from terminal velocity to slightly subsonic for
the 10 cm length of the reaction tube, along with a
slight delay to regain terminal velocity from expansion
out the 1 cm diameter orifice. The second effect is
the counter current injection of the reactant gas causing
a further decrease of the velocity down the tube. Taking
both of these effects into account, a reasonable estimate
for the residence time is between 150 and 200 μs.

Gas Density

From the known flow rate and pulse length of the
main nozzle it is easy to place a lower limit of 40 torr
for the effective stagnation pressure of the helium gas
near the exit of the reaction tube. This limit is set
by considering the area change upon entering the larger
diameter reaction tube. Although a better estimate can
be calculated using the average flow velocity ($.59 \times 10^5$ cm/s),
the mass flow rate (3000 torr liter second), and temperature
(320 K) of the gas within the reaction tube. This leads
to an average density of 65 torr for static helium.

Due to viscous drag effects on the walls and
injection needles along with the counter directed
flow of reactants, it is likely that a pressure gradi-
ent along the tube should exist. Reasonable estimates
for the pressure at the entrance, middle, and exit of
the reaction tube, therefore are 100, 65, and 40 torr,
respectively.

F. Results

The first few examples of these metal cluster
reactions will focus on the reaction of a few simple
small molecules such as N_2, Co, and D_2 with both nio-
bium and cobalt clusters. These metals are particularly
good subjects for these studies because both have only
one naturally occuring isotope which makes the interpre-
tation of their reaction product mass spectra more in-
formative. A presentation of similar reactions with
copper, nickel, and iron clusters will also be made,
although since these metals have multiple isotopes their
reaction product mass spectra are somewhat less revealing.

Carbon Monoxide Chemisorption

A reasonable place to begin is with the chemisorption
of carbon monoxide since it is in most respects the
simplest reaction to be considered. With every metal we
have investigated (including most the metals discussed in
this thesis) carbon monoxide was found to readily chemisorb

on all clusters with more than two atoms. For example,
Figure 20 displays a limited region of the time of flight
mass spectrum for niobium clusters reacting with CO. The
figure shows both the mass spectrum of the metal cluster
beam with only pure helium injected through the reactant
needles (the control spectrum) as well as the spectrum
when CO was injected into the reaction tube. As shown in
the figure, both the niobium trimer and tetramer react
readily, producing a depletion of the parent cluster signal.
In the case of CO chemisorption the ionization signal lost
in the metal cluster channel reappears in higher channels
in the form of $Nb_n(CO)_m$ reaction products with $m = 1-3$.
Although not shown in Figure 20, all higher clusters of
niobium were found to react with CO in a similar manner.
With the limited mass resolution it was impossible to
follow the successive additions of CO's to each cluster
beyond three, but, at least up to this extent of reaction,
all niobium clusters showed the same tendency to chemisorb
multiple CO molecules.

In contrast with this facile reaction for the higher
clusters, the Nb atom and dimer were found to be remarkably
inert. Even with far higher concentration of CO than used
in Figure 20, no significant reaction of Nb or Nb_2 was
observed. In reactions of atoms and dimers, however, we
do not claim this lack of apparent reaction is necessarily

Figure 20. Reaction study of small niobium
clusters with CO. The dashed mass
spectrum is that of the control ex-
periment where only pure helium was
injected into the reaction tube. The
solid trace was observed when 2.4 sccm
$(cm^3$ atm/minute) of CO was injected
(with a pure helium carrier) into
the reaction tube. The features
growing in due to formation of $Nb_n(CO)_m$
reaction products are blackened in for
emphasis. Corresponding reaction
products for the Nb_nO cluster oxides
are observable as small peaks on the
baseline.
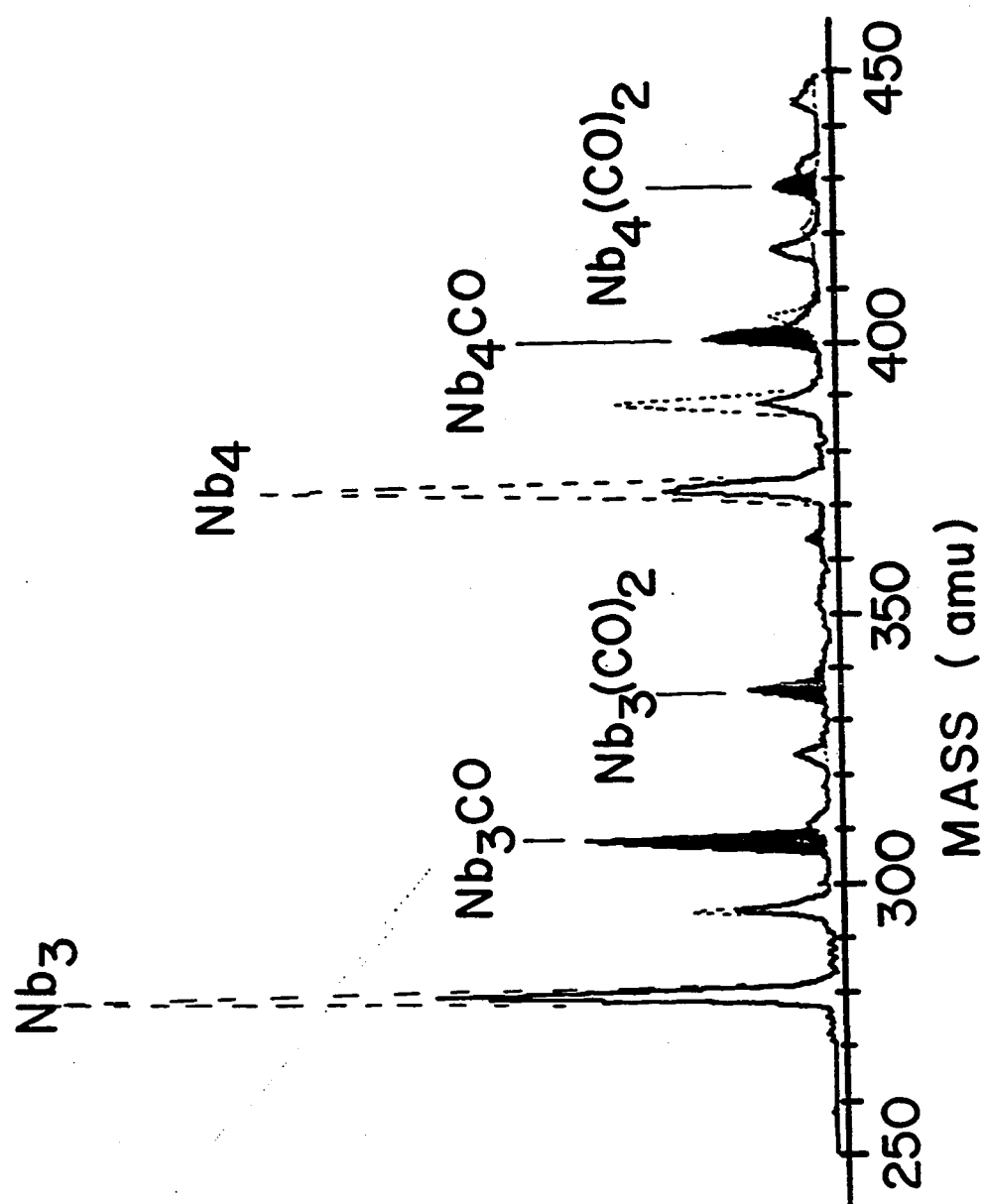
significant. These are gas phase addition reactions where thermalizing collisions with the helium buffer gas are essential to take away the energy of reaction and stabilize the reaction product. The 50-100 torr, 320 K helium buffer gas conditions of the reaction tube provide thermalizing helium collisions with reaction products on the order of once every few nanoseconds. In the case of the larger clusters, the unimolecular decomposition time of the reaction complex is certainly much longer than this, and the required bath gas collisions will always occur prior to decomposition. In the case of clusters with only a few atoms on the other hand, the absence of observable reaction products may simply mean that the reaction complex is too short-lived to survive until the final expansion region where cooling occurs. In the case of Nb_2 + CO, a rough estimate of the lifetime of the Nb_2CO reaction complex (with an energy in excess of the 1 eV binding energy by kT) shows the observed absence of reaction here is on the verge of being significant: the calculated lifetime (RRK)[84] is on the order of 10^{-7} second. Since so little is presently known with certainty about the critical parameters that go into such a lifetime calculation for a metal cluster -- CO complex, we prefer to stay on the conservative side, and not draw any firm

conclusions as to the reactivity of the atom and dimer for any of the metals and reaction partners considered in this study.

The chemisorption of CO on metal clusters was found to be generally facile, with very little change as a function of cluster size. This can be seen in Figure 21 which plots a coarse estimate of the relative reaction rates for CO chemisorption as a function of cluster size for both niobium and cobalt, obtained from a series of mass spectra taken at various CO concentrations. These relative rate data are based on the following simple picture. The chemisorption reaction for Nb_n was assumed to proceed in a single elementary step of the form
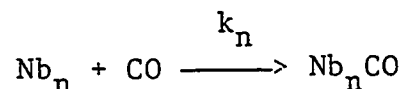
$$Nb_n + CO \xrightarrow{k_n} Nb_nCO$$

for which the elementary rate expression is[84]

$$\frac{d[Nb_n]}{dt} = k_n[Nb_n][CO].$$

Assuming that CO is in such excess that its concentration change is negligible, integration gives an expression for the rate constant, k_n, in terms of the measured fraction of Nb_n left unreacted (D_n), CO concentration ([CO]), and reaction time (t):

$$k_n = {}^-([CO]t)^{-1}\ln D_n$$

Figure 21. Relative reaction rates for CO
chemisorption for cobalt and ni-
obium clusters. Estimated error
bounds for these relative rate
measurements are ± 20%.
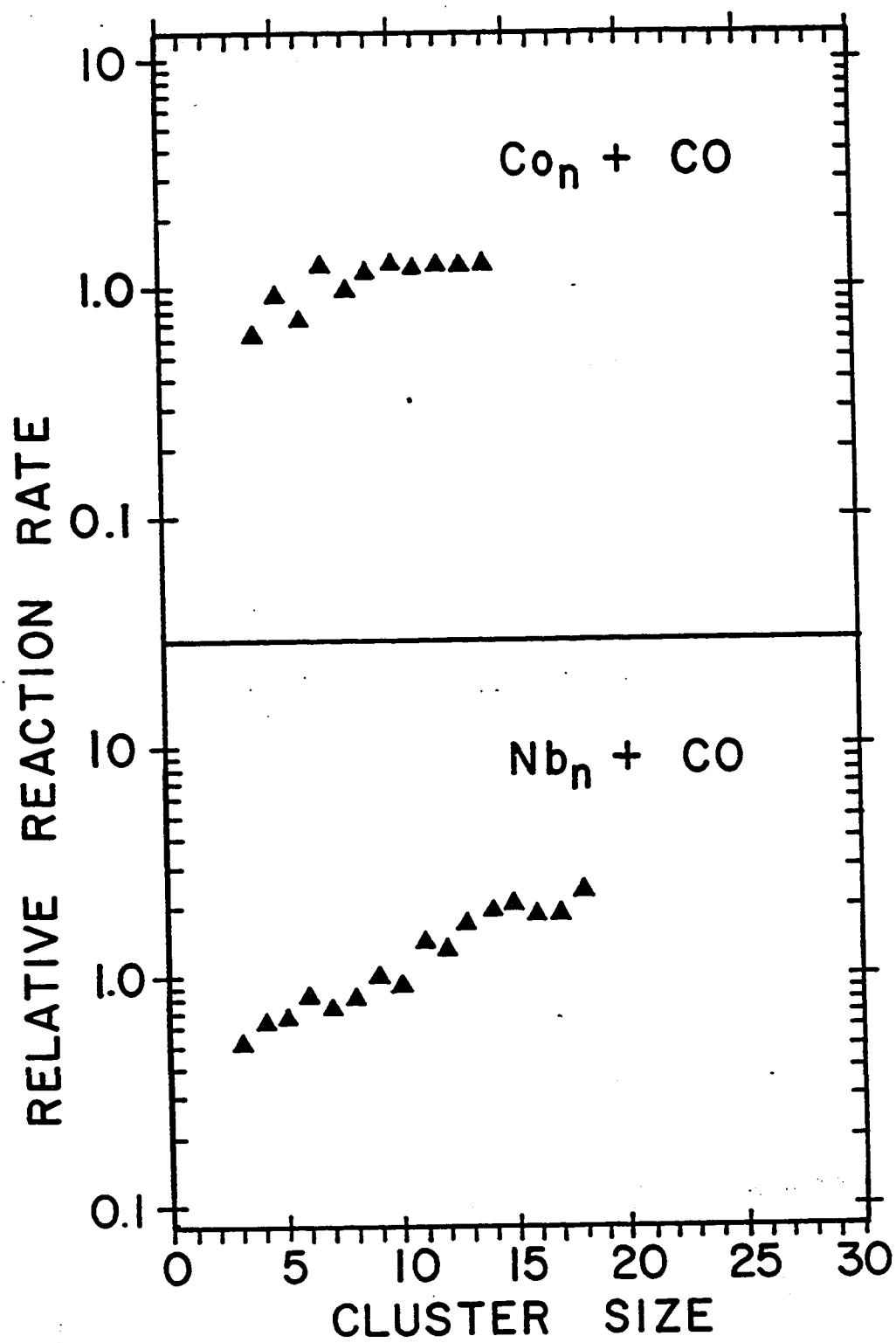
where $D_n = [Nb_n]_{reaction} / [Nb_n]_{control}$

From these initial survey studies of cluster chemisorption reactions, we have only a rough knowledge of the average CO concentrations and reaction times appropriate to the reaction tube. Although it is possible to make reasonable estimates of these parameters and arrive at a coarse measure of the absolute reaction rates, k_n, we have far more confidence in taking the ratio of the reaction rate for the n-th cluster to that for some reference cluster measured in the same mass spectrum. For this reason the rates plotted in this thesis for the various studied chemisorptions are relative reaction rates,

$$R_n = \ln D_n / \ln D_r$$

where D_n is the measured unreacted fraction of the n-th cluster, and D_r is the corresponding unreacted fraction of a reference cluster.

For the data in Figure 21, Co_8 and Nb_9 were picked as the reference clusters for the top and bottom panels, respectively. The measured relative rates are seen to increase quite gradually with increasing cluster size, the rate of increase differing a bit between the two metals.

There is little in these CO chemisorption data to suggest that anything particularly dramatic is changing as

the size of the metal cluster increases. Either there
is not much difference among this range of small clusters,
or CO chemisorption is not a very discriminating probe.
One indication that CO is not very discriminating can be
found in Figure 20 where careful examination of the small
peaks near the baseline shows that the extent of CO chemi-
sorption for the various niobium cluster oxides is much
the same as the corresponding niobium clusters. These
oxides are formed in the high temperature plasma of
the laser vaporization cluster source from trace oxygen
contaminants in the helium carrier gas. Certainly the
addition of an oxygen atom to a small metal cluster like
Nb_3 would be expected to produce a major reorganization
of the electronic structure. Nevertheless CO chemisorp-
tion occurs as if nothing had changed.

Dissociative Chemisorption of D_2 on Cobalt Clusters

Despite the above indication from CO chemisorption
that there was little difference between one cluster and
another, there are other reactions for which different
sized clusters are actually very different. The first
indication that this is true came in a study of the
chemisorption of D_2 on clusters of cobalt, which appeared
as a Communication earlier.[75a] Figure 22 shows a more
extensive series of mass spectra for this important re-
action. As seen in the figure, the clusters display

Figure 22. Chemisorption study of D_2 on cobalt
clusters. The control mass spectrum
was performed with only pure helium
injected in as the reactant gas. The
lower two mass spectra were taken with
3.6 sccm and 5.0 sccm flow of injected
D_2 reactant, respectively. The sharp
peaks seen in the bottom-most trace
for clusters with more than 10 atoms
are all due to cobalt clusters with more
than one molecule of D_2 chemisorbed.

COBALT CLUSTERS

control

3.6 sccm D$_2$

5.0 sccm D$_2$
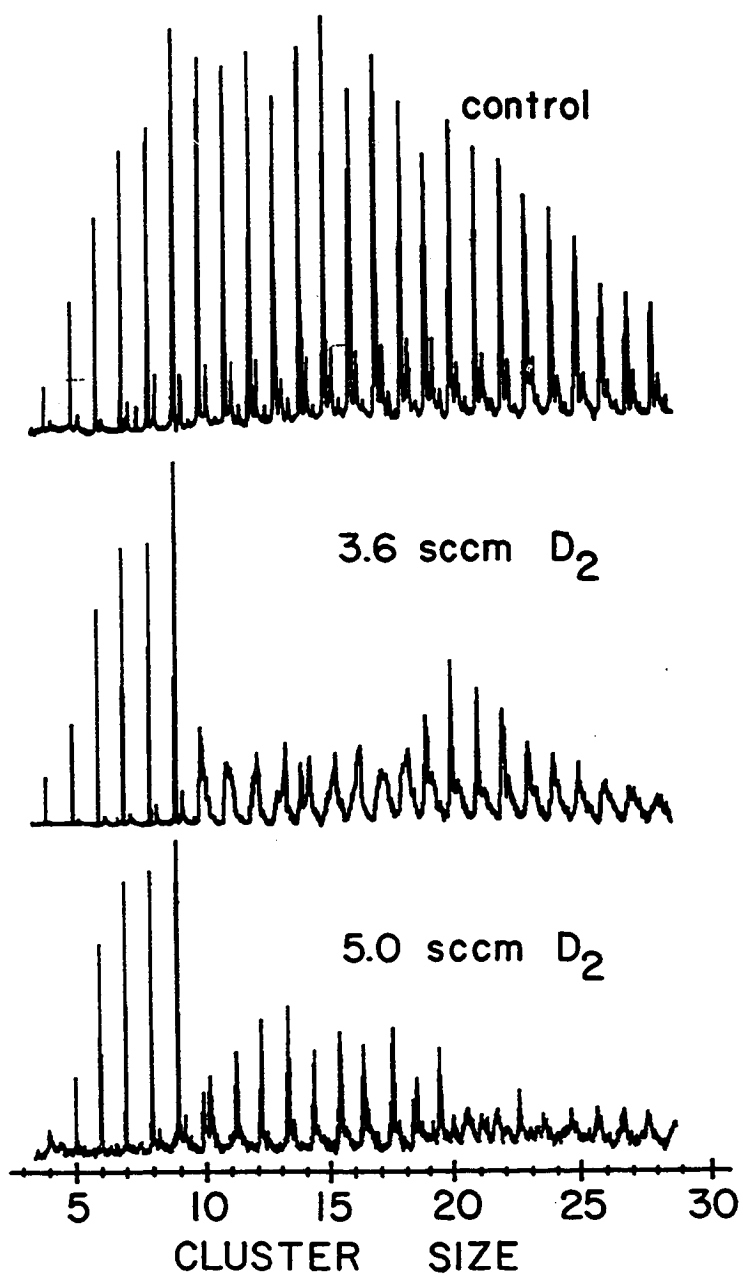
CLUSTER SIZE

very dramatic size dependencies in their reaction with D_2. Note particularly the rapid onset of high reactivity on going from 9 to 10 atoms per cluster. At the time it was first discovered, this was the most abrupt change ever observed in any property of a metal cluster as a function of size.

As with CO chemisorption, reaction with D_2 was not found to occur on the cobalt atom or dimer. Again, it is not clear whether this is a simple kinetic effect associated with the short lifetime of the reaction complex or whether these species are inherently unreactive. The cobalt trimer, however, does react strongly. Figure 23 shows this trimer region in sufficient detail to resolve individual reaction products produced by the successive addition of up to three D_2 molecules.

The bottom panel of Figure 22 taken with a fairly high D_2 concentration is misleading. It looks as though the clusters in the 10-20 atom size range have returned, as though the reactivity were less at higher concentrations than at lower ones. The sharp peaks that look like the clusters are actually shifted to higher mass because the clusters have picked up a certain number of D_2 molecules and then stopped reacting. This titration-like[85] behavior is shown in more detail in Figure 24 where the control and D_2 reaction mass spectra are superimposed for clusters in

Figure 23. Detail of the D_2 chemisorption
experiment on Co trimer. The
dashed mass spectrum is the con-
trol experiment (only pure helium
as the reactant), the solid trace
is the observed mass spectrum with
an average reactant flow of 7.4 sccm
D_2. Note that only reaction products
with even numbers of deuterium atoms
are observed. Careful examination of
the baseline reveals that the Co_3C
carbide and Co_3O oxide which are pro-
duced in small amounts in the laser
plasma of the cluster source also
chemisorb D_2 strongly.

Co₃

Co₃D₂

Co₃D₄

Co₃D₆

MASS (amu)
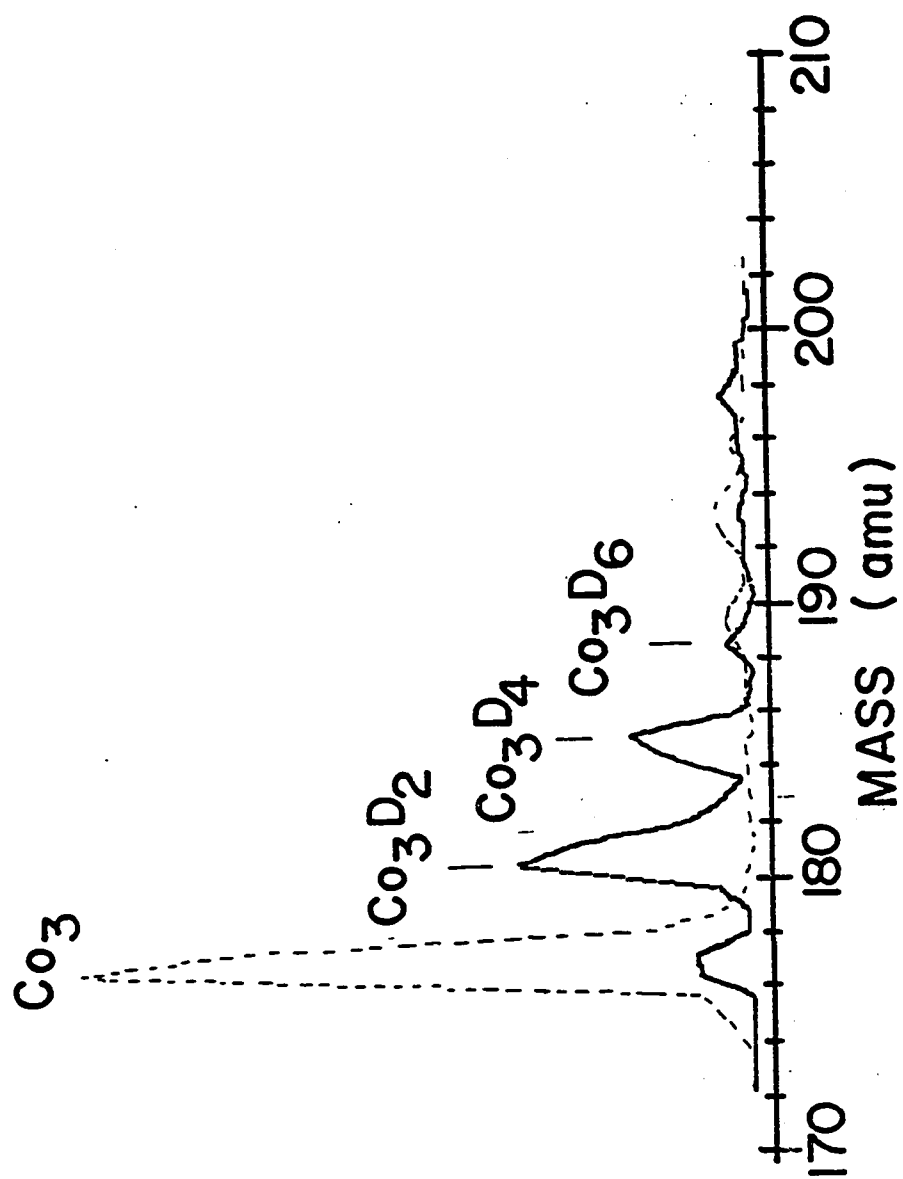
the 9-16 atom range. Here the mass shift for each cluster is clear enough to permit a measure of the number of D_2 molecules required to "titrate" the cluster: 5 for Co_{11-12}, 6 for Co_{13-14}, and 7 for Co_{15-16}.

There is also some indication in this reaction data that D_2 chemisorption on cobalt clusters is auto-catalytic. As shown in Figure 22, there is only a very small concentration range over which clusters with inter-mediate amounts of chemisorbed D_2 are observed. This may be due to an increase in the effective reaction rate after adsorption of the first D_2 molecule. This point should be checked in more detail when later, more quanti-tative versions of these cluster chemisorption experi-ments are available.

Chemisorption of D_2 is particularly interesting in that there is only one plausible way for the D_2 to bind to the cluster tightly enough to survive passage through the reaction tube and be observed in the molecular beam: D_2 must dissociatively chemisorb. Remember that the re-action products, whatever their nature, are exposed in the reaction tube to 50-100 torr helium buffer gas at a temperature of 320 K. In the last section it was argued that any reaction product will be thermalized to the buf-fer gas temperature within a few microseconds. Under these highly collisional conditions at room temperature

only quite strongly chemisorbed species will remain
on the clusters. Their rate for desorption should be
well approximated by an Arrhenius expression[84]

$$k_{desorption} = A \exp(-E_a/RT)$$

where E_a is the heat of desorption, R is the gas con-
stant, and T is the cluster temperature (320 K). This
is the approach used in the surface chemistry technique
of thermal desorption, where a large body of data has
been accumulated in the application of this equation to
wide ranges of real molecular desorptions. It is usually
found that the pre-exponential factor,[86] A, is on the order
of 10^{14} to 10^{15} s^{-1} for surface desorption. This value
is 10-100 times larger than usually encountered in simple
gas phase molecular decompositions, a fact that Zeiri,
Redondo, and Goddard[87] have ascribed to hindered rotations
of the chemisorbed molecule on the bulk surface. In the
case of small clusters with only 2 to 30 atoms, we are not
yet in the bulk surface limit, so an intermediate pre-expo-
ential factor of 10^{14} seems reasonable.

For many of the clusters shown in Figures 22,23 and
24 the extent of reaction with D_2 is nearly complete, for
essentially all the cluster signals have been replaced by
reaction products. Since the reaction tube has a residence
time of 150-200 microseconds, the typical reaction product
we see in the beam must have survived in the reaction tube

Figure 24.   Detail of D_2 chemisorption experiment
in the 9-16 atom cluster range showing
evidence for titration in the chemi-
sorption reaction. The dashed mass
spectrum corresponds to the pure he-
lium control experiment, the solid
trace to a flow of 5.0 sccm D_2 injected
into the reaction tube. The D_2 chemi-
sorption process appears to shut off at
five molecules of D_2 for Co_{11} and Co_{12},
six for Co_{13} and Co_{14}, and seven for
Co_{15} and Co_{16}.

COBALT CLUSTERS + D$_2$

9 10 11 12 13 14 15 16

MASS (amu)

500 600 700 800 900 1000
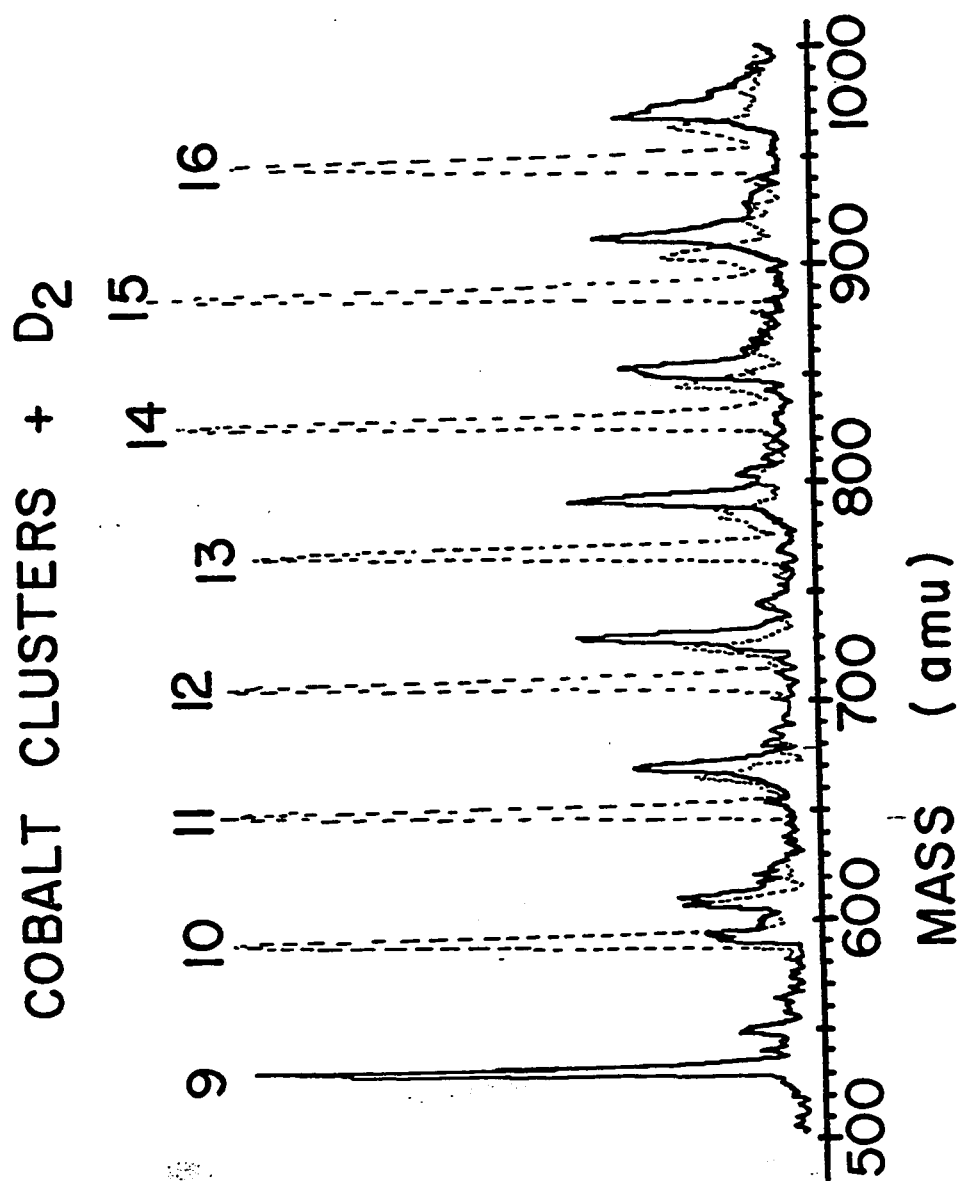
for at least 80 microseconds without having the D_2 desorb off the cluster. The desorption rate must therefore be slower than 10^4 s^{-1}. The Arrhenius equation and this maximum desorption rate together imply that the minimum heat of desorption for a reaction product to be stable in the reaction tube is 13 kcal mole^{-1}.

Hydrogen chemisorption is one of the best known of all surface chemistries. There are known molecular chemisorption states on some transition metal surfaces, but these are very weakly bound and are stable only at cryogenic temperatures. All known room temperature chemisorption states of H_2[88,89] on transition metal surfaces are dissociative, with the two hydrogens well separated at different binding sites on the surfaces.

So what is measured here in these gas phase reaction experiments with D_2 on metal clusters is the activation barrier on the entrance channel to dissociative chemisorption. This is a reaction that requires the concerted weakening of the strong H-H bond while simultaneously making two new bonds to the metal cluster. Transition metals are uniquely capable of such chemistry, and here we are beginning to see the onset of the behavior on the surface of small clusters.

Dissociative Chemisorption of N_2 on Cobalt Clusters

A parallel to these D_2 chemisorption studies is a related study using N_2. Figure 25, shows a characteristic mass spectrum for a control experiment along with spectra for two different concentrations of N_2 in the reaction tube. Without a magnifying glass and a ruler it is a bit difficult to see the details, but it is clear that the reactivity pattern obtained here with N_2 is similar to that observed in Figure 22 for reaction with D_2. However, the sharpest change in reactivity is clearly in the vicinity of Co_{19} and Co_{20}.

This similarity is quite clearly seen in Figure 26 which plots the measured relative reactivities as a function of cobalt cluster size for both the D_2 and N_2 chemisorption reactions. These relative reactivity plots were obtained from measured depletion ratios for each cluster as seen in a variety of experiments at different concentrations, similar to those described previously for the CO chemisorption experiments. Although we have endeavored to make these accurate as possible, the reader is cautioned not to take these relative rate measurements too literally. We have not plotted the estimated error bounds in the relative rate figures because these errors are highly correlated and inclusion in the figure simply makes it more difficult to see the reactivity pattern.

Figure 25. Chemisorption study of N_2 on cobalt
clusters. Careful examination of
the mass spectra (particularly the
middle trace taken with 3.5 sccm flow
of N_2) reveals features due to reaction
products with one or more N_2 molecules
chemisorbed on the cobalt clusters.
The higher concentration trace at the
bottom is a particularly graphic demon-
stration of the comparative inertness
of Co_{19} and Co_{20}.

COBALT   CLUSTERS

control

3.5 sccm N_2

8.5 sccm N_2
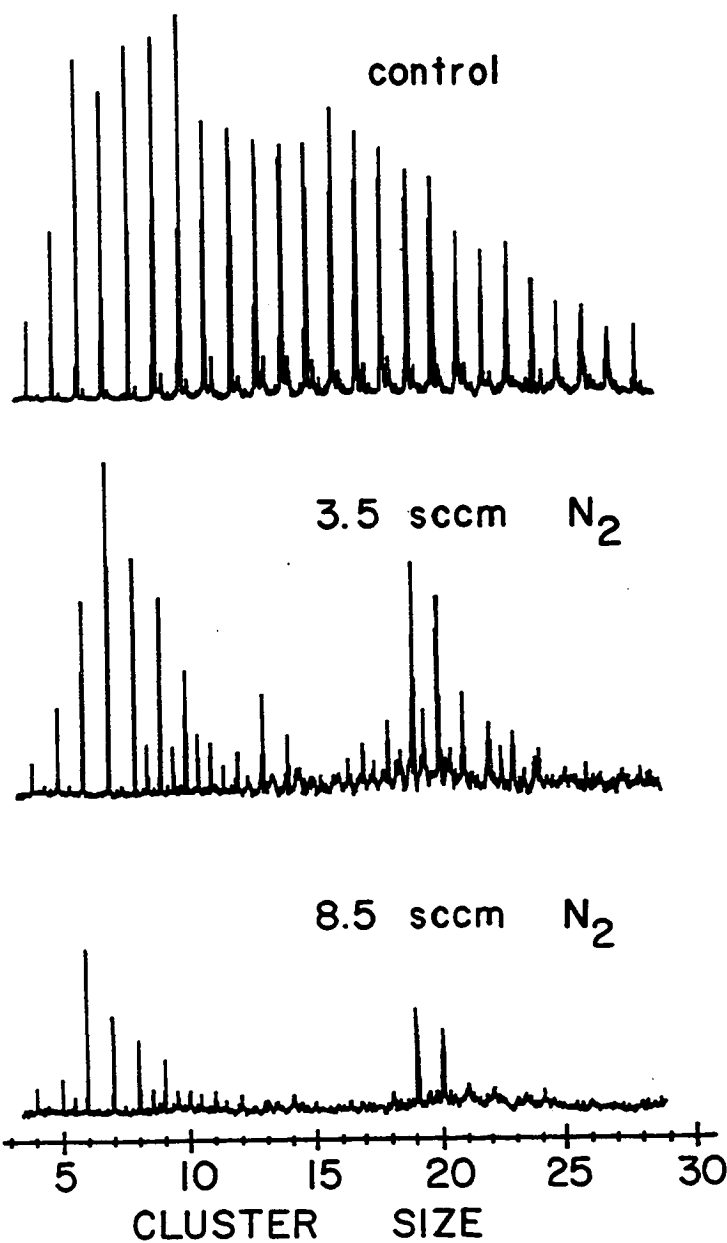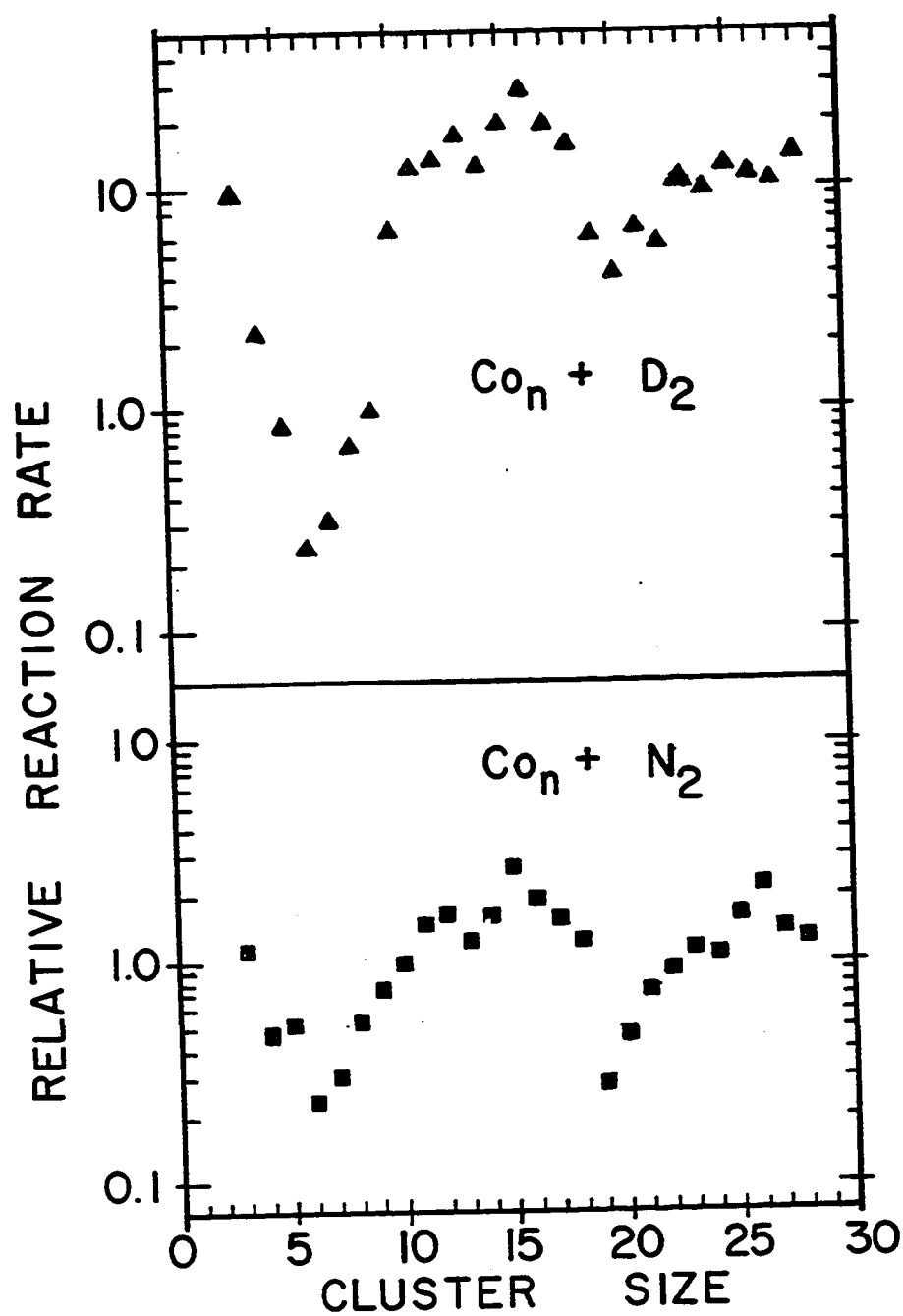
CLUSTER   SIZE

Figure 26. Relative reaction rates of cobalt
clusters with D_2 and N_2. Note the
striking similarity in the reactivity
patterns for these two reactants. The
estimated errors for these relative
rates is ±20% except for rates greater
than 10 or less than 0.1 compared to
the reference rate; for these extreme
rates the measurements are only of semi-
quantitative significance.

The estimated error bounds range from ± 20% for relative
rates near unity to over 100% for some of the extreme
points corresponding to clusters with either far faster
relative rates, or far slower as compared to the reaction
rate of the reference cluster. The effect of these errors
has been to smooth out the extremes. When more accurate
reaction rate data is obtained we expect the patterns
seen here to be even more pronounced.

The striking similarity in reactivity pattern seen
in Figure 26 for D_2 and N_2 chemisorption on cobalt clusters
is particularly impressive when one recalls how little
variation in reactivity was seen in CO chemisorption on
these same clusters (see Figure 21). Without question,
the mechanism of N_2 chemisorption must be more similar to
the dissociative chemisorption of hydrogen (deuterium)
than it is to the (presumably) molecular chemisorption of
CO.

As with D_2, chemisorption of N_2 is known to be largely
a dissociative process on transition metal surfaces at
room temperature. Single crystal data is not yet available
for N_2 adsorption on cobalt, but a great deal has been
learned recently about the adjacent elements in the
periodic table: iron and nickel. The tightest bound
molecular form of N_2 now known on an iron single crystal
surface is the σ adsorption state[90] on the Fe(111)
surface. This σ state is bound by 31 kj mole^{-1}, has a

markedly reduced N--N vibration frequency (1490 cm^{-1} as compared to 2194 cm^{-1} for free N_2), and is believed to be π-bonded parallel to the surface. This molecularly bound σ state partially desorbs at 170 K, the remainder dissociating to form a surface nitride. In the case of nickel,[91] recent angle resolved photoemisson data have shown that the γ adsorption state of N_2 on Ni(100) is molecularly adsorbed perpendicular to the surface. This also is too weakly bound to survive at room temperature. It desorbes at only 140 K. Even though no data is yet available in the case of cobalt, it is reasonable to expect that it too will exhibit only weak binding for molecular N_2. For these reasons, the 320 K adsorption data for N_2 shown in Figures 25 and 26 quite likely refer to a dissociative chemisorption process.

Chemisorption of D_2 and N_2 on Niobium Clusters

Results from the extension of these D_2 and N_2 chemisorption experiments to niobium clusters are presented in Figures 27-30. Once again dramatic changes in reactivity were observed as a function of cluster size. For both the D_2 and N_2 chemisorptions the clusters with 8,10, and 16 atoms are far less reactive than clusters with only one atom more or less. Figure 29 presents a particularly clear view of these sharp reactivity differences for N_2 chemisorption on niobium clusters in the

Figure 27. Chemisorption study of D_2 on niobium clusters. Note the negligible reactivity of Nb_8, Nb_{10}, and Nb_{16}, and the absence of titration behavior in the strongly reacting clusters.

NIOBIUM CLUSTERS

control

6.5 sccm D_2
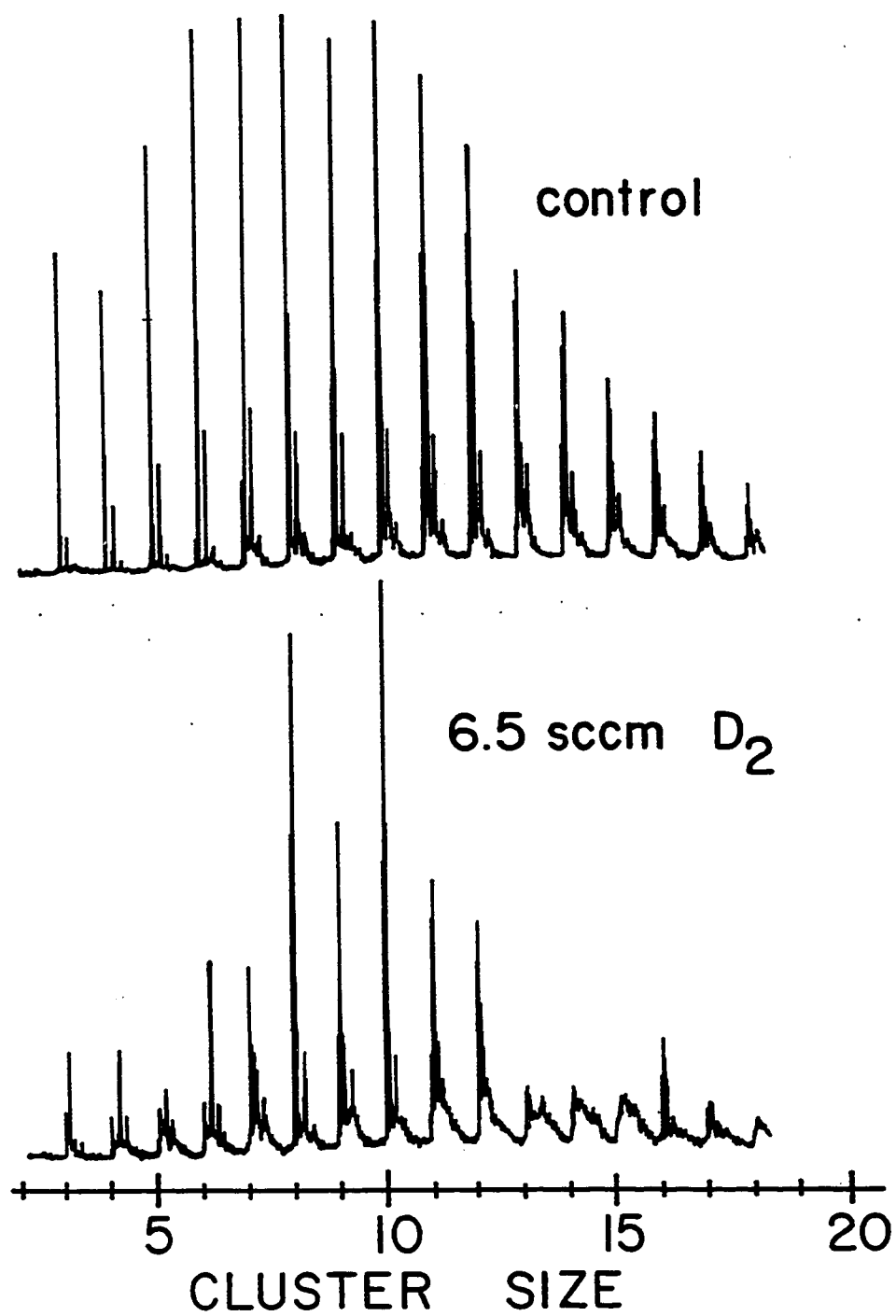
CLUSTER SIZE

Figure 28. Chemisorption study of N_2 on niobium
clusters. The sharp peaks in the small
cluster region of the lower mass spectrum
are due to the N_2 chemisorption product,
whereas the peaks seen in roughly the
correct position for the 8-12 and 16th
cluster of niobium are, in fact, due to
the unreacted cluster.

NIOBIUM CLUSTERS

control

2.8 sccm N_2

CLUSTER SIZE

Figure 29. Detail of small cluster region
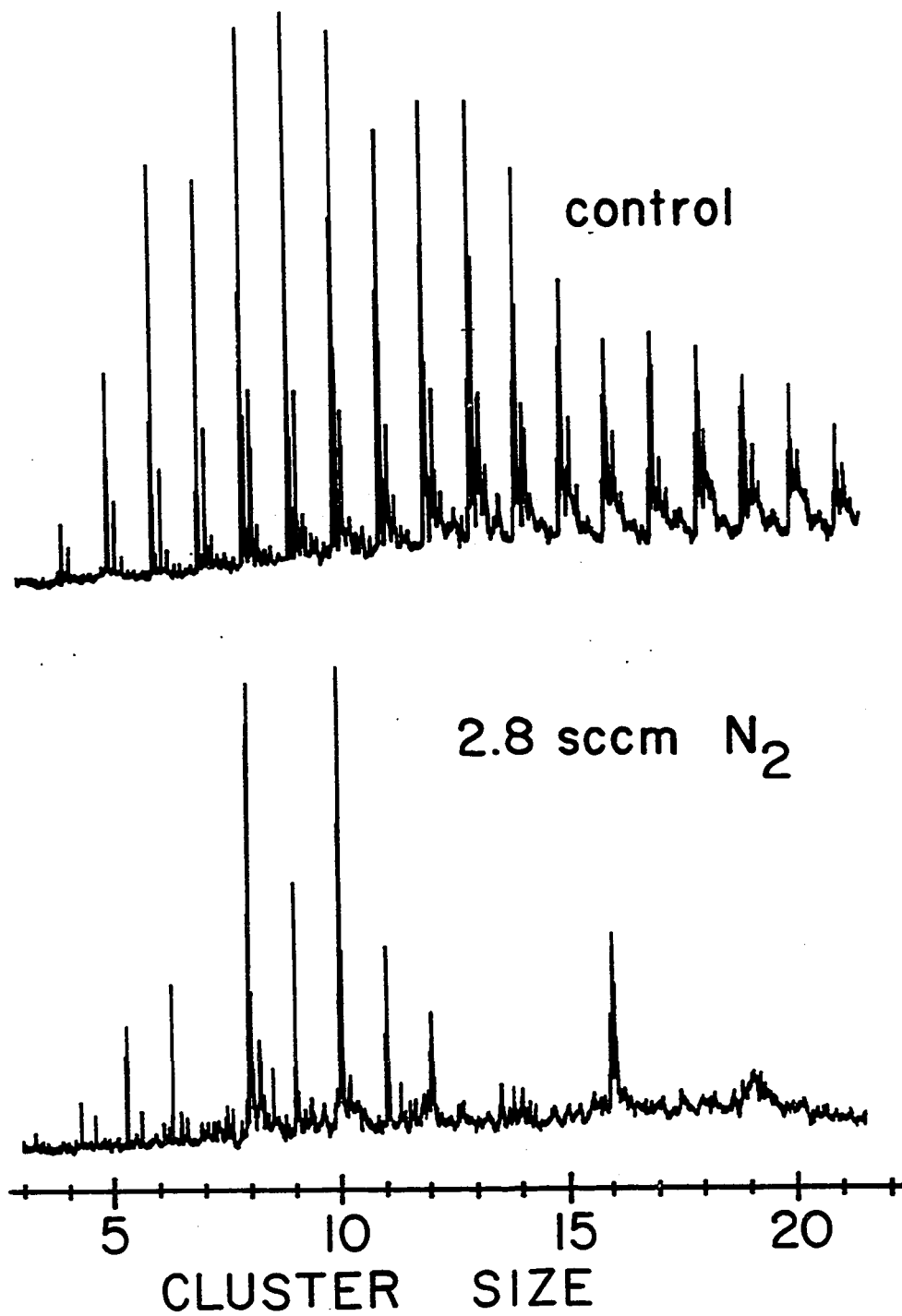of the N_2 chemisorption study on
niobium. Peaks due to N_2 chemi-
sorption reaction products have
been blackened in for emphasis.
Note that the reactivity of the
Nb_nO oxides is often markedly dif-
ferent from the corresponding pure
niobium clusters -- see the Nb_3 and
Nb_8 clusters particularly in this
regard.

NIOBIUM CLUSTERS
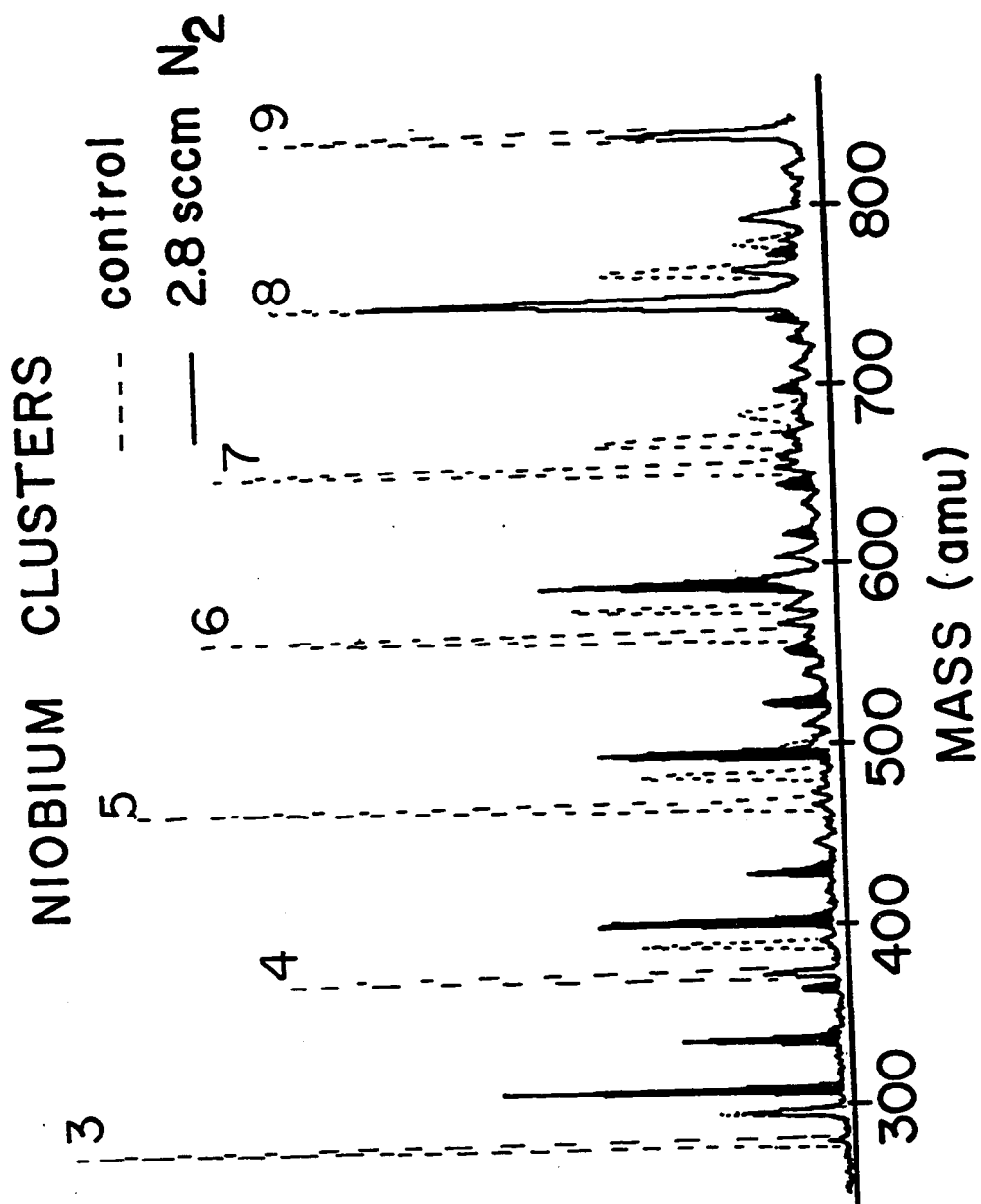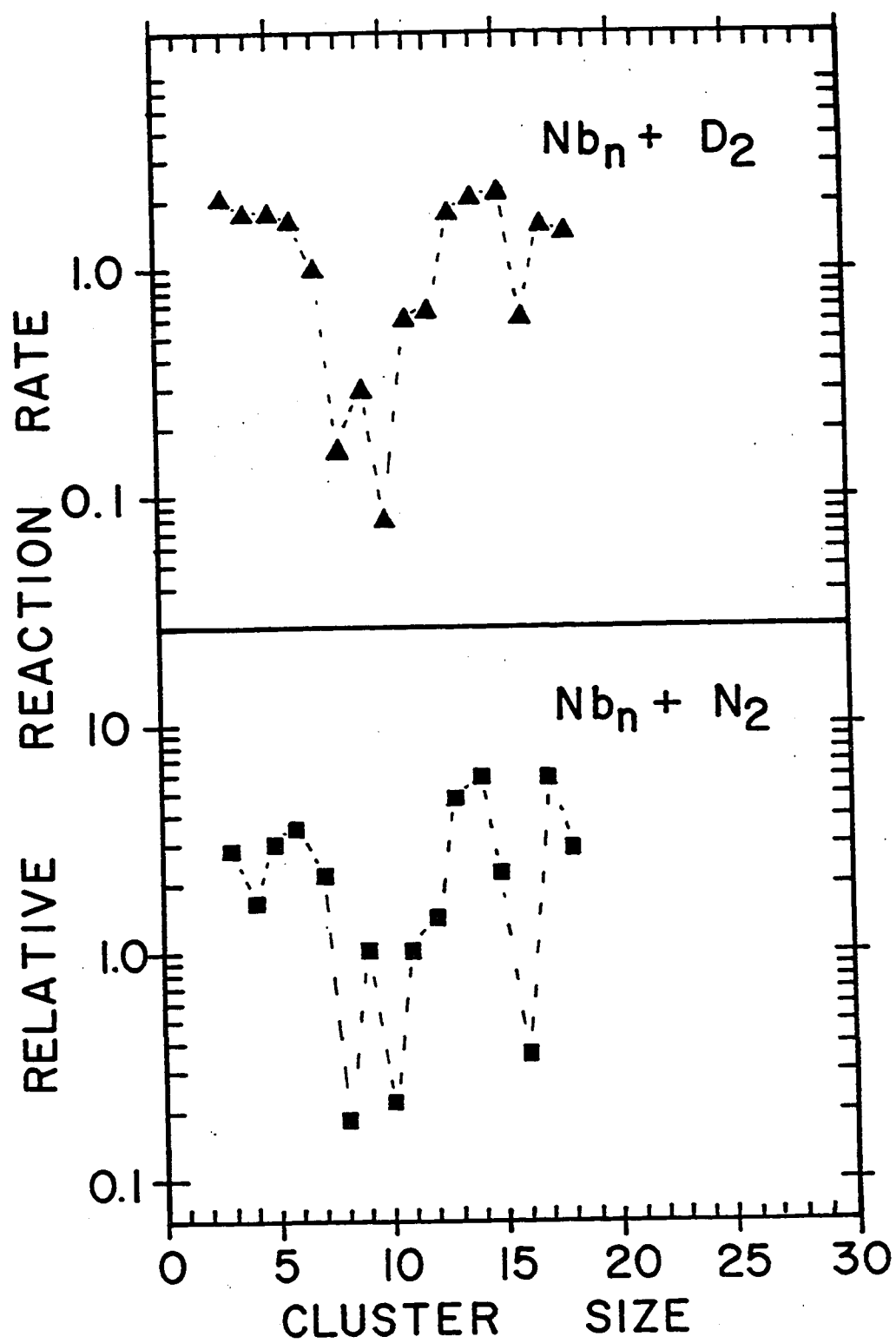
control
2.8 sccm N_2

MASS (amu)

Figure 30. Relative reaction rates of niobium clusters with D_2 and N_2. Note the similarity in the reactivity patterns for these two reactants. Estimated error bounds for these relative rates are ±20% except for the extremely low and high reactivity points which are only semi-quantitative.

3-9 size range. Note, for example, that the niobium trimer has nearly disappeared from the mass spectrum, the missing ion signal reappearing in peaks corresponding to Nb_3N_2, Nb_3N_4, and Nb_3N_6. In sharp contrast, the Nb_8 cluster has been largely unaffected by the N_2 reactant.

Also note that the reactivity of the corresponding cluster oxides is often sharply different than the metal cluster. Nb_3O, for example, is seen in Figure 29 to be far less reactive than Nb_3, while Nb_8O is far more reactive than Nb_8. In direct contrast to the observations for CO chemisorption, the pattern of reactivity of the niobium cluster oxides for D_2 and N_2 chemisorption is quite different from that of the clusters.

The relative reaction rates measured as a function of cluster size for D_2 and N_2 on niobium are presented in Figure 30. Again we emphasize that the errors in these measured relative rates are considerable. Particularly for the very fast and very slow relative rates, the measured values are likely to be biased due to the difficulty in measuring very large and very small depletions. Very slow relative rates will tend to be over-estimated, very fast rates will tend to be under-estimated. However, the gross pattern of reactivity, is well determined by the current measurements.

Copper Clusters - A Check for Hydrogen Chemisorption

Dissociative hydrogen chemisorption is a surface chemistry that is peculiar to transition metals with open d-shells.[92] Copper is an interesting test case since here the 3d band is fairly narrow and situated below the Fermi level. Molecular hydrogen[93] is known to chemisorb on copper surfaces, but this process is known to possess an activation barrier in the range of 3 to 5 kcal/mole, depending upon the crystal face. Calculations[94] of the electronic structure of copper clusters indicate the 3d band remains narrow and filled, lying well below the Fermi level, so it is reasonable to suspect that copper clusters will be unreactive toward H_2.

As an added check on our interpretation of the D_2 chemisorption experiments with cobalt and niobium clusters, we therefore extended the hydrogen reaction studies to copper clusters. Figure 31 shows the result of this experiment. As expected, no evidence of reaction was observed with H_2 (which should react faster than D_2) at a concentration over an order of magnitude higher than used in the previous experiments with cobalt and niobium.

Nickel and Iron Cluster Chemisorption Experiments

Nickel is a particularly important transition metal for detailed cluster beam studies since it is by far one of the easiest of the open d-shell transition metals to

Figure 31. Chemisorption study of H_2 on copper
clusters demonstrating no significant
evidence of reaction.

COPPER   CLUSTERS

control

83 sccm H_2
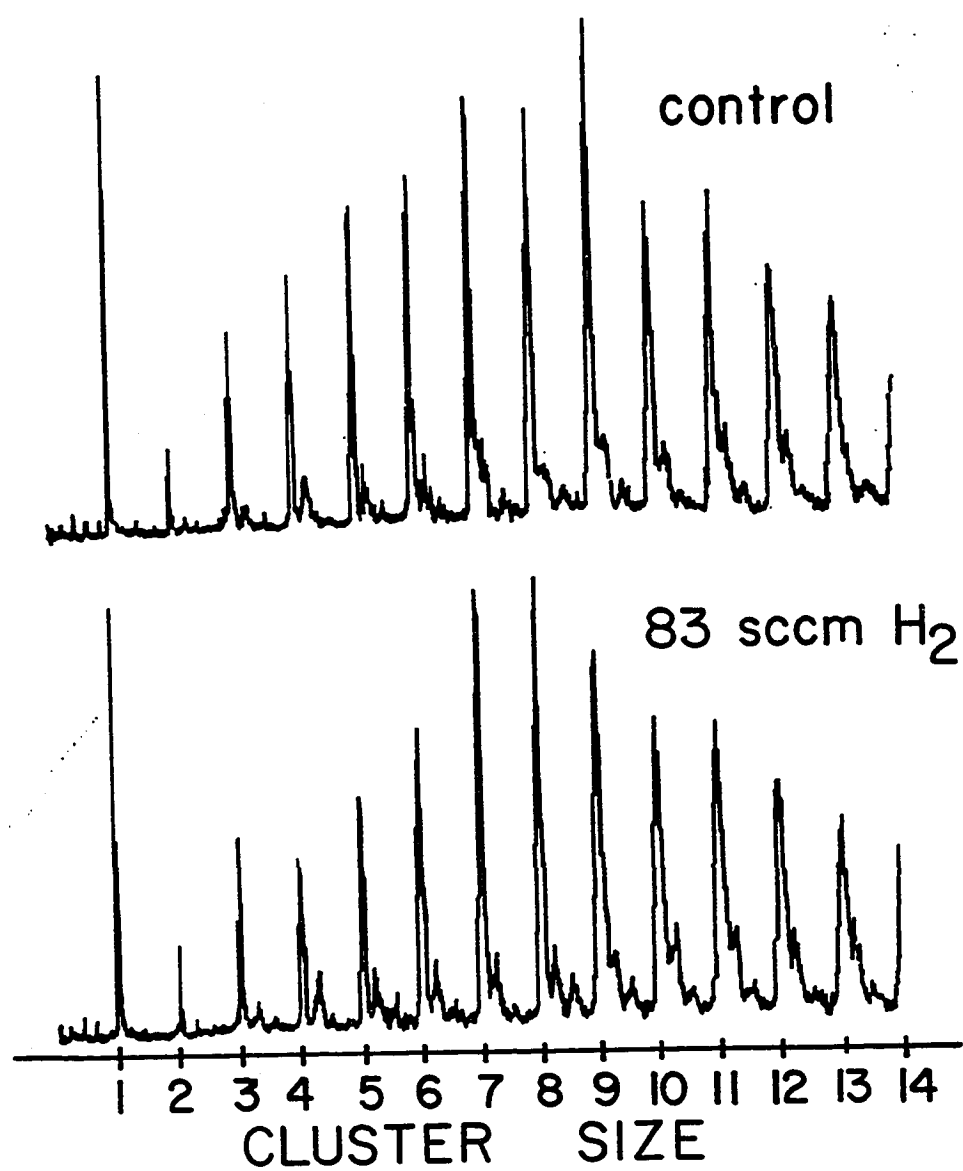
CLUSTER   SIZE

handle in quantum chemical calculations[94] Figure 32
shows the results of a D_2 chemisorption experiment on
nickel clusters using the new fast-flow reaction tube.
Deuterium is found to chemisorb readily, but displays
only a mild, nearly monotonic increase in reaction rate
as a function of cluster size. In light of the dramatic
effects seen with cobalt and niobium clusters, smooth
reactivity variation with cluster size is rather sur-
prising. Due to time constraints on the molecular beam
apparatus, no other chemisorption experiments were done
for nickel.

Iron completes the list of metals we have explored
in these first chemisorption experiments with the new
apparatus. Figure 33 presents mass spectra from a D_2
chemisorption experiment. Once again, a highly size-
dependent reactivity pattern is found for dissociative
D_2 chemisorption. Relative rates abstracted from
experiments such as these have been plotted along with
similar data from the nickel chemisorption experiments
in Figure 34.

An extensive attempt was made to measure the
relative reactivity patterns for N_2 chemisorption on
iron clusters. Unfortunately, the iron clusters turned
out to be almost inert to N_2 chemisorption. Figure 35
shows the results of one experiment where an order of

Figure 32. Chemisorption study of D_2 on
nickel clusters. The dashed
mass spectrum pertains to the
control experiment using only
pure helium as a reactant; the
solid line is the spectrum ob-
tained with a flow of 12 sccm
D_2.

NICKEL CLUSTERS

----- control

—— 12 sccm D$_2$
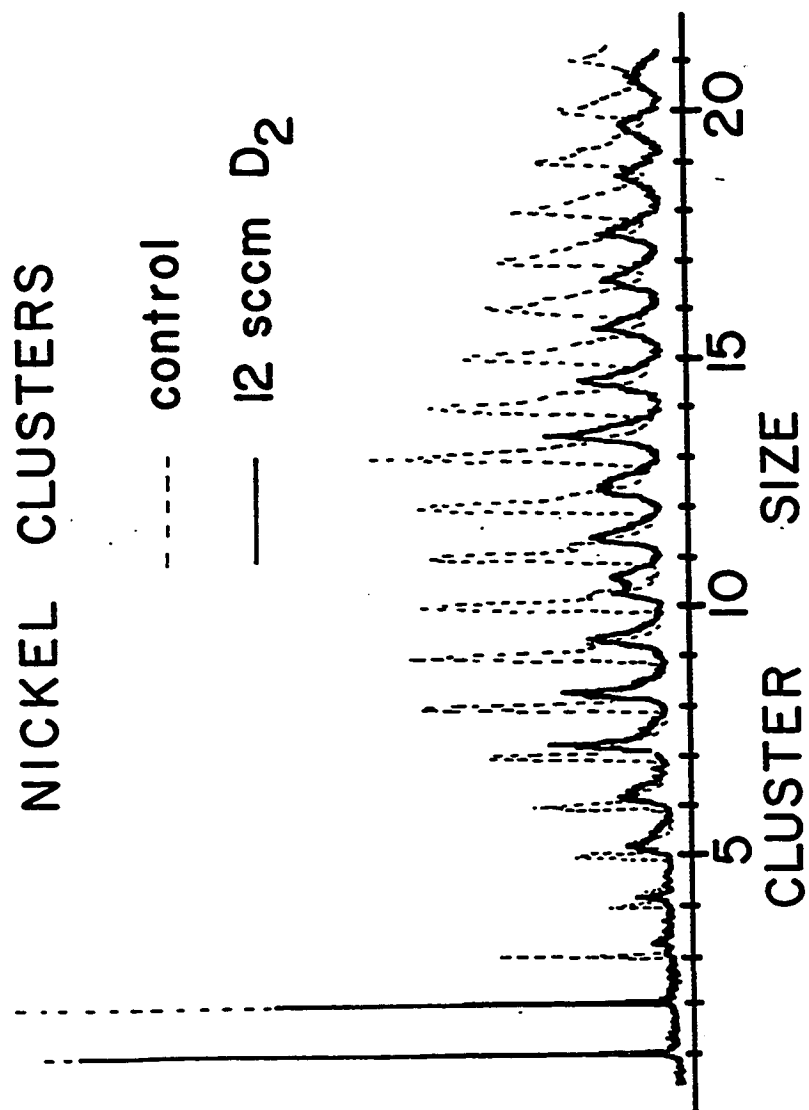
CLUSTER SIZE

Figure 33. Chemisorption study of D_2 on iron clusters.

IRON CLUSTERS
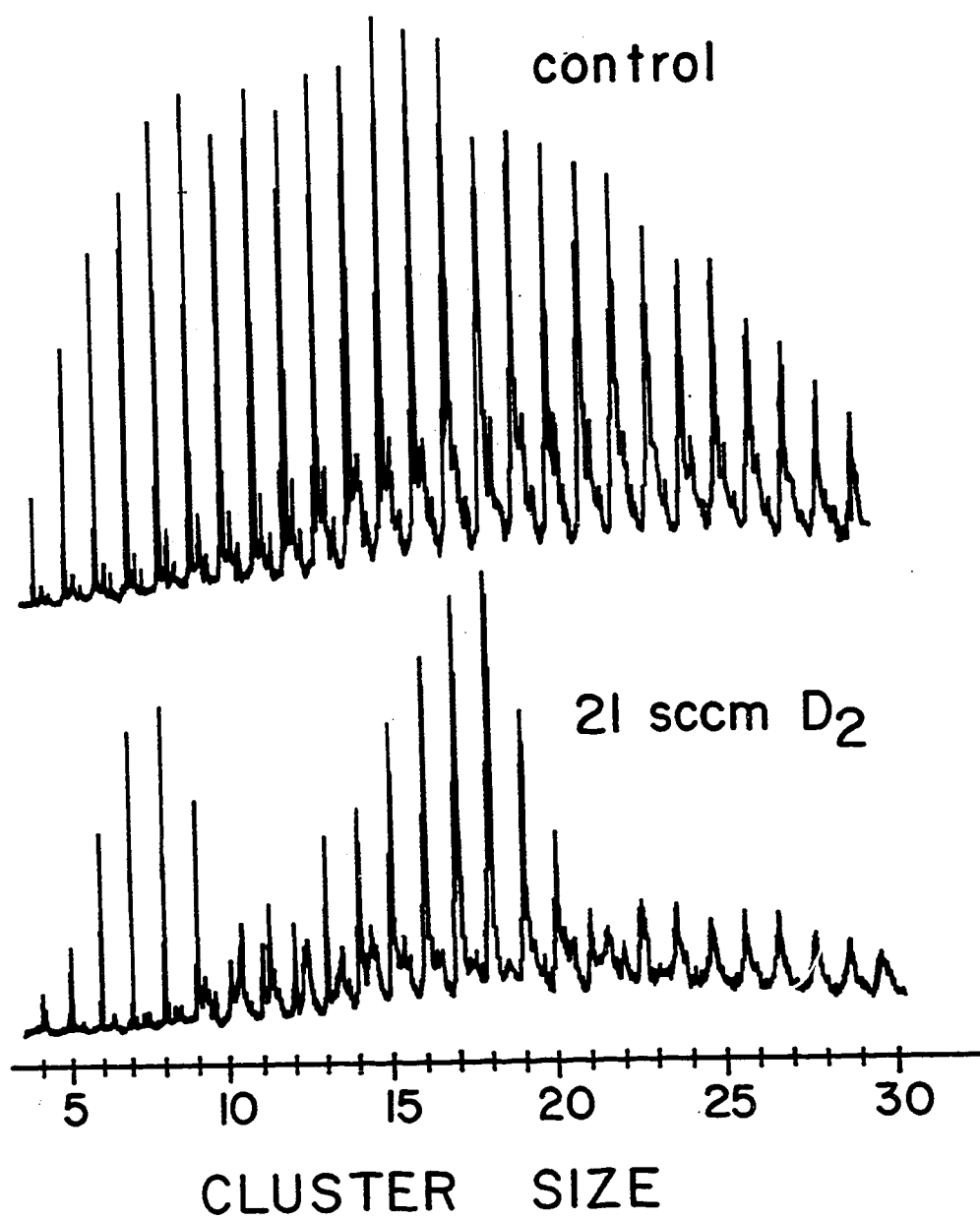
CLUSTER SIZE

Figure 34. Chemisorption study of N_2 on iron
clusters. The lower trace was taken
with sufficient N_2 flowing into the
reaction tube to lengthen the arrival
time of the clusters by 30-40 micro-
seconds. Even so, very little reaction
is evident here. Looking closely, there
is clear evidence of new peaks growing
in at 28 amu to higher mass of some of
the clusters -- particularly in the
region of Fe_{11} -- due to some formation
of N_2 chemisorption products. The sat-
ellite peaks seen at 16 and 32 amu to
higher mass of the iron clusters in
these mass spectra are due to iron
cluster ·oxides made in the laser plasma
of the cluster source.

IRON CLUSTERS

control

30 sccm N_2

CLUSTER   SIZE

Figure 35. Relative reaction rates for nickel
            and iron chemisorption reactions
            with D_2.

magnitude higher N_2 concentration was used than in
the experiments with cobalt and niobium clusters.
Even at this high concentration there is only a slight
indication of reaction (Fe_{11}, for example does show a
weak but clear $Fe_{11}N_2$ feature growing at 28 amu to high
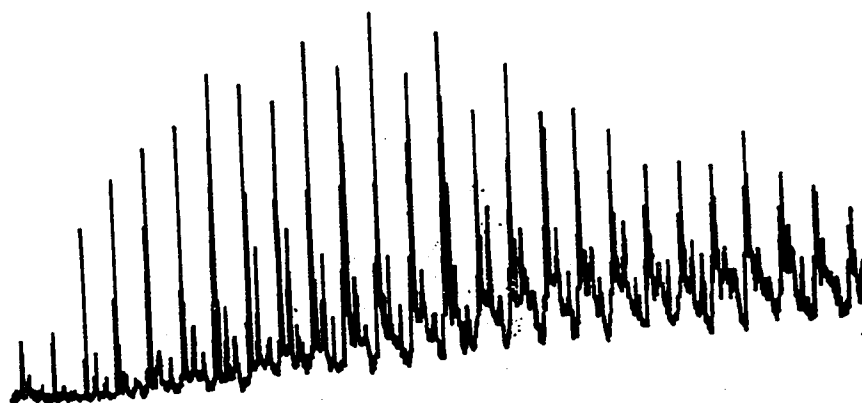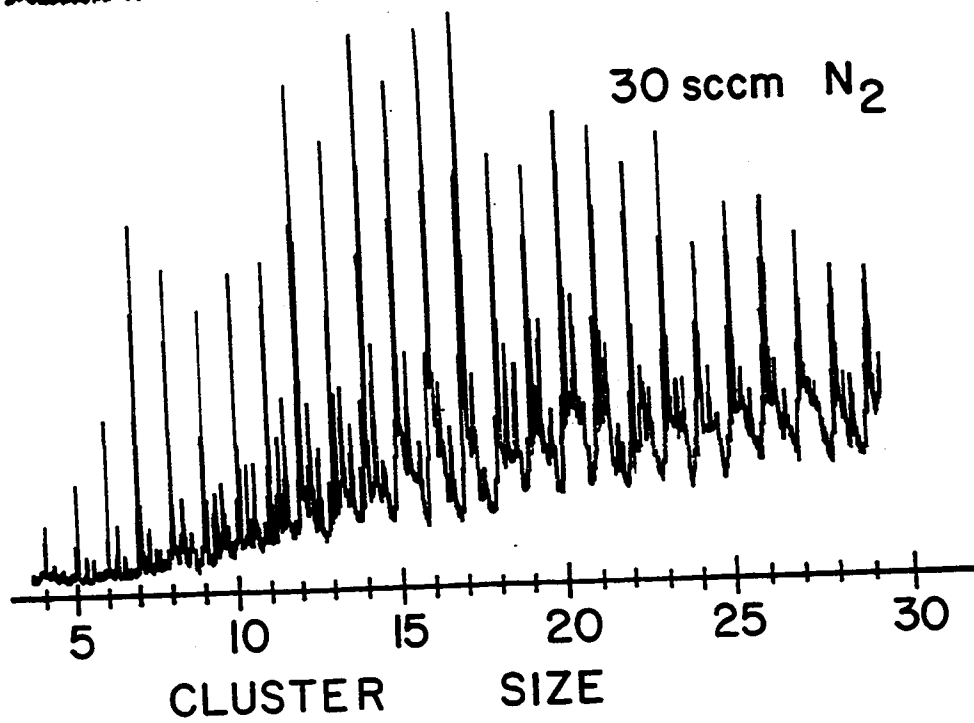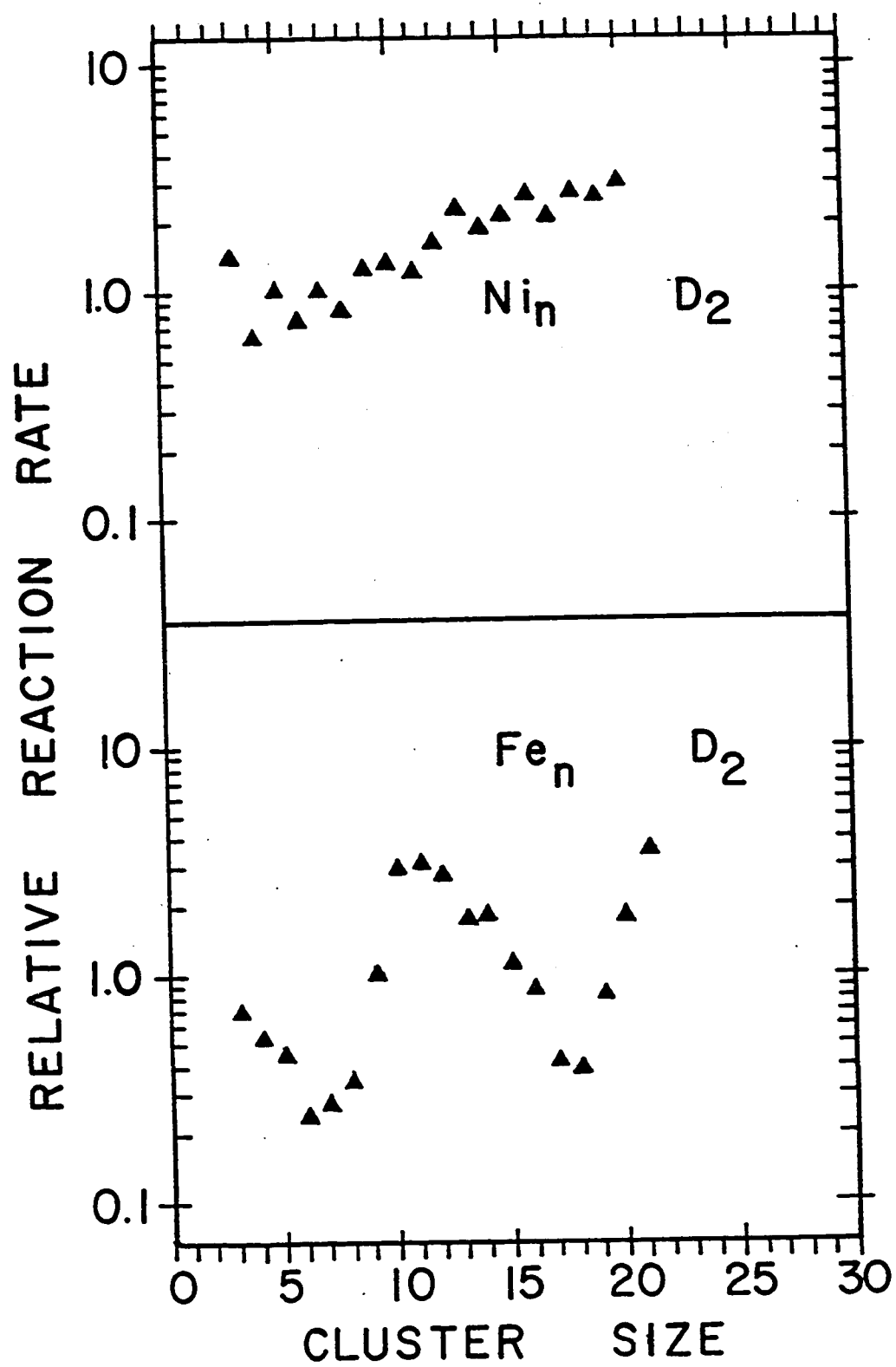mass in the lower spectrum of Figure 35).

At the relatively high concentrations of injected
N_2 reactant used in the experiment of Figure 35, the
cluster arrival time at the detector was observed to
increase by 20 to 40 microseconds (to a total flight
time of 800 microseconds). An experiment with argon
injected instead of N_2 revealed this time shift to be
a kinetic effect associated with the heavier mass of
the reactant gas as compared to the normal helium car-
rier. We do not fully understand as yet the detailed
mechanism for this delay. Even at the highest reactant
concentrations only a few percent of the total gas in
the reaction tube was due to the injected heavy reac-
tant -- not enough to produce a significant lowering
of the terminal beam velocity. Since the increase in
cluster arrival time was greatest for the heavier clusters,
the effect may be due to the heavier reactant gas being
more effective in slowing and redirecting the heavy
clusters in the post-shock region at the entrance of
the reaction tube, thus increasing the effective resi-
dence time prior to the main supersonic expansion.

Whatever the cause of the extra delay in the arrival time of the clusters at the detector, it made it difficult to be precise about the extent of reaction of iron clusters with N_2. However, it is clear that the reaction rate is far slower than seen in the cases of cobalt and niobium at much lower N_2 concentrations. Furthermore, those few cases where Fe_nN_2 reaction products are seen in the highest concentration studies are just the clusters that were found to be most reactive in D_2 chemisorption.

These low reactivity results for N_2 dissociative chemisorption on iron clusters are perfectly in accord with the extensive single crystal studies of Ertl and co-workers[95] in their studies of N_2 dissociation as the rate limiting step in ammonia synthesis on iron catalysts.

G. Conclusions

From the data presented within the last section it was shown that the reactivity of metal clusters depends on the reactant, cluster size, and metal. These initial studies have obtained the first data demonstrating that for certain reactants the reactivity as a function of cluster size changes dramatically. For example, the relative reactivity for N_2 chemisorption on niobium clusters shows that Nb_{16} is over an order of magnitude less reactive than Nb_{15} or Nb_{17}.

As also shown in the last section certain restrictions can be placed on the reaction products due to the conditions in the reaction tube. It was estimated that the minimum binding energy of these chemisorption reaction products is at least 13 kcal/mole in order to be observed. In the case of molecular hydrogen (or D_2), there is only one type of chemisorption having such a strong binding energy, that is, it must dissociatively chemisorb. Also in the case of N_2 these requirements support the argument that dissociative chemisorption is involved for its reaction on clusters. This is due to the fact that the strongest known N_2 molecular chemisorption state on a transition metal (N_2 on rhodium)[96] is completely desorbed by 300K. The D_2 and N_2 chemisorption reactions reported here are therefore almost certainly dissociative processes producing strongly bound surface hydrides and nitrides.

For this type of dissociative chemisorption, consensus is that the critical interaction involves electron donation from the surface of the metal into the anti-bonding molecular orbitals of the species, weakening the binding energy of the reacting molecule. Since this process involves partial electron transfer from the metal to the diatomic, it would seem reasonable to suppose that as the ionization potential of the cluster is decreased, the reactivity should increase.

In a recent publication by Whetten et al.[97], they investigated the reaction of H_2 and D_2 on iron clusters and have, in fact, pointed out such a correlation. They have measured the reactive rates of dissociative chemisorption of D_2 and H_2 on iron clusters in the range of Fe_8 to Fe_{25}, and with ionization threshold data previously obtained[98] have correlated the local minimum in D_2 chemisorption reaction rate to a local maximum in the ionization threshold for F_{17} and F_{18}. In this paper they show that the reaction rate seems to correlate well with the ionization potential for clusters of iron in the range of 8 to 25 atoms which seems to support the mechanism of electron donation from the metal to an anti-bonding orbital of H_2 (or D_2). Although in the data presented here, as well as that of Riley et al.,[76,85] there are two minima in the D_2 reaction rate dependence on cluster size for iron. The first minimum occurs near Fe_6 (a region not reported by Whetten et al.) and this minimum does <u>not</u> correspond to a maximum in the ionization threshold of iron clusters which suggests that there may also be other factors involved.

The reaction rate of D_2 on copper clusters also indicates that ionization potential alone is not the only factor involved in determining the relative rate for these reactions. Copper clusters show an inability

to dissociatively chemisorb D_2 (see Figure 31), although the ionization potential of copper clusters (1-25) has been shown by Powers et al.[99] to be just as low as those for the highly reactive iron clusters. From the evidence, it can concluded that orbital electron donation into the anti-bonding orbital of D_2 (or H_2) is definitely not the only factor involved in determing the reaction rate on these clusters.

The dissociative chemisorption of molecular hydrogen on metal surfaces has been considered a chemistry unique to transition metals. This suggests that the surface d-orbitals must be the critical factor involved in these reactions. Recent ab initio calculations by Siegbahn et al.[100] have examined H_2 chemisorption on various surface sites of small nickel clusters both with and without the use of 3d orbitals at the chemisorption site. Their results predict that the 3d orbitals are crucial in lowering the activation barrier to dissociative chemisorption. Therefore, it can be suggested that these studies are actually monitoring the "d" character of the frontier orbitals on the surface of the metal cluster. Although, as of this time, no definite conclusions can be drawn concerning exactly what the parameters are which control these relative reactivities. In comparing the relative reactivities of D_2 and N_2 on clusters of cobalt and niobium

it can be seen that there are some differences however, they are slight and the overall patterns are actually very similar. Therefore, it is suspected that whatever factors control the D_2 dissociative chemisorption rate also control it for N_2.

In contast, the reaction of CO on cobalt and niobium clusters shows a drastically different pattern of reactivity from that of H_2 or N_2. This pattern is a more gradual monotonic increase of reactivity with increasing cluster size. As mentioned in the last section, CO is thought to be molecularly chemisorbed, which in fact may explain its reactivity pattern as compared with H_2 and N_2, suggesting that molecular chemisorption is a much less constrained process.

REFERENCES

1. G. A. Ozin, Faraday Symp. Chem. Soc. 14,7 (1980).

2. M. Moskovits, Acc. Chem. Res. 12, 229 (1979).

3. D. A. Lindsay and G. A. Thompson, J. Chem. Phys. 77, 1114 (1982).

4. V. E. Bondybey and J. H. English, J. Chem. Phys. 73, 42 (1980).

5a. E. Schumacher, W. H. Gerber, H. P. Harri, M. Hoffman, and E. Scholl, ACS Symp. Series No. 197, Metal Bonding and Interaction in High Temperature Systems, edited by J. Gole and W. C. Stwalley (1982) p. 83.

b. A. Hermann, E. Schumacher, and L. Woste, Helv. Chim. Acta 61, 453 (1978).

6. D. R. Preuss, S. A. Pace and J. L. Gole, J. Chem. Phys. 71, 3553 (1978).

7. S. J. Riley, E. K. Parks, C. R. Mao, L. G. Pobo, and S. Wexler, J. Phys. Chem. 86, 3911 (1982).

8. C. Breton, C. DeMichelis, W. Hecq, and M. Mattioli, Revue de Physique Appliquee, 1193 (June 1980).

9. I. G. Karasev, V. M. Kirillow, V. E. Norskii, V. I. Samoilv, and P. I. Ulyakov, Soviet Physics - Technical Physics 15, No. 9, 1523 (1971).

10. E. H. Piepmeir and D. E. Osten, Appl. Spectrosc. 25, No. 6, 642 (1971).

11. S. Leach and M. Velghe, J. Quant. Spectrosc. Radiat. Transfer 16, 861, Pergamon Press (1976).

12. P. Dhez, D. Jaegle, S. Leach, and M. Velghe, J. of Applied Physics 40, No. 6, 2545 (1969).

13. T. G. Dietz, M. A. Duncan, D. E. Powers, and R. E. Smalley, J. Chem. Phys. 74, 6511 (1981).

14. D. E. Powers, S. G. Hansen, M. E. Geusic, A. C. Puiu, J. B. Hopkins, T. G. Dietz, M. A. Duncan, P. R. R. Langridge-Smith, and R. E. Smalley, J. Phys. Chem. 86, 2556 (1982).

15. D. E. Powers, S. G. Hansen, M. E. Geusic, D. L. Michalopoulos, and R. E. Smalley, J. Chem. Phys. 78(6) (1983).

16. V. E. Bondybey, J. Phys. Chem. 86, 3396 (1982).

17. V. E. Bondybey and J. H. English, J. Chem. Phys. 76, 2165 (1982).

18a. M. G. Liverman, Ph.D. Thesis, Rice University (1980).

  b. M. A. Duncan, Ph.D. Thesis, Rice University (1981).

  c. T. G. Dietz, PhD. Thesis, Rice University (1981).

19. T. G. Dietz, M. A. Duncan, M. G. Liverman, and R. E. Smalley, J. Chem. Phys. 73, 4816 (1980).

20. W. C. Wiley and I. H. McLaren, Rev. Sci. Instrum. 26(12), 1150 (1955).

21. T. E. Adams, B. H. Rockney, R. J. S. Morrison, and E. R. Grant, Rev. Sci. Instrum. 52, 1469 (1981).

22. M. R. Adriaens, W. Allison, and B. F. Fauerbacher, J. Phys. E: Sci. Instrum. 14, 1375 (1981).

23a. J. H. Brophy and C. T. Rettner, Opt. Lett. 4, 337 (1978).

23b. J. H. Brophy and C. T. Rettner, Chem. Phys. Lett. 67, 351 (1979).

24. C. T. Rettner and J. H. Brophy, J. Chem. Phys. 56, 53 (1981).

25. P. M. Johnson, M. Berman, and D. Zakheim, J. Chem. Phys. 62, 2500 (1975).

26. D. H. Parker and M. A. El-Sayed, J. Chem. Phys. 42, 376 (1979).

27. K. Klabunde, Chemistry of Free Atoms and Particles (Academic Press: New York, 1980).

28. W. Weltner, Jr. and R. J. Van Zee, Ann. Rev. Phys. Chem. 35, 291 (1984).

29. K. Gingerich, Faraday discussions of the Royal Society of Chemistry, No. 14, Faraday Symposium, 14 (1980).

30a. F. A. Cotton, Acc. Chem. Res. 6, 368 (1973).

30b. F. A. Cotton, Acc. Chem. Res. 11, 225 (1979).

30c. F. A. Cotton and M. H. Chisholm, Chem. Eng. News 60(26), 40 (1982).

31. W. C. Troger and H. B. Gray, Acc. Chem. Res. 11, 233 (1978).

32. J. G. Norman, Jr., H. J. Kolari, B. H. Gray, and W. C. Troger, Inorg. Chem. 16, 987 (1977).

33. A. B. Anderson, J. Chem. Phys. 64, 4046 (1976).

34. W. Klotzbücher and G. A. Ozin, Inorg. Chem. 16, 984 (1977).

35. C. Wood, M. Doran, I. H. Hillier, and M. F. Guest, Symp. Faraday Soc. 14, 159 (1980).

36a. M. M. Goodgame and W. A. Goddard III, J. Phys. Chem. 85, 215 (1981).

 b. M. M. Goodgame and W. A. Goddard III, Phys. Rev. Lett. 48, 135 (1982).

37. A. Kant and B. J. Strauss, J. Chem. Phys. 45, 3161 (1966).

38. Y. M. Efremov, A. N. Samoilova, and L. V. Gurvich, Opt. Spectrosc. 36, 381 (1974).

39. D. L. Michalopoulos, M. E. Geusic, S. G. Hansen, D. E. Powers, and R. E. Smalley, J. Phys. Chem. 86, 3914 (1982).

40. I. N. Levine, Molecular Spectroscopy (John Wiley and Sons, Inc.: New York, 1975).

41. G. Herzberg, Spectra of Diatomic Molecules (Van Nostrand Reinhold: New York, 1950).

42. V. E. Bondybey and J. H. English, Chem. Phys. Lett. 94(5), 443 (1983).

43. S. J. Riley, E. K. Parks, L. G. Pobo, and S. Wexler, J. Chem. Phys. 79(6), 2577 (1983).

44. M. D. Morse, G. P. Hansen, P. R. R. Langridge-Smith, Lan-Sun Zheng, M. E. Geusic, D. L. Michalopoulos, and R. E. Smalley, J. Chem. Phys. 80(11), 5400 (1984).

45. P. R. R. Langridge-Smith, M. D. Morse, G. P. Hansen, R. E. Smalley, and A. J. Merer, J. Chem. Phys. 80(2), 593 (1984).

46. Y. M. Efremov, A. N. Samoilova, V. B. Kozhukosky, and L. V. Gurvich, J. Mol. Spectrosc. 73, 40 (1970).

47. J. B. Hopkins, P. R. R. Langridge-Smith, M. D. Morse, and R. E. Smalley, J. Chem. Phys. 78(4), 1627 (1983).

48. M. M. Goodgame and W. A. Goddard III, Phys. Rev. Lett. 54, 661 (1985).

49. N. A. Baykara, B. N. McMasters, and D. R. Salahub, Mol.Phys. 52(4), 891 (1984).

50. M. M. Goodgame and W. A. Goddard III, Phys. Rev. Lett. 48, 135 (1982).

51. T. H. Upton and W. A. Goddard III, J. Am. Chem. Soc. 100, 5659 (1978).

52. J. Shim, J. P. Dahl, and H. Johansen, Int. J. Quantum Chem. 15, 311 (1979).

53. M. D. Morse, J. B. Hopkins, P. R. R. Langridge-Smith, and R. E. Smalley, J. Chem. Phys. 79, 5316 (1983).

54. P. W. Merill, Publ. Astron. Soc. Pac. 38, 175 (1926).

55. B. Kleman, Astrophys. J. 123, 162 (1956).

56a. A. E. Douglas, Astrophys. J. 114, 466 (1951).

   b. D. A. Ramsay, Adv. Spectrosc. 1, 1 (1959).

   c. L. Gauisset, G. Herzberg, A. Laberquist, and R. Rosen, Astrophys. J. 142, 45 (1965).

57. W. Weltner and D. McLeod, J. Chem. Phys. 41, 235 (1964).

58. R. D. Verma and S. Nagaraj, Can. J. Phys. 52, 1938 (1974).

59. V. E. Bondybey, J. Phys. Chem. 86, 3396 (1982).

60a. S. Green, Astrophys. J. 266, 895 (1983).

  b. S. E. Cummins, S. Green, P. Thaddeus, and R. A. Linke, Ap. J. 226, 331 (1983).

61. S. Green, Ann. Rev. Phys. Chem. 32, 103 (1981).

62. D. L. Michalopoulos, M. E. Geusic, P. R. R. Langridge-Smith, and R. E. Smalley, J. Chem. Phys. 80(8), 3556 (1984).

63. C. H. Townes and A. L. Schawlow, Microwave Spectroscopy (Dover Publications, Incs.: New York, 1975).

64. G. Herzberg, Electronic Spectra and Electronic Structure of Polyatomic Molecules (Van Nostrand Reinhold: New York, 1966).

65. P. C. Cross, J. Chem. Phys. 12, 210 (1944).

66. P. R. Bevington, Data Reduction and Error Analysis for the Physical Sciences (McGraw-Hill: New York, 1969).

67. R. S. Grev and H. F. Schaefer III, J. Chem. Phys. 80, 3552 (1984).

68. P. Thaddeus, S. E. Cummins, and R. A. Linke, Astrophys. J. Lett. (submitted April 18, 1984).

69. G. A. Somorjai, Chemistry In Two Dimensions; Surfaces (Cornell Univ.: Ithaca, NY, 1981)

70. F. C. Tompkins, Chemisorption of Gases on Metals (Academic Press: New York, 1978).

71a. G. A. Ozin, Symp. Faraday Soc. 14, 7 (1980).

  b. G. A. Ozin and C. Gracie, J. Phys. Chem. 88, 643 (1984).

  c. G. A. Ozin and J. G. McCaffrey, J. Phys. Chem. 88, 645 (1984).

72a. Z. K. Ismail, R. H. Hauge, L. Fredin, J. W. Kaufman, and J. L. Margrave, J. Chem. Phys. 77, 1617 (1982).

  b. Z. H. Kafafi, R. H. Hauge, L. Fredin, W. E. Billups, and J. L. Margrave, J. C. S. Chem. Commun. 1230 (1983).

73. D. A. Garland and D. M. Lindsay, J. Chem. Phys.
     80, 4761 (1984).

74a. C. Cosse, M. Fouassier, T. Mejean, M. Tranquille,
     D. P. DiLella, and M. Moskovits, J. Chem. Phys.
     73, 6076 (1980).

  b. M. Moskovitz and D. P. DiLella, in Metal Bonding and
     Interactions In High Temperature Systems, ACS Sympo-
     sium Series 179, ed. J. L. Gole and W. C. Stwalley
     (Am. Chem. Soc., Washington, D. C. 1982) p. 153.

75a. M. E. Geusic, M. D. Morse, and R. E. Smalley, J.
     Chem. Phys. 82(1), 590 (1985).

  b. M. E. Geusic, M. D. Morse, S. C. O'Brien, and R. E.
     Smalley, J. Chem. Phys. (submitted January 1985).

  c. M. D. Morse, M. E. Geusic, J. Heath, and R. E. Smalley,
     J. Chem. Phys. (submitted January 1985).

76. S. C. Richtsmeirer, E. K. Parks, K. Liu, L. G. Pobo,
     and S. J. Riley, J. Chem. Phys. 82 (1985).

77a. D. J. Trevor, R. L. Whetten, D. M. Cox, and A. Kaldor,
     J. Am. Chem. Soc. 107, 518 (1985).

  b. R. L. Whetten, D. M. Cox, D. J. Trevor, and A. Kaldor,
     J. Phys. Chem. 89, 566 (1985).

78. M. J. Zucrow and J. D. Hoffman, Gas Dynamics Vol. 1
     (John Wiley and Sons, Inc.: New York, 1976).

79. H. W. Liepmann and A. Roshko, Elements of Gas Dynamics
     (John Wiley and Sons, Inc.: New York, 1957).

80. J. B. Anderson, in Molecular Beams and Low Density Gas
     Dynamics, P. P. Wegner, Ed. (Marcl Dekkar: New York,
     1974) pp. 1-91.

81. H. Askenhas and F. S. Sherman, Rarified Gas Dynamics,
     4, 84 (1966).

82. J. K. Vennard and R. L. Street, Elementary Fluid
     Mechanics, 5th ed. (John Wiley and Sons, Inc.: New York,
     1975) p. 301.

83. J. P. Toennies and K. Winkelman, J. Chem. Phys. 66,
     3965 (1977).

84. J. Nicholas, Chemical Kinetics (Harper and Row: New York, 1976).

85. E. K. Parks, K. Liu, S. C. Richtsmeirer, L. G. Pobo, and S. J. Riley, J. Chem. Phys.

86. L. D. Schmidt, Catalysis Rev. Sci. Eng. 9, 115 (1974).

87. Y. Zeiri, A. Redondo, and W. A. Goddard III, Surf. Sci. 131, 221 (1983).

88. E. Shustorvich, R. C. Baetzold, and E. L. Muetterties, J. Phys. Chem. 87, 1100 (1983).

89a. T. H. Upton and W. A. Goddard III, in Critical Reviews in Solid State and Material Sciences (CRC, Boca Raton, Florida, 1981).

   b. T. H. Upton and W. A. Goddard III, Phys. Rev. Lett. 42, 472 (1979).

90. M. Grunze, M. Golze, W. Hirschwald, H. J. Freund, H. Pulm, V. Seip, M. C. Tsai, G. Ertl, and J. Kuppers, Phys. Rev. Lett. 53, 850 (1984).

91. P. A. Doben, Y. Sakiska, and T. H. Rhodin, Surf. Sci. 147, 89 (1984).

92. J. F. Janak, A. R. Williams, and V. L. Moruzzi, Phys. Rev. B. 11, 1522 (1975).

93a. M. Balooch, M. J. Cardillo, D. R. Miller, and R. E. Stickney, Surf. Sci. 46, 358 (1974).

   b. M. Balooch and R. E. Stickney, Surf. Sci. 44, 310 (1974).

94a. R. P. Messmer, T. C. Caves, and C. M. Kao, Chem. Phys. Lett. 90, 296 (1982).

   b. R. P. Messmer, S. K. Knudson, K. H. Johnson, J. B. Diamond, and C. Y. Yang, Phys. Rev. B. 13, 1396 (1976).

95a. G. Ertl, J. Vac. Sci. and Technol. A 1, 15 (1983).

   b. G. Ertl, S. B. Lee, and M. Weiss, Surf. Sci. 114, 515 (1982).

   c. G. Ertl, M. Huber, S. B. Lee, Z. Paal, and M. Weiss, Appl. Surf. Sci. 8, 373 (1982).

96. H. A. Hendricks, A. Hoek, and B. E. Nieuwenhuys, Surf. Sci. 135, 81 (1984).

97. R. L. Whetten, D. M. Cox, D. J. Trevor, and A. Kaldor, Phys. Rev. Lett.

98. E. A. Rohlfing, D. M. Cox, A. Kaldor, and K. H. Johnson, J. Chem. Phys. 81, 3846 (1984).

99. D. E. Powers, S. G. Hansen, M. E. Geusic, D. L. Michalopoulos, and R. E. Smalley, J. Chem. Phys. 78, 2866 (1983).

100. P. E. M. Siegbahn, M. R. A. Blomberg, and C. W. Bauschlicher, Jr., J. Chem. Phys. 81, 2103 (1984).

APPENDIX 1

New Electronic States of Chromium Dimer

During the search for spectra of Cr_3, further vibronic features were accidently obtained for Cr_2 in the 4900-5300 Å region. Figure 36 shows the vibronic scan of this region for the 52-52 isotope of chromium dimer. It can be seen that there are two prominent features at 19,396.12 and 19,907.64 cm^{-1} with weaker bands 452 cm^{-1} to the red of each. Bondybey has reported $\Delta G_{\frac{1}{2}}'' = 452$ cm for the 4600 Å spectral band of Cr_2, indicating that the bands arise from the same lower state (the ground state).

High resolution spectra of the 19,396 and 19,907 cm^{-1} bands show the rotational structure characteristic of a $^1\Sigma_u^+ \leftarrow {}^1\Sigma_g^+$ transition for the 52-52 (odd levels and Q-branch missing) and 50-52 (all J levels present, missing Q-branch) isotopic modifications (see Figure 37). Rotational analysis of the 19,396 cm^{-1} band provides further verification within experimental error that the lower state is the $^1\Sigma_g^+$ ground state. It also determines the excited state bond length to be r'=1.635 Å (see Table VI). Under high resolution the 19,905 cm^{-1} band is seen to be a doublet with a splitting of 2.93 cm^{-1}. The data shows that both bands arise from the ground state and terminate in a $^1\Sigma_u^+$ upper state. Both show identical bond lengths of r'=1.730 Å (see Table VII).

From the rotational and isotopic information presented it is reasonable to suggest that there are three electronic states present. Two of these are $^1\Sigma_u^+$ in this region. High

resolution rotational spectra of the remaining bands was
not possible due to low signal noise. The three electronic
states will be labeled as System I, II, and III since it
is the author's feeling that lower lying states will be
found in the future.

System I.

System I as seen in Figure 36 lies to the low energy
(red) side of the spectrum with the 19,396 cm^{-1} band
assigned as the origin (0-0) band due to the small iso-
tope shift of -.343 cm^{-1}. The only other possible member
of the upper state progression (v'-0) is seen at 19,970 cm^{-1}.
However, since the anharmonicity constant of the excited
state would have to be 180 cm^{-1}, this band can be ruled out.
To the red of the origin (0-0) band 452 cm^{-1} is a weak
feature which is assigned as the 0-1.

System II.

This system consists of two bands related by the
$\Delta G_{\frac{1}{2}}"=452$ cm^{-1}. The 19,970 cm^{-1} band has a larger isotope
shift of +5.55 cm^{-1} and therefore is for the most part a
member of the upper state progression (v'-0) with v$\geq$1.
To the red 451 cm^{-1} of this band lies a feature so the
19,970 and 19,519 cm^{-1} bands are assigned as the 1-0 and
1-1, respectively.

System III.

The first member of the upper state progression which
under high resolution was seen to be a doublet is located

at 19,905 cm^{-1}. Evidence from the 50-52 Cr_2 spectra, where this band is seen as a single level, suggests that the doubling is due to a level from a perturbing system which has gained oscillator strength through the 19,905 cm^{-1} band. Because of the large isotope shift of +4.89 cm^{-1}, it is apparent that this band does not correspond to the origin (0-0) band but is instead, most likely, a member of the v'-0 progression with $v \geq 1$. Using the approximate relationship of $w^i = \rho w$ where $\rho = \sqrt{\frac{\mu}{\mu i}}$ and where μ is equal to the reduced mass of the 52-52 isotope of Cr_2, and assuming the upper state level to be v'=1 (without substantial shifting of the 19,907 cm^{-1} band due to perturbation), it may be calculated that the upper state vibrational frequency should be approximately w' = 480 cm^{-1}.

As seen in Figure 36 there is a band at 20,375 cm^{-1} which gives $\Delta G'_{3/2}$=472 cm^{-1}. This evidence seems to support the assignment of the 19,907 and 20,375 cm^{-1} bands as the 1-0 and 2-0 bands, respectively. Each of these bands show a band 452 cm^{-1} to the red which are assigned as the 1-1 and 2-1. Also, 445 cm^{-1} to the red of the 2-1 band lies another band which could possibly be the 2-2 band. The fact that the origin (0-0) band is not seen may be either due the Franck-Condon factors or predissociation.

Summary

The line positions are given for the three systems in Table VII. From the high resolution and isotopic

information it is shown that two of these states
(Systems I and III) are $^1\Sigma_u^+$ with bond lengths of 1.63
and 1.73 Å, respectively. The molecular constants
obtained for these two states are given in Table VI.

Table VI. Molecular Constants

System I	System III
$\nu_{0-0} = 19{,}396.12 \pm 2$	$\nu_{1-0} = 19{,}905.64 \pm 2$
$B_{0'} = .2417 \pm .003$	$B_{1'} = .2165 \pm .003$
$B_{0''} = .2289 \pm .003$	$B_{0''} = .2289 \pm .003$
$r_{0'} = 1.635 \pm .01$	$r_{1'} = 1.730 \pm .01$
$r_{0''} = 1.684 \pm .01$	$r_{0''} = 1.684 \pm .01$
	$\Delta G_{3/2'} = 474.89 \pm 2$

All values are given in cm^{-1}, except r is in $\overset{\circ}{A}$.

Table VII. Band Positions

	System I		Isotope Shift
	52-52	50-52	
0-1	18,944.02	18,947.69	+3.94
0-0	19,396.12	19,395.77	-.343
	System II		Isotope Shift
	52-52	50-52	
1-1	19,519.91		
1-0	19,970.66	19,976.21	+5.55
	System III		Isotope Shift
	52-52	50-52	
1-1	19,455.05		
2-2	19,477.91	19,477.81	-1.1
	19,904.71(Perturber)		
1-0	19,907.64	19,912.53	+4.89
2-1	19,923.51		
2-0	20,375.60		

Uncertainty in band positions estimated to be ± 2 cm^{-1}.

Figure 36.   R2PI vibronic scan of Cr_2 in the
5300-4900 Å region.

$^{52}Cr_2$ (4900-5300 Å)

SYSTEM I

SYSTEM III

SYSTEM II

0-0

0-1

1-0

2-0

RELATIVE FREQUENCY (cm^{-1})

-600 -400 -200 0 200 400 600 800
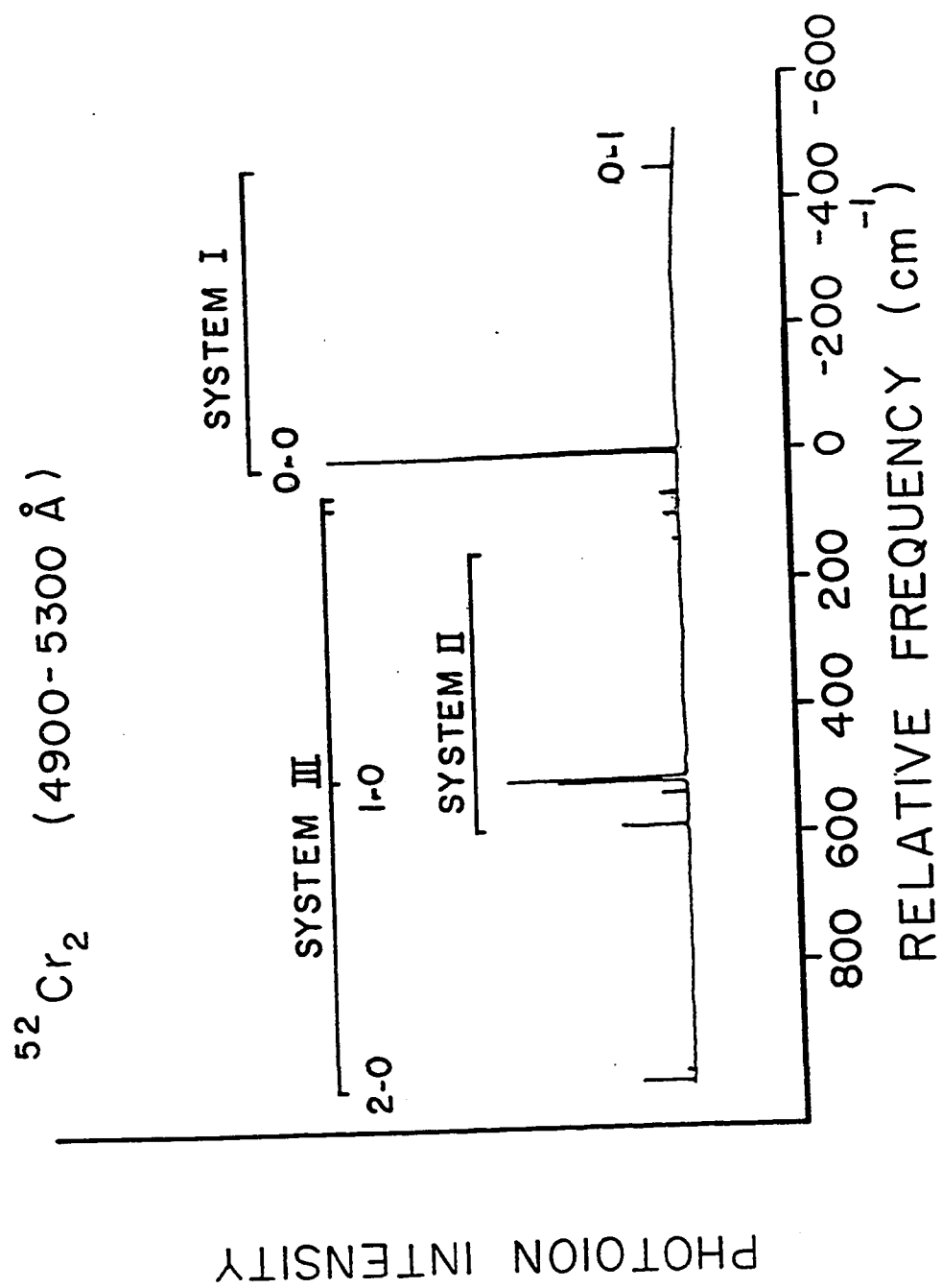
PHOTOION INTENSITY

Figure 37. High resolution spectroscopic scans
of the origin (0-0) transition of
the 50-52 and 52-52 isotopic species
for System I.